อนุพันธ์ควิโนลีนที่มีเฮเทอโรไซเคิลห้าเหลี่ยมสำหรับการตรวจวัดไอออนโลหะ

นายภาสกร หาญเศรษฐการ

วิทยานิพนธ์นี้เป็นส่วนหนึ่งของการศึกษาตามหลักสูตรปริญญาวิทยาศาสตรมหาบัณฑิต
สาขาวิชาเคมี ภาควิชาเคมี
คณะวิทยาศาสตร์ จุฬาลงกรณ์มหาวิทยาลัย
ปีการศึกษา 2559

Quinoline derivatives containing 5-membered heterocycles for metal ion detection

Mr. Pasakorn Hansetagan

A Thesis Submitted in Partial Fulfillment of the Requirements

for the Degree of Master of Science Program in Chemistry

Department of Chemistry

Faculty of Science

Chulalongkorn University

Academic Year 2016

Thesis Title	Quinoline derivatives containing 5- membered heterocycles for metal ion detection
By	Mr. Pasakorn Hansetagan
Field of Study	Chemistry
Thesis Advisor	Assistant Professor Anawat Ajavakom, Ph.D.
Thesis Co-Advisor	Professor Mongkol Sukwattanasinitt, Ph.D.

Accepted by the Faculty of Science, Chulalongkorn University in Partial Fulfillment of the Requirements for the Master's Degree

....Dean of the Faculty of Science

(Associate Professor Polkit Sangvanich, Ph.D.)

THESIS COMMITTEE

....Chairman

(Associate Professor Vudhichai Parasuk, Ph.D.)

....Thesis Advisor

(Assistant Professor Anawat Ajavakom, Ph.D.)

....Thesis Co-Advisor

(Professor Mongkol Sukwattanasinitt, Ph.D.)

....Examiner

(Associate Professor Paitoon Rashatasakhon, Ph.D.)

....External Examiner

(Assistant Professor Nakorn Niamnont, Ph.D.)

ภาสกร หาญเศรษฐการ : อนุพันธ์ควิโนลีนที่มีเฮเทอโรไซเคิลห้าเหลี่ยมสำหรับการตรวจวัดไอออนโลหะ (Quinoline derivatives containing 5-membered heterocycles for metal ion detection) อ.ที่ปรึกษาวิทยานิพนธ์หลัก: ผศ. ดร.อนวัช อาชวาคม , อ.ที่ปรึกษาวิทยานิพนธ์ร่วม: ศ. ดร.มงคล สุขวัฒนาสินิทธิ์, 72 หน้า.

การออกแบบและสังเคราะห์ตัวรับรู้เรื่องแสงสำหรับไอออนโลหะเป็นเรื่องที่น่าสนใจ เนื่องจากตัวรับรู้เหล่านี้มีความว่องไวสูง และมีความจำเพาะสูง ทั้งยังมีความสามารถช่วยให้เห็นภาพเรื่องแสง เพื่อใช้ในการตรวจวิเคราะห์ในทางชีวภาพ และในสิ่งแวดล้อม ในงานวิจัยนี้รายงานอนุพันธ์เอสเธอร์และเอไมด์ซึ่งมีวงเฮเทอโรไซคลิกชนิดห้าเหลี่ยมแบบอะโรแมติกและอะลิฟาติกอยู่ใน 8-ไฮดรอกซีควิโนลีนและ 8-อะมิโนควิโนลีนตามลำดับ ถูกใช้เป็นตัวรับรู้เรื่องแสงแบบเพิ่มสัญญาณสำหรับไอออนโลหะ เพื่อศึกษาผลการเลือกจำเพาะกับไอออนโลหะ โดยในสารละลายเตเตระไฮโดรฟิวแรน พบว่ามีเพียงอนุพันธ์เอไมด์ของ 8-อะมิโนควิโนลีนที่ต่อด้วยวง L-โปรลีน (AQPro) ที่มีสัญญาณาณการเรื่องแสงที่เพิ่มกับไอออนของสังกะสี (Zn^{2+}) โดยมีค่าเรื่องแสงเพิ่มขึ้นถึง 18 เท่า โดยการเพิ่มขึ้นสัญญาณเรื่องแสงของสารประกอบเชิงซ้อนระหว่าง AQPro และ Zn^{2+} เกี่ยวข้องกับการเกิดปรากฏการณ์ chelation enhanced fluorescence (CHEF) และการยับยั้ง photo induced electron transfer (PET) ซึ่งเกิดจากการหลุดออกหรือสูญเสียโปรตอนของเอไมด์ของ AQPro ซึ่งยืนยันผลจากการวิธีการทางสเปกโทรสโกปีได้แก่ ^{1}H NMR, MS การเปลี่ยนไปของสัญญาณการดูดกลืนแสง (absorption) และการปลดปล่อย (emission) ทั้งนี้ Job's plot และ ^{1}H NMR เผยให้เห็นว่า มีการเกิดสารประกอบเชิงซ้อนแบบ 1:1 และ 2:1 ระหว่าง AQPro และ Zn^{2+} และแต่ละอันมีค่าคงที่ในการเกิดสารประกอบเชิงซ้อนเท่ากับ 5.0×10^2 M^{-1} และ 1.5×10^4 M^{-2} สำหรับสารประกอบเชิงซ้อนแบบ 1:1 and 2:1 ตามลำดับ นอกจากนั้นความเข้มข้นต่ำสุด (LOD) ของการตรวจวัด Zn^{2+} โดยใช้สาร AQPro มีค่าอยู่ที่ 25.7 nM

ภาควิชา	เคมี	ลายมือชื่อนิสิต	....
สาขาวิชา	เคมี	ลายมือชื่อ อ.ที่ปรึกษาหลัก	....
ปีการศึกษา	2559	ลายมือชื่อ อ.ที่ปรึกษาร่วม	....

5772102223 : MAJOR CHEMISTRY

KEYWORDS: 8-AMINO QUINOLINE / 8-HYDROXYQUINOLINE / FLUORESCENCE SENSOR / HETEROCYCLES / METAL IONS SENSOR

PASAKORN HANSETAGAN: Quinoline derivatives containing 5-membered heterocycles for metal ion detection. ADVISOR: ASST. PROF. ANAWAT AJAVAKOM, Ph.D., CO-ADVISOR: PROF. MONGKOL SUKWATTANASINITT, Ph.D., 72 pp.

The design and synthesis of fluorescent sensors for metal ions are interesting because of their high sensitivity, high selectivity and imaging capability derivable for analysis of biological and environmental systems. Herein, ester and amide derivatives containing 5-membered heterocyclic aromatic and aliphatic rings of 8-hydroxyquinoline and 8-aminoquinoline, respectively, are evaluated as fluorescent sensors for metal cations to explore their effects on the metal ion binding selectivity. In THF solution, the amide derivative of 8-aminoquinoline bearing L-proline (AQPro) exhibited fluorescence enhancement, a remarkable 18-fold increase of the quantum yield, with Zn^{2+}. The fluorescence enhancement of the complexation between AQPro and Zn^{2+} involves the chelation enhanced fluorescence (CHEF) and suppressed photo induced electron transfer (PET) which is promoted by the deprotonation of the amide proton as confirmed by ^{1}H NMR, MS absorption and emission spectroscopy. The Job's plot of fluorescence intensity and ^{1}H NMR spectroscopy revealed that both 1:1 and 2:1 stoichiometric binding ratio between AQPro and Zn^{2+} are possible and gave the association constant (K_a) of 5.0×10^2 M^{-1} and 1.5×10^4 M^{-2} for the 1:1 and 2:1 complexation, respectively. Furthermore, the limit of fluorescence detection of Zn^{2+} with AQPro in THF solution was as low as 25.7 nM.

Department:	Chemistry	Student's Signature	....
Field of Study:	Chemistry	Advisor's Signature	....
Academic Year:	2016	Co-Advisor's Signature	....

ACKNOWLEDGEMENTS

CONTENTS

LIST OF FIGURES

จุฬาลงกรณ์มหาวิทยาลัย
CHULALONGKORN UNIVERSITY

LIST OF TABLES

CHAPTER I

INTRODUCTION

1.1   Fluorescence

One form of quantum mechanical process (photoluminescence) is the term of fluorescence occurring between the ground and excited states of a molecule that can be basically described by the Jablonski energy diagram (Figure 1.1). The molecule (usually an aromatic compound or highly conjugated molecule) is in ground electronic state (S_0) which is a singlet state at normal condition. Upon the absorption of light with appropriate energy, an electron, usually one of the valence electrons, of the molecule is excited to a higher energy level and the molecule assumes excited electronic states (e.g. S_1 or S_2 excited state). Absorption of light occurs extremely fast, approximately a femtosecond that the time necessary for the electron to travel within the molecule. The electronic transition occurs without geometrical change which is normally called vertical transition. This can be explained from the Frank-Condon principle that a nucleus is much heavier than an electron. Thus, the motions of nuclear are much slower than the motions of electron. However, if the geometry in excited state is not the same as the ground state, the initial electronic excitation occurs geometrically relaxed to the most stable vibrational state of S_1 via vibration and rotation without light emitting. This non-radiative decay is also very fast, between 10^{-14} and 10^{-10} s. If the initial excited state is higher than S_1, the molecule may relax to the most stable vibrational state of S_1 via the coupling of geometrical and electronic relaxation which is termed as internal conversion. Then, the most stable vibrational state of S_1 may return to S_0 by two possible radiative pathways. First, the excited molecules may reduce its energy by emitting a photon which is termed fluorescence. The time required for this process typically in nano-second scale which is slower than most geometrical relaxation and competitive with some other nonradiative pathways. With part of the energy already lost via nonradiative geometrical relaxation and internal conversion, fluorescence spectrum is observed at longer wavelength than the corresponding absorption spectrum. The energy of a fluorescent photon is thus always

less than that of the exciting photon. The difference in wavelengths of the maximum emission and maximum absorption is called Strokes shift; $\Delta\lambda = \lambda_{em} - \lambda_{abs} > 0$. The molecules with many possible geometrical changes will have larger Strokes shift. However, in rigid molecules for which S_1 and S_0 have very similar geometries, and solvation, the stokes shift will be small. Another pathway that a molecule may take in the dissipation of energy is called intersystem crossing (ISC). The electron changes spin multiplicity from an excited singlet state to an excited triplet state (T_1). Usually, the transitions between S_1 to T_1 in common organic molecule are forbidden by the spin conservation rule. However, the ISC is allowed with spin-orbit coupling which is usually observed for a molecule containing heavy atoms like bromine or iodine. After the ISC process, radiative relaxation from T_1 back to S_0 is known as phosphorescence. This is the slowest process in the Jablonski diagram, several orders of magnitude slower than fluorescence, typically in the scale of microseconds to several minutes. It can continue to glow even after the excitation source is turned off.
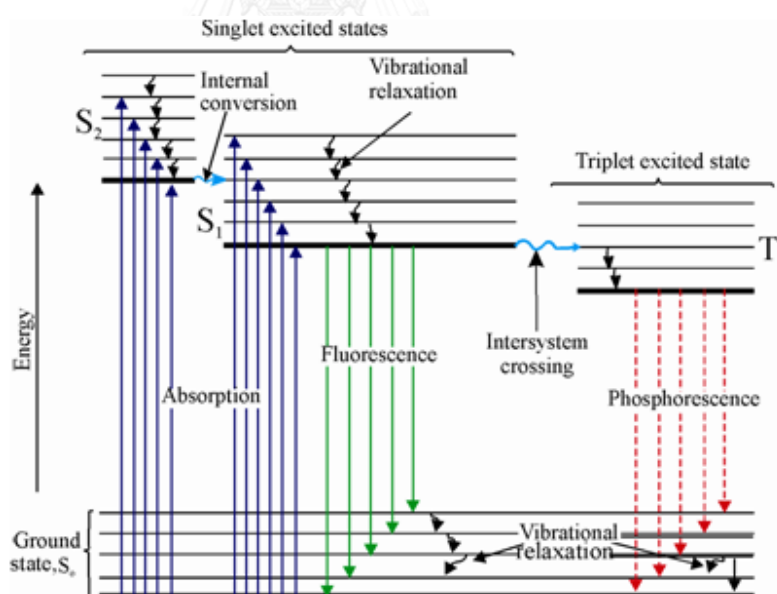
Figure 1.1 Jablonski diagram [1].

1.2   Fluorescence chemosensors

Recently, the fluorescent sensors have been developed for easy to use, short response time and no sample destruction. They were designed for detection of several analytes. Fluorescent technique has several special features such as high sensitivity and high selectivity with ability to allow visual detection and optical imaging.

1.2.1   Sensing modes

Generally, fluorescent chemosensor contains two main components: one is a selective binding site (receptor) another is the signal source (fluorophore) which provides the means of signaling this binding, whether by fluorescence turn-on, turn-off or wavelength shift (Figure 1.2). Fluorescent turn-on mode is fluorescent sensor that gives enhanced fluorescence signal upon interaction with an analyte. In contrast, turn-off mode must have fluorophore unit which its high emission intensity diminishes upon interaction with an analyte. For the wavelength shift mode, the sensing molecule may change its electronic structure or at least its geometry upon the interaction with an analyte that leads to a new fluorescence signal at different wavelength. The ideal sensors should not be affected by environmental interference (signal-selectivity), such as photochemical reactions, concentration and matrixes (pH, polarity, temperature, etc.).
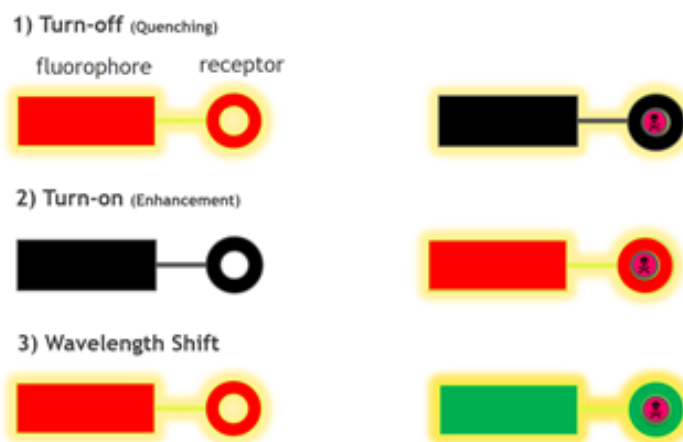
Figure 1.2 mode of fluorescence sensor.

1.3   Sensing mechanism

The photophysical mechanisms control the response of a fluorophore to analyte binding as follows; photoinduced electron transfer (PET) [2-9], intramolecular charge transfer (ICT) [3-5, 7-9], excited-state intramolecular proton transfer (ESIPT) [10-14], Föster resonance energy transfer (FRET) [15, 16], Isomerization [17], aggregation-induced enhancement fluorescence (AIE) [13, 18, 19], aggregation-caused quenching (ACQ) [20], and excimer/exciplex formation [3-5, 9, 21]. A chemosensor may transduce the chemical interaction event into fluorescent signals based on one or more of these processes. A design of sensing system having more than one process working synergistically to enhance the fluorescence responses is challenging.

1.3.1   Photoinduced electron transfer (PET)

PET process occurs when receptor or analyte has either its highest occupied molecular orbital (HOMO) (donor) or the lowest unoccupied molecular orbital (LUMO) (acceptor) level between HOMO and LUMO gap of the fluorophore.

In the first case, when an electron of fluorophore is excited to its LUMO level. A HOMO electron of donor presumably transfers to the HOMO level of excited fluorophore which acts as the electron acceptor. Then, the excited electron in LUMO level can transfer to the HOMO level of donor (Figure 1.3, left). In the latter case, the excited electron in LUMO level of fluorophore transfer to the LUMO level of the acceptor before transferring back to the half-filled HOMO level itself of the fluorophore (Figure 1.3, right). The electron transfer process is a non-radiative process which results in quenching of the fluorescence. So, the fluorescent sensor in turn-off and turn-on mode can be designed based on promoting or inhibiting of the PET process.
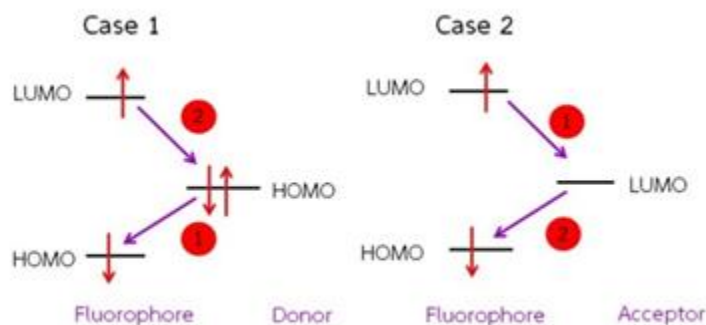
Figure 1.3 Schematic diagram of PET process [22].

1.3.2   Intramolecular charge transfer (ICT)

The locally excited (LE) state is the initial most stable excited state of S_1. In certain case, a molecule in LE state may undergoes another geometrical relaxation along with redistribution of electron density, especially when the molecule contains both electron withdrawing and donating groups connected *via* π-conjugated system. The relaxation process produces a new longer energy excited state called internal charge transfer (ICT) state having significantly different geometry and dipole moment from the LE state (Figure 1.4). After that, the ICT state relaxes to ground state either by non-radiative decay or radiative decay. Depending on the energy band gap, this relaxation may provide light within or outside the visible light spectrum [23, 24]. If detectable, this emission from ICT state is at a longer wavelength and enhanced by polar solvent as the ICT excited state more populated by the solvent stabilization. Because of multi-step process, ICT emission usually has lower fluorescence quantum yield compared with LE state. The fluorescent sensor can be designed based on the degree of the ICT process to be turn-off or turn-on or wavelength shift mode.
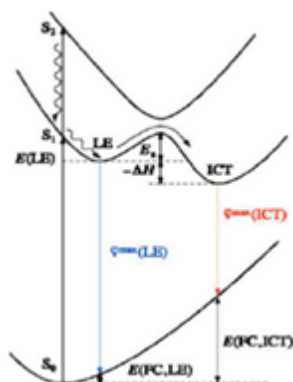
Figure 1.4 Potential energy surfaces of the ground state, S_0 is excited to S_1 then relaxed to LE and ICT state [23].

1.3.3 Excited state intramolecular proton transfer (ESIPT)

The ESIPT process generally associates with the transfer of proton from a hydroxyl group (or amino) to carbonyl oxygen (or imine nitrogen) with a six- or five-membered ring hydrogen bonding configuration intermediate [25]. The classical example of the ESIPT photophysical process was observed for 2-(20-hydroxyphenyl)-benzoxazole (HBO) (Figure 1.5). After irradiation, the excited HBO in enol form (E*) is converted to the excited keto form (K*) in the sub picosecond time scale resulting in significantly red-shift emission compared with the absorption and unusually large Stoke shift. A large Stoke shift is beneficial in fluorescence sensing to avoid the self-absorption or the inner filter effect. The fluorescent sensor that designed with a large wavelength shift can be achieved with ESIPT process.
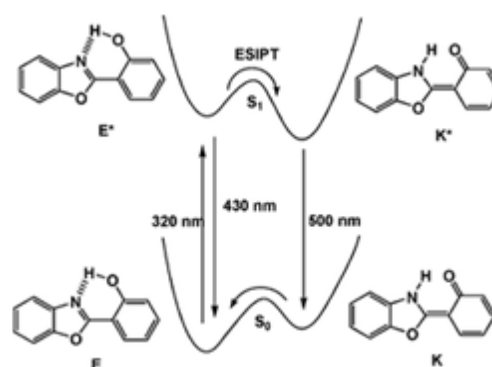
Figure 1.5 ESIPT process of 2-(20-hydroxyphenyl)-benzoxazole (HBO) [25].

1.3.4   The FÖster resonance energy transfer (FRET)

FÖster resonance energy transfer (FRET) is a dynamic quenching mechanism in which the process can occur when emission spectrum of the energy donor (D) overlaps with the absorption spectrum (A) of the acceptor (Figure 1.6) [9]. FRET drops quickly with the distance of donor and acceptor, but increases with the spectral overlap between the donor emission and acceptor, and the relative orientation of the donor and acceptor dipole moment. The idea of an oscillating diploe supports this theory that can get an energy exchange with a second dipole which has a similar resonance frequency. So, resonance energy transfer is similar behavior of coupled oscillators. Measurements of FRET efficiency can be used as a research tool in biology and chemistry, both *in vitro* and *in vivo* to determine the distance between two fluorophores [26]. The sensing application in the term of turn-off and wavelength shift mode can be designed based on FRET process
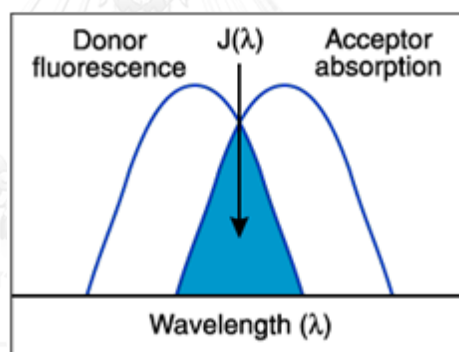
Figure 1.6 Spectral overlap between donor and acceptor in order to transfer energy.

The sensing compounds in this thesis have been designed on PET and ICT.

1.4   Quinoline-Based fluorescence sensors

Quinolines are one of the most interesting classes of heterocyclic compounds forming fluorescent complex with metal ions. The prime example is tris-(8-hydroxyquinoline) aluminum AlQ_3 which is highly fluorescent in both solution and solid state that it has been used as a standard green emissive material for organic light-emitting diodes (OLEDs) [27- 32] . Quinoline and its derivatives, mainly 8-

Hydroxyquinolines and 8-Aminoquinoline, are important fluorescence sensor for detecting metal ions [33-35]. Derivatives of 8-aminoquinoline with an aryl sulfonamide [36] (Figure 1.7) are the first and most widely applied fluorescent chemosensors for Zn^{2+} in biological sample. They are highly selective sensor for Zn^{2+} in the presence of high concentration of Ca^{2+} and Mg^{2+}, which is very important for in *vivo* application. However, their poor water solubility has limited their applications [37].
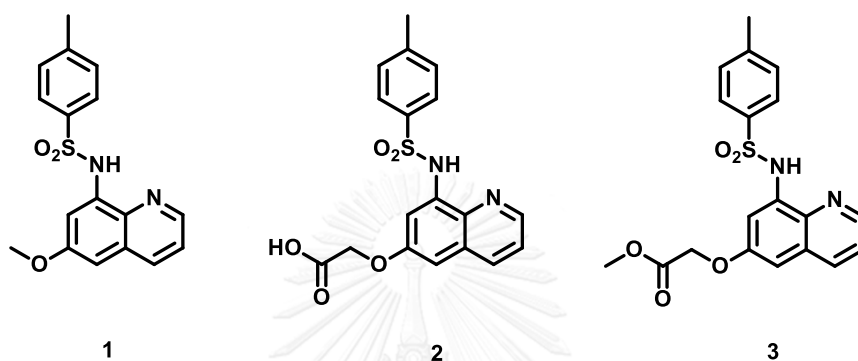
Figure 1.7 Derivative of 8-aminoquinoline with an aryl sulfonamide [36].

In 2008, Zhang et al. [38] reported a water-soluble and ratiometric chemosensor **AQZ**, based on 8-aminoquinoline for Zn^{2+} ion, which displayed 8-fold increase in fluorescence quantum yield (Figure 1.8) and a 75 nm red-shift of the emission peak from 440 to 515 nm. The association constant (K_a) was determined as = 6.7 x 10^6 in methanol/water 1:9 (v/v). **AQZ** was applied for sensing of Zn^{2+} in yeast cells.
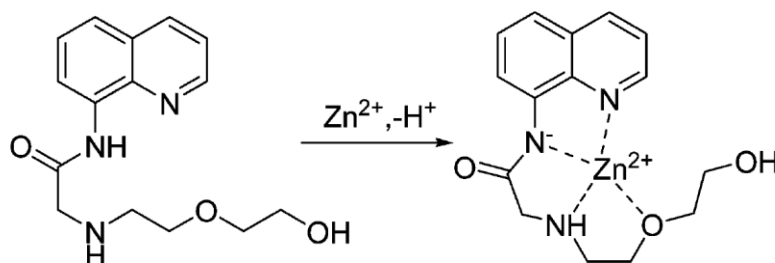
Figure 1. 8 Proposed of **AQZ**-Zn^{2+} complexation resulting in fluorescence enhancement [38].

In 2011, Xiaobo et al. [39] designed and synthesized a pair of carboxamido quinoline pendants onto trans-1,2-diaminocyclohexane scaffold via *N*-alkylation, multifunctionalized (**ACAQ** in Figure 1.9). In 50% methanol/aqueous buffer pH 7.4 solution, **ACAQ** showed a selective ratiometric fluorescence changes with a shift from 410 to 490 nm upon excitation at 316 nm in response to the complexation with Zn^{2+}. The enhancement ratio of I_{490}/I_{410} was found to be as high as 12-Fold. The limit of detection (LOD) of **ACAQ** with Zn^{2+} was 28.3 nM. The K_a determined in methanol/water 50:50 (v/v) was 1.8×10^6 M^{-1}. Two stoichiometric complexes were observed by ^{1}H NMR spectroscopy at different **ACAQ**:Zn^{2+} ratios. **ACAQ** was also applied for Zn^{2+} sensing in HK-1 cells.
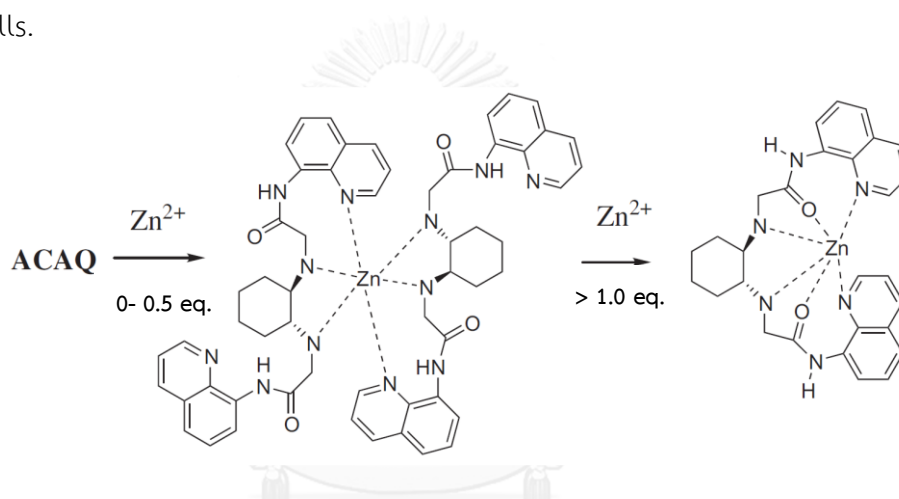
Figure 1.9 Proposed two complexes observed by ^{1}H NMR spectroscopy at different **ACAQ**:Zn^{2+} ratios [39].

In the same year, Parul et al. [40] designed and synthesized *N*-(quinoline-8-yl)-2-[3-(triethoxysilyl)propylamino]acetamide on ordered mesoporous silica material, MCM-41, for Zn^{2+} fluorescent sensing application (Figure 1.10). The **QTEPA-modified MCM-41** showed 3-fold fluorescence emission enhancement and about a 55 nm red shift. The K_a value was determined to be 5.7×10^3 M^{-1} in aqueous buffer solution with the limit of detection (LOD) of 0.1 μM.
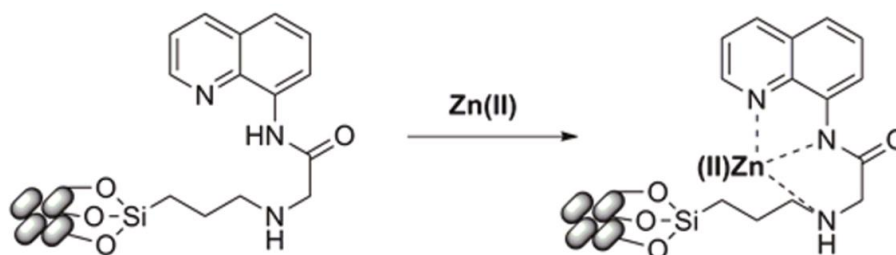
Figure 1.10 Proposed binding of **QTEPA-modified MCM-41** and Zn^{2+} [40].

In 2012, Zhang et al. [41] synthesized a series of carboxamidoquinoline based fluorescent sensors, the **AQZ** family (Figure 1.11a). The substituents and their positions on the quinoline ring were varied for tuning its fluorescence sensing properties. All synthesized **AQZ** derivatives showed high fluorescence enhancement sensitivity for Zn^{2+} in aqueous buffer solution. The derivatives containing morpholine (**AQZ4MP** and **AQZ2MP**) also showed very high selectivity (Figure 1.11b). The apparent dissociation constants (K_d) of the Zn^{2+} complexes were 10^{-5}-10^{-6} M.
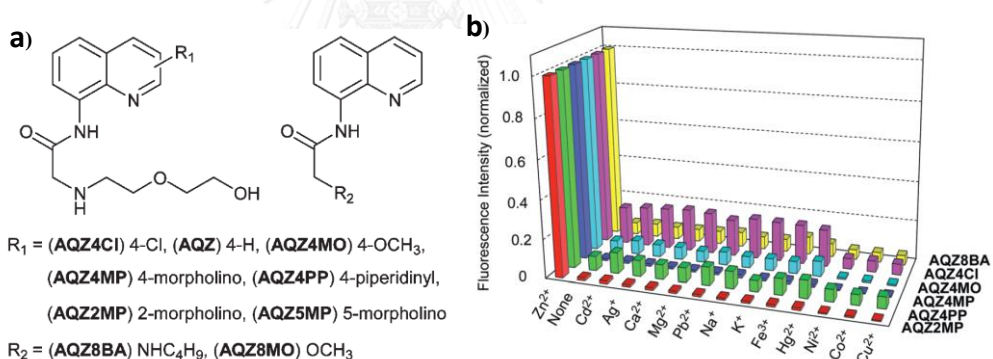
Figure 1.11 (a) Structure of **AQZ** derivatives and (b) normalize selectivity graph of **AQZ** family with various metal ions [41].

In 2013, Zhengping et al. [42] developed (*N*-Quinolin-8-yl-2-[quinoline-8-ylcarbamoylmethly)-amino]-acetamide, **NQA**) as a new fluorescent sensor for Zn^{2+}. **NQA** displayed selectivity for Zn^{2+} in the presence of other metal in aqueous solution (Figure 1.12) with the K_a of 8.69 x 10^5 M^{-1} and the LOD of 0.2 nM. Furthermore, the fluorescent changes of **NQA** upon the addition of cation (Cu^{2+} and Zn^{2+}) are utilized to construct an inhibit logic gate at the molecular level, using Cu^{2+} and Zn^{2+} as chemical inputs and the fluorescence intensity as output.
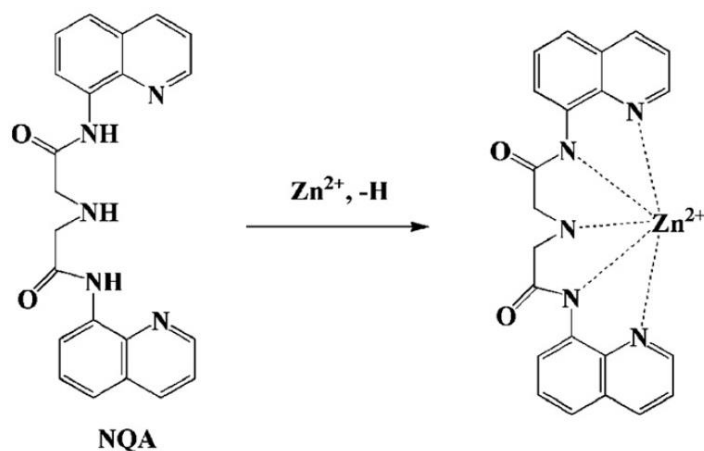
Figure 1. 12 Proposed binding between **NQA** and Zn^{2+} resulting in fluorescence enhancement [42].

In the same year, Yang et al. [43] synthesized a quinoline based acetamidoquinoline bearing picolylamine (**R-1**) for the dual detection of Zn^{2+} and Cd^{2+} in aqueous solution. Upon binding to both metal ions, fluorescence enhancement at 497 nm, corresponding to the 77 nm red shift, was observed. The binding constants between sensor and metal ions were calculated to be 1.64 x 10^5 M^{-1} for Zn^{2+} and 6.30 x 10^4 M^{-1} for Cd^{2+}. The detection limits were calculated to be 3.2 µM and 170 µM for Zn^{2+} and Cd^{2+}, respectively. The fluorescence of **R-1**/Cd^{2+} complex reduced by addition of excess cysteine. However, the fluorescence of **R-1**/Zn^{2+} complex unchanged with the addition of cysteine. Thus, by using **R-1** and cysteine, Zn^{2+} and Cd^{2+} could be readily distinguished (Figure 1.13).
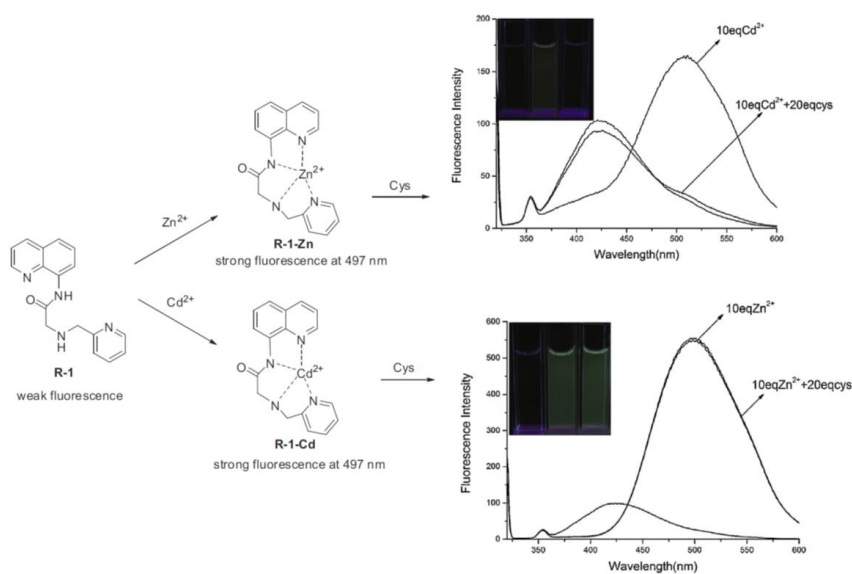
Figure 1.13 Proposed complexation of Zn^{2+} and Cd^{2+} with **R-1** and cysteine [43].

In the same year, Shyamaprosad et al. [44] synthesized a new sensor, **TAQ** as shown in Figure 1.14. **TAQ** showed good water solubility and high selectivity for Zn^{2+} sensing; about a 15-fold increase in fluorescence quantum yield and a 100 nm red-shift of fluorescence emission upon binding Zn^{2+} in aqueous HEPES buffer solution are observed. The K_a value between **TAQ** and Zn^{2+} was 4×10^4 M^{-1} and the LOD was 3.2 µM. The Zn^{2+}-**TAQ** complex can also be used in killing human lung cancer cells (A549).
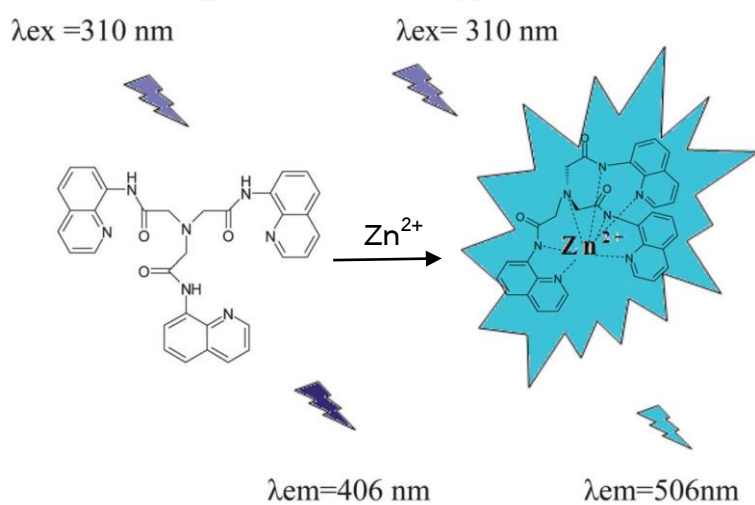
Figure 1.14 Probable host-quest binding beteen **TAQ** and Zn^{2+} [44].

In 2015, Yue el al. [45] reported a novel quinoline based fluorescent Zn^{2+} chemosensor **HAQT**. **HQAT** exhibited excellent sensitivity and selectivity with a fluorescence enhancement to Zn^{2+} over other cations in Tris buffer (pH = 7. 4, CH_3OH/H_2O = 4:1, v/v) (Figure 1.15). The detetion limit for Zn^{2+} by **HAQT** reached 25.6 µM and the K_a vaule between **HAQT** and Zn^{2+} was $5. 2 \times 10^5$ M^{-1}. The stoichiometric ratio of the **HAQT**-Zn^{2+} complex was determined to be 1:1 according to the Job's plot. These advantages allowed for the application of **HAQT** to detect Zn^{2+} in real water samples.
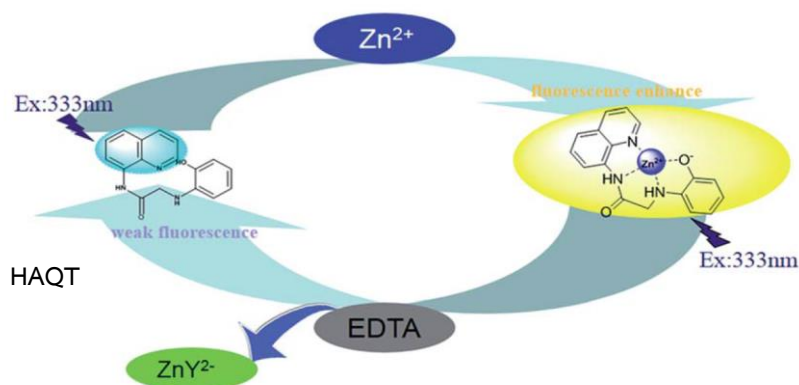
Figure 1.15 Proposed mechanism of the sensing of Zn^{2+} and EDTA [45].

In the same year, Choi et al. [46] synthesized compound **1** based on 8-aminoquinoline for detection of Zn^{2+}. Compound **1** showed selective fluorescence enhancement at 536 nm with Zn^{2+} in aqueous solution (Figure 1. 16). The detection limit of compound **1** for Zn^{2+} was 4.48 µM and the association constant (K_a) was 1.4×10^4 M^{-1}. Moreover, the sensing mechanism of Zn^{2+} by compound **1** was proposed to be the inhibition of PET process which supported by theoretical calculations.
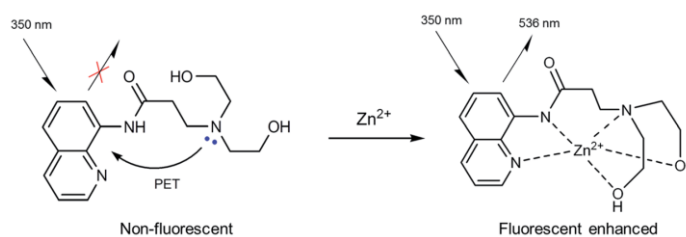
Figure 1.16 Proposed sensing mechanism of **1** for Zn^{2+} [46].

1.5 Objectives of this research

According to the literature review, there was know literature reports concerning to the synthesis and application of quinoline derivatives bearing 5- membered heterocyclic rings as fluorescent sensor. Therefore, the aim of this research is to synthesize and evaluate a series of quinoline derivatives of 8- hydroxyquinoline (**HQ**) and 8- aminoquinoline (**AQ**) which having heterocyclic aromatic and aliphatic rings as fluorescent chemosensors for metal ions. (Figure 17.) We expected that the difference of heterocyclic aromatic and apliphatic rings such as furan (**F**), thiophene (**T**), pyrrole (**P**), tetrahydrofuran (**THF**), tetrahydrothiophene (**THT**) and L-proline (**Pro**), can show different selectivity with various metal ions.
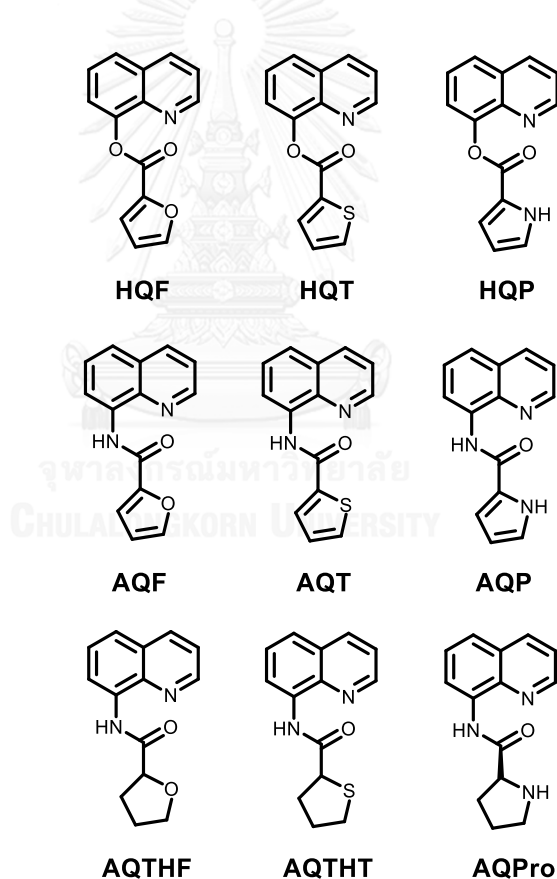
Figure 1.17 Nine target molecules

CHAPTER II

EXPERIMENT

2.1 Reagent, chemicals and Materials

8- Aminoquinoline, 8-Hydroxyquinoline and *N*-(3-dimethyl-aminopropyl)-*N'*-ethylcarbodiimide hydrochloride (EDC) were purchased from TCI Tokyo Chemical Industry. 2-Furoyl chloride, *N*-(*tert*-butoxycarbonyl)-L-proline, 2-thiophene-carbonyl chloride, pyrrole-2-carboxylic acid, tetrahydro-2-furoic acid, tetrahydrothiophene-2-carboxylic acid, triethylamine (TEA), 4-dimethyl-aminopyridine (DMAP), 98% oxalyl chloride, ammonium chloride, trifluoroacetic acid and sodium bicarbonate were purchased from Sigma Aldrich. In anhydrous reactions, dichloromethane was dried by using a Pure Solv MD3 solvent drying system. All column chromatography was operated using Merck silica gel 60 (70-230 mesh). Thin layer chromatography (TLC) was performed on silica gel plates (Merck F245) visualized under an ultraviolet lamp (254 nm). Solvents used for extraction and chromatography such as CH_2Cl_2, hexane and ethyl acetate were commercial grade and distilled before use. Solvents used for sensing study such as methanol, ethanol, isopropanol, dimethysulfoxide, acetronitrile and tetrahydrofuran were AR grade purchased from LABSCAN (Thailand). Milli-Q water was used in all aqueous experiments unless specified otherwise.

2.2 Analytical instruments

The ^{1}H NMR spectra were acquired on a Varian Mercury NMR spectrometer at 400 MHz and ^{13}C NMR spectra were obtained from a Bruker NMR spectrometer at 100 MHz. Mass spectra were recorded on an electrospray ionization (ESI). The absorption and emission spectra were acquired from solutions of the fluorophore in a quart cuvette with 1 cm light path. Absorption spectra were measured by using Varian Cary 50 UV- vis spectrophotometer. Fluorescence spectra were recorded on a Varian Cary Eclipse spectrofluorometer. All color photographs were taken with Panasonic Lumix-GF8 digital camera under normal room light or in a dark box equipped with a black light lamp (354 nm, 8 W).

2.3   Synthesis of fluorophores

2.3.1   Synthesis of compound **AQF**: *N*-(quinolin-8-yl) furan-2-carboxamide

AQT1

69 %yield
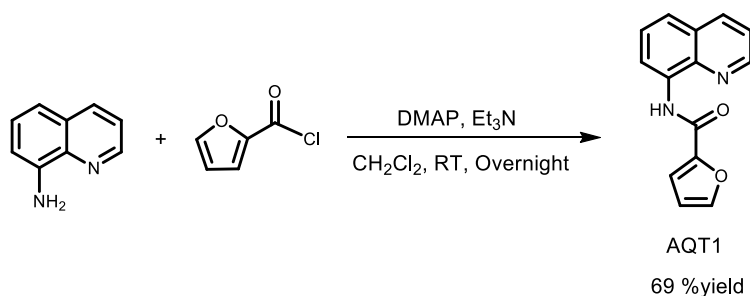
8‑Aminoquinoline (200 mg, 1.39 mmol), DMAP (56 mg, 0.45 mmol) and trimethylamine (0.23 mL, 1.67 mmol) were dissolved in dry CH_2Cl_2 (10 mL) under nitrogen gas. The mixture was cooled to 0°C before 2‑furoyl chloride (0.27 mL, 2.77 mmol) was added dropwise while stirring at room temperature. The reaction mixture was stirred overnight at roomtemperature and quenched with water (10 mL). The mixture was then extracted with CH_2Cl_2 (3 x 10 mL). The organic layer was separated, combined and dried over anhydrous magnesium sulfate. The solution was filtered and concentrated with a rotary evaporator followed by recrystallization from hexane/EtOAc 4:1 to afford **AQF** as a white solid (228 mg, 69% yield). ^{1}H NMR (DMSO-d_6, 400 MHz): δ (ppm) 10.68 (s, 1H), 9.01 (d, J = 4.2 Hz, 1H), 8.73 (d, J = 7.6 Hz, 1H), 8.48 (d, J = 8.3 Hz, 1H), 8.08 (b, 1H), 7.75 (d, J = 8.2 Hz, 1H) 7.70 (dd, J = 4.2 Hz, 8.3 Hz, 1H), 7.66 (m, 1H) 7.38 (d, J = 3.3 Hz, 1H), 6.80 (dd, J = 1.4 Hz, 3.3 Hz, 1H). ^{13}C NMR (DMSO-d_6, 100 MHz) : δ (ppm) 155.4, 149.2, 147.3, 146.1, 137.7, 136.8, 133.5, 127.8, 127.1, 122.4, 122.3, 116.0, 115.5, 112.8. HRMS: *m/z* calculated for $[C_{14}H_{11}N_2O_2]^+$ is 239.0815; found 239.0831 $[M+H^+]$.

2.3.2   Synthesis of compound **AQT**: *N*-(quinolin-8-yl) thiophene-2-carboxamide

AQT
59 %yield
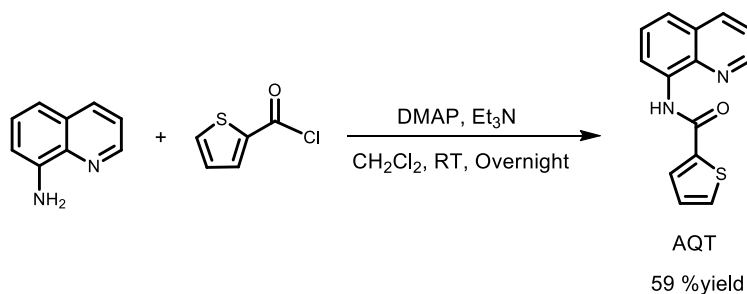
       AQT was synthesized by a similar procedure as the synthesis of **AQF** but 2-furoyl chloride was replaced with thiophenecarbonyl chloride (0.3 mL, 2.77 mmol). **AQT** was obtained as a white solid (210 mg, 59% yield). ^{1}H NMR (DMSO-d_6, 400 MHz): (ppm) δ 10.56 (s, 1H), 9.00 (d, *J* = 4.2 Hz, 1H), 8.60 (d, *J* = 7.6 Hz, 1H), 8.47 (d, *J* = 8.3 Hz, 1H), 8.01 (d, *J* = 3.7 Hz, 1H), 7.96 (d, *J* = 4.9 Hz, 1H), 7.76 (d, *J* = 8.2 Hz, 1H), 7.7 (dd, *J* = 4.2 Hz, 8.3 Hz, 1H), 7.66 (m, 1H), 7.3 (t, *J* = 4.1 Hz, 1H). ^{13}C NMR (DMSO-d_6, 100 MHz) : δ (ppm) 159.3, 149.2, 139.1, 138.3, 136.7, 133.7, 132.3, 129.2, 128.5, 127.8, 126.9, 122.5, 122.3, 117.0. HRMS: *m/z* calculated for $[C_{14}H_{10}NaN_2OS]^+$ is 277.0406; found 277.0424 [M+Na$^+$].

2.3.3   Synthesis of compound **AQP**: *N*-(quinolin-8-yl)-1*H*-pyrrole-2-carboxamide

AQP
12 %yield
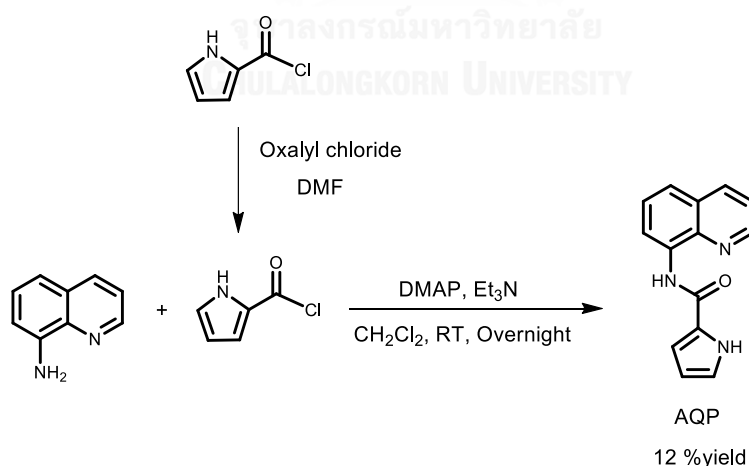
       AQP was synthesized by a similar procedure as the synthesis of **AQF** but 2-furoyl chloride was replaced with pyrrole-2-carbonyl chloride, which generated *insitu* by refluxing pyrrole-2-carboxylic acid (308 mg, 2.77 mmol), and a catalytic amount of DMF in oxalyl chloride (0.5 mL, 5.54 mmol) for 3 h. The crude product was purified by

silica gel column chromatrography using 20% ethyl acetate in hexane as an eluent to afford **AQP** as a yellow solid (39 mg, 12% yield). ^{1}H NMR (DMSO-d_6, 400 MHz): **δ** (ppm) 11.95 (s, 1H), 10.26 (s, 1H), 8.98 (d, J = 2.7 Hz, 1H), 8.67 (d, J = 7.6 Hz, 1H), 8.45 (d, J = 6.9 Hz, 1H), 7.67 (m, 3H). 7.07 (b, 1H), 6.96 (b, 1H), 6.27 (m, 1H). ^{13}C NMR (DMSO-d_6, 100 MHz) : **δ** (ppm) 158.5, 149.0, 137.9, 136.7, 134.3, 127.8, 127.0, 125.9, 123.4, 122.2, 121.4, 115.9, 110.6, 109.4. HRMS: m/z calculated for $[C_{14}H_{11}NaN_3O]^+$ is 260.0794; found 260.0813 [M+Na$^+$].

2.3.4   Synthesis of compound **AQPro-Boc**: (S)-*tert*-butyl 2-(quinolin-8-ylcarbamoyl) pyrrolidine-1-carboxylate

AQPro-Boc
99 %yield
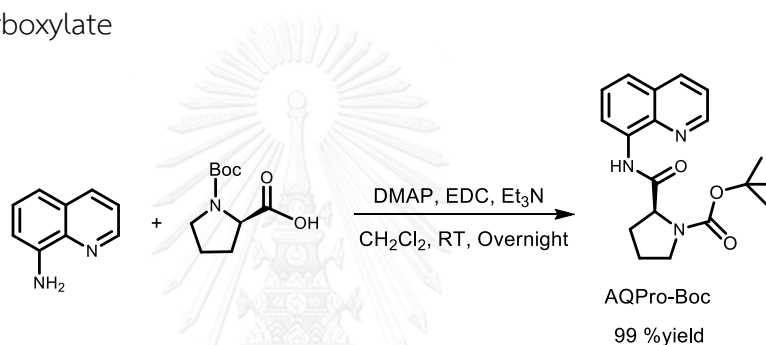
8-Aminoquinoline (200 mg, 1.39 mmol), DMAP (8.47 mg, 0.07 mmol) and triethylamine (0.19 mL, 0.14 mmol) were dissolved in dry CH$_2$Cl$_2$ (20 mL). N-(*tert*-Butoxycarbonyl)-L-proline (894 mg, 4.16 mmol) was added to the mixer and chilled to 0 °C followed by the addition of EDC (798 mg, 4.16 mmol). The reaction mixture was stirred at 0°C for 30 minutes and stirred overnight at room temperature. The reaction mixture was extracted with ammonium chloride. The combined organic layer was dried over magnesium sulfate, filtered, and concentrated with a rotary evaporator. The crude product was eluted through a silica gel column using 40% ethyl acetate in hexane as an eluent to afford **AQPro-Boc** as a white solid (469 mg, 99% yield). ^{1}H NMR (DMSO-d_6, 400 MHz): **δ** (ppm) 10.35 (s, 1H), 8.90 (b, 1H), 8.64 (d, J = 7.5 Hz, 1H), 8.41 (d, J = 8.3 Hz, 1H), 7.68 (d, J = 8.1 Hz, 1H), 7.63 (dd, J = 4.2 Hz, 8.3 Hz, 1H), 7.60 (m, 1H), 4.49 (dd, J = 4.0 Hz, 8.4 Hz, 1H), 3.44 (m, 2H), 2.26 (b, 1H), 2.04 (b, 1H), 1.87 (m, 2H), 1.45 (s, 3H), 1.22 (s, 6H). ^{13}C NMR (DMSO-d_6, 100 MHz) : **δ** (ppm) 171.5, 148.9, 138.0, 136, 134.0, 127.8, 127.0, 122.2, 122.0, 116.1, 79.0, 61.2, 46.7, 30.9, 29.6, 28.1, 27.8, 24.0, 23.4. HRMS: m/z calculated for $[C_{19}H_{23}NaN_3O_3]^+$ is 364.1632; found 364.1630 [M + Na$^+$].

2.3.5   Synthesis of compound **AQPro**: (*S*)-*N*-(quinolin-8-yl) pyrrolidine-2-carboxamide

AQ-Boc-Pro   AQPro

99 %yield   92 %yield
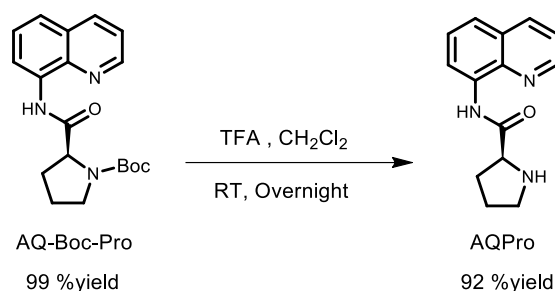
The deprotection of the Boc group was achieved by using trifluoroacetic acid (10mL, 0.1mmol). **Boc-AQPro** (469 mg, 1.37 mmol) was dissolved in CH_2Cl_2 (10 mL). The reaction mixture was stirred overnight at room temperature. Solvent and excess TFA were removed with a rotary evaporator and then the reaction mixture was neutralized with saturated sodium bicarbonate solution followed by addition of CH_2Cl_2 (10 mL). The organic layer was separated and dried over magnesium sulfate, filtered, and concentrated with a rotary evaporator. **AQPro** was obtained as a white solid (304 mg, 92 %yield). ^{1}H NMR (DMSO-d_6, 400 MHz): δ (ppm) 10.82 (s, 1H), 8.95 (d, *J* = 4.2 Hz, 1H), 8.54 (d, *J* = 7.6 Hz, 1H), 8.42 (d, *J* = 8.3 Hz, 1H), 7.73 (d, *J* = 8.2 Hz, 1H), 7.64 (dd, *J* = 4.2 Hz, 8.3 Hz, 1H), 7.60 (t, *J* = 8.1 Hz, 1H), 4.76 (t, *J* = 7.5 Hz, 1H), 1.97 (m, 3H). ^{1}H NMR (methanol-d_4, 400 MHz): δ (ppm) 8.94 (dd, *J* = 1.5 Hz, 4.2 Hz, 1H), 8.65 (d, *J* = 8.0 Hz, 1H), 8.37 (d, *J* = 1.5 Hz, 8.3 Hz, 1H), 7.73 (d, *J* = 9.0 Hz, 1H), 7.61 (m, 2H), 4.77 (m, 1H), 3.53 (dt, *J* = 7.1 Hz, 11.4 Hz, H), 3.44 (dt, *J* = 7.1 Hz, 11.4 Hz, H), 2.27 (m, 1H), 2.17 (m, 1H). ^{13}C NMR (DMSO-d_6, 100 MHz) : δ (ppm) 167.7, 149.2, 138.5, 136.6, 133.7, 127.9, 123.2, 122.3, 118.1, 60.1, 46.0, 29.9, 23.7. NMR (methanol-d_4, 100 MHz) : δ (ppm) 168.4, 150.3, 140.3, 137.8, 134.9, 129.7, 127.9, 124.6, 123.2, 119.5, 62.1, 47.5, 31.2, 25.21. HRMS: *m/z* calculated for $[C_{14}H_{16}N_3O]^+$ is 242.1293; found 242.1300 [M + H$^+$].

2.3.6   Synthesis of compound **AQTHF**: *N*-(quinoline-8-yl) tetrahydrofuran-2-carboxamide
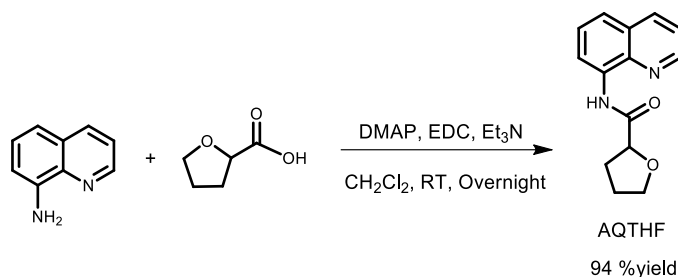
AQTHF
94 %yield

AQTHF was synthesized by a similar procedure as the synthesis of **Boc-AQPro** but *N*-(*tert*-butoxycarbonyl)-L-proline was replaced with tetrahydro-2-furoic acid (550 mg, 4.16 mmol). After recrystallization in methanol, **AQTHF** was obtained as a white solid (316 mg, 94% yield). ^{1}H NMR (DMSO-*d$_6$*, 400 MHz): δ (ppm) 10.73 (s,1H), 8.93 (m, 1H), 8.66 (d, *J* = 7.5 Hz, 1H), 8.41 (d, *J* = 8.2 Hz, 1H), 7.68 (d, *J* = 8.1 Hz, 1H), 7.63 (dd, *J* =4.2 Hz, 8.2 Hz, 1H), 7.58 (m ,1H), 4.54 (dd, *J* = 6.0 Hz, 8.0 Hz, 1H), 4.04 (dd, *J* = 7.1 Hz, 14.2 Hz, 1H), 3.95 (dd, 7.2 Hz, 14.2 Hz, 1H), 2.28 (m, 1H), 2.05 (m, 1H), 1.89 (b, 1H). ^{13}C NMR (DMSO-*d$_6$*, 100 MHz) : δ (ppm) 171.4, 149.3, 137.9, 136.6, 133.4, 127.8, 126.9, 122.2, 122.1, 115.6, 78.4, 69.1, 29.8, 25.1. HRMS: *m/z* calculated for $[C_{14}H_{14}NaN_2O_2]^+$ is 265.0953; found 265.0959 [M+Na$^+$].

2.3.7 Synthesis of compound **AQTHT**: *N*-(quinolin-8-yl) tetrahydrothiophene-2-carboxamide
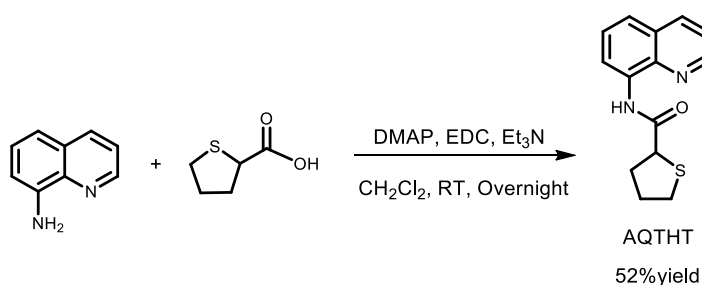
AQTHT
52%yield

AQTHT was synthesized by a similar procedure as the synthesis of **Boc-AQPro** but *N*-(*tert*-butoxycarbonyl)-L-proline was replaced with tetrahydrothiophene-2-carboxylic acid (549 mg, 4.16 mmol). The crude product was purified by silica gel column chromatrography using dichloromethane as an eluent to afford **AQTHT** as a

yellow liquid (186 mg, 52%yield) ^{1}H NMR (DMSO-d_6, 400 MHz): δ (ppm) 10.71 (s, 1H), 8.95 (d, J = 4.1 Hz, 1H), 8.65 (d, J = 7.6 Hz, 1H), 8.42 (d, J = 8.2 Hz), 7.69 (d, J = 8.1 Hz, 1H), 7.65 (dd, J = 4.1 Hz, 8.2 Hz, 1H), 7.59 (t, J = 7.9 Hz, 1H), 4.38 (dd, J = 5.0 Hz, 6.7 Hz, 1H), 3.04 (m, 1H), 2.93 (m, 1H), 2.31 (m, 1H), 2.13 (m, 1H), 2.04 (b, 2H). ^{13}C NMR (DMSO-d_6, 100 MHz) : δ (ppm) 171.0, 149.1, 138.1, 136.6, 134.1, 129.3, 127.8, 126.9, 122.2, 122.1, 116.1, 50.7, 34.5, 32.7, 30.2. HRMS: m/z calculated for [$C_{14}H_{14}NaN_2OS$] is 281.0725; found 281.0721 [M + Na$^+$].

2.3.8 Synthesis of compound HQF: quinolin-8-yl furan-2-carboxylate
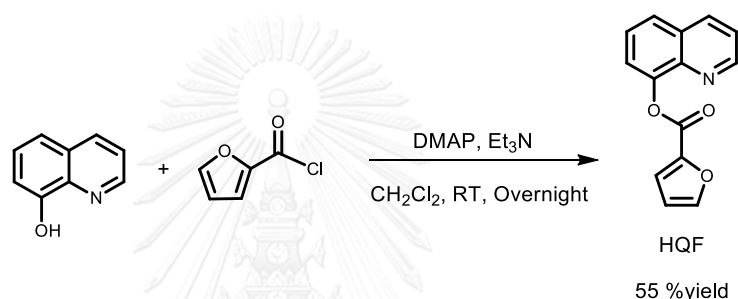
HQF was synthesized by a similar procedure as the synthesis of AQF but 8-aminoquinoline was replaced with 8-Hydroxyquinoline (200 mg, 1.37 mmol). HQF was obtained as a white solid (180 mg, 55 %yield). ^{1}H NMR (DMSO-d_6, 400 MHz): δ (ppm) 8.87 (d, J = 4.1 Hz, 1H), 8.46 (d, J = 8.3 Hz, 1H), 8.13 (d, J = 1.7 Hz, 1H), 7.96 (d, J = 7.3 Hz, 1H), 7.68 (m, 2H), 7.63 (m, 1H), 7.60 (dd, J = 4.1 Hz, 8.3 Hz, 1H), 6.83 (dd, J = 1.7 Hz, 3.5 Hz, 1H). ^{13}C NMR (DMSO-d_6, 100 MHz) : δ (ppm) 164.3, 140.7, 130.3, 128.0, 125.1, 119.9, 118.4, 114.0, 113.6, 107.8, 70.5, 61.4, 21.9, 16.9. HRMS: m/z calculated for [$C_{14}H_9NaNO_3$]$^+$ is 262.0480; found 262.0482 [M+Na$^+$].

2.3.9 Synthesis of compound HQT: quinolin-8-yl thiophene-2-carboxylate
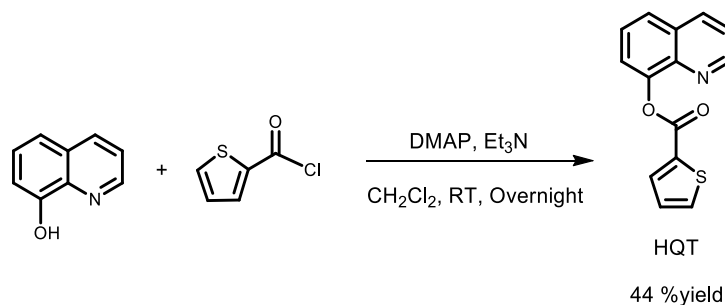
HQT was synthesized by a similar procedure as the synthesis of AQF but 8-aminoquinoline and 2-furoyl chloride were replaced with 8-hydroxyquinoline (200 mg, 1.37 mmol) and thiophenecarbonyl chloride (0.3 mL, 2.77 mmol). HQT was obtained as a white solid (153 mg, 44 %yield). ^{1}H NMR (DMSO-d_6, 400 MHz): δ (ppm) 8.86 (m, 1H), 8.46 (d, J = 8.2 Hz, 1H), 8.11 (d, J = 5.6 Hz, 1H), 8.07 (m, 1H), 7.96 (d, J = 7.6 Hz, 1H), 7.67 (m, 2H), 7.60 (m, 1H), 7.33 (m, 1H). ^{13}C NMR (DMSO-d_6, 100 MHz) : δ (ppm) 161.0, 150.7, 146.6, 140.5, 136.2, 135.2, 135.1, 131.8, 129.1, 128.7, 126.5, 126.4, 122.2, 121.8. HRMS: m/z calculated for $[C_{14}H_9NaNO_2S]^+$ is 278.0252; found 278.0257 $[M+Na^+]$.

2.3.9   Synthesis of compound HQP: quinolin-8-yl 1H-pyrrole-2-carboxylate
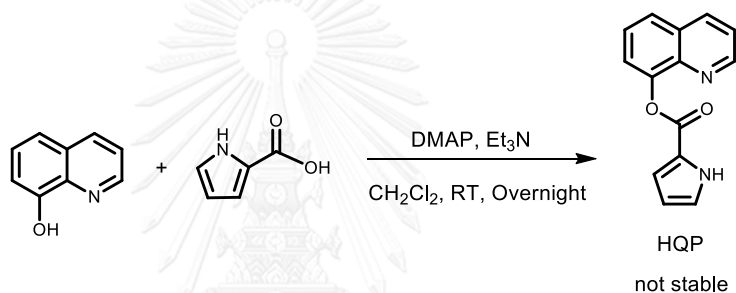
HQP was synthesized by a similar procedure as the synthesis of AQF but 8-aminoquinoline and 2-furoyl chloride were replaced with 8-hydroxyquinoline (200 mg, 1.37 mmol) and pyrrole-2-carbonyl chloride (307.5 mg, 2.77 mmol). The product was decomposed back to 8-hydroxyquinoline upon the purification with silica gel column chromatrography. HQP was obtained as a trace amount of yellow crude oil. ^{1}H NMR (DMSO-d_6, 400 MHz): δ (ppm) 11.20 (s, 1H), 8.86 (dd, J = 1.4 Hz, 4.1 Hz, 1H), 8.44 (dd, J = 1.4 Hz, 8.3 Hz, 1H), 7.92 (dd, J = 2.2 Hz, 1H), 7.65 (m, 2H) 7.58 (dd, J = 4.1 Hz, 8.3 Hz, 1H), 7.15 (d, J = 1.3 Hz, 1H), 7.07 (m, 1H), 6.29 (d, J = 2.1, 1H).

2.4   Photophysical property study

2.4.1   UV-visible spectroscopy

The absorption spectra were acquired from THF solutions of the fluorophores in a quart cuvette (Starna 29-F/Q/10) with 1 cm light path recorded from 250 nm to

600 nm at ambient temperature. The analytical sample solutions were prepared from dilution of the 10 mM stock solutions in THF.

Molar absorption coefficient (ε)

Molar absorption coefficients (ε) of all fluorophores were estimated from UV absorption spectra of analytical samples in THF solution for the sensor base on 8-aminoquinoline derivatives at various concentrations. The intensities at absorption maximum wavelength (λ_{max}) of each compound were plotted against the concentrations. Each plot should be a straight-line intercepting at the origin and the molar absorption coefficients (ε) can be obtained from slope of the plot according to the following equation:

$$A = \varepsilon bC$$

where b is the cell path length (1 cm), A is the absorbance and C is the molar concentration.

UV-vis titration for determination of K_a

The 10 µL of **AQPro** stock solution (10 mM) was diluted with 980 µL of THF in quartz cuvette. The volumes at 1-10 µL of $Zn(NO_3)_2$ stock solutions (10 mM and 100 mM) was added into **AQPro** solution. The final volume of the mixture was adjusted to 1 mL with THF. The fluorophore solution mixed with THF without the metal ion was used as the blank solution. The absorption spectra of the blank solution and the mixtures were recorded from 250 nm to 600 nm at ambient temperature. The absorbance of the mixture and blank solution of each metal ion was plotted against the wavelength. The absorbance of the mixture of each metal ion was plotted against the $[Zn^{2+}]/[Fluorophore]$ mole ratio as shown in Figure 2.1. The association constant (K_a) was calculated using Bindfit v0. 5 program available from http://app.supramolecular.org/bindfit/.
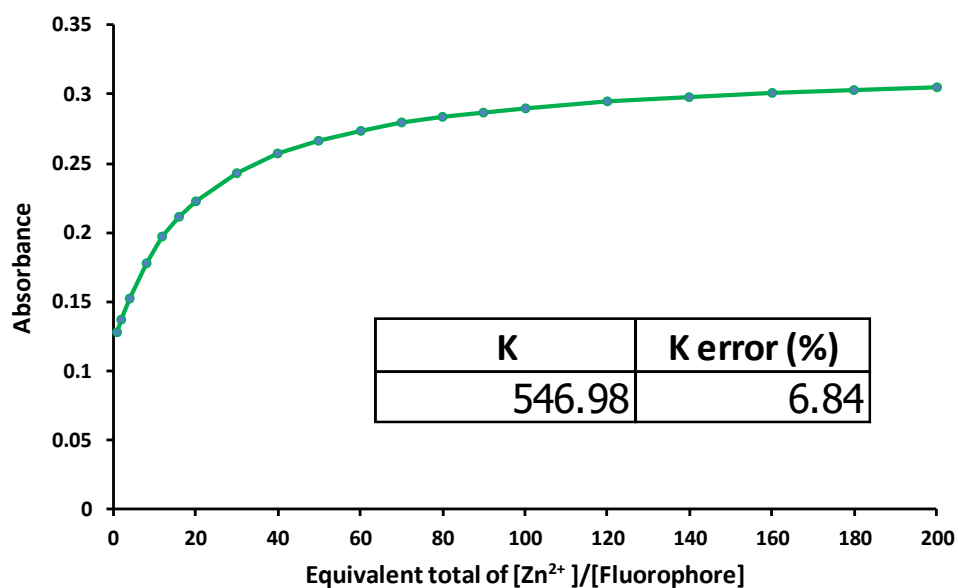
Figure 2.1 The example of curve line from Bindfit v0.5 program.

2.4.2   Fluorescence spectroscopy

The fluorescence spectra were acquired from THF solutions of the fluorophores in a quart cuvette (Starna 29-F/Q/10) with 1 cm light path recorded from 380 nm to 700 nm at ambient temperature using an excitation wavelength of 370 nm. The analytical sample solutions were prepared from dilution of the 10 mM stock solutions in THF.

Fluorescence quantum yields

The fluorescence quantum yield of each fluorophore and complex of **AQPro** with Zn^{2+} ions were determined from the THF solutions using relative fluorescence quantum yield measurement [47]. Quinine sulphate in 0.5 M H_2SO_4 (Φ_{ST} = 0.54: λ_{ex} 336 nm) or fluorescein in 0.1 NaOH (Φ_{ST} = 0.95: λ_{ex} 496 nm) were used as the standard references. The UV-vis absorption and fluorescence spectra of the sample and reference solutions were recorded at seven concentrations. The maximum absorbance of all solutions should never exceed 0.1. The maximum absorption wavelength (λ_{max}) was used as excitation wavelength (λ_{ex}) for each compound. The integrated fluorescence intensities of each spectrum were plotted against the absorbance at the

λ_{max}. The plot for each compound should be a straight-line intercepting at the origin. The fluorescence quantum yield ($\mathbf{\Phi}$) was obtained from the slope ($\mathbf{m}$) of the plot according to the following equation:

$$\Phi_X = \Phi_R \left(\frac{m_X}{m_R}\right)\left(\frac{\eta_X^2}{\eta_R^2}\right)$$

where η is the refractive index of the solvent and the subscripts x and R denote the sample and reference, respectively.

Selectivity study

The stock solution (10 mM) of the metal cation tested were prepared by dissolving their nitrate salts i.e. $LiNO_3$, $NaNO_3$, KNO_3, $Mg(NO_3)_2$, $Ca(NO_3)_2$, $Ba(NO_3)_2$, $Al(NO_3)_3$, $Fe(NO_3)_3$, $Cr(NO_3)_3$, $Co(NO_3)_2$, $Cu(NO_3)_2$, $Ni(NO_3)_2$, $Zn(NO_3)_2$, $Cd(NO_3)_2$, $AgNO_3$, $Pb(NO_3)_2$, acetate salt i.e. $Fe(OAc)_2$, and chloride salt i.e. $HgCl_2$ in Milli-Q water. The fluorophore solution (1 mM, 10 µL) in THF was mixed with each metal ion stock solution (10 µL). The volume of each mixture was adjusted by THF to 1 mL to afford the final concentration of 100 µM metal ion and 10 µM fluorophore. The fluorophore solution mixed with THF without the metal ion was used as the blank solution. The fluorescence spectra of the blank solution and the mixtures were acquired using an excitation wavelength of 370 nm. The ratio between the fluorescence intensity of the mixture and blank solution (I/I_0) of each metal ion was used for selectivity comparison.

Limit of detection (LOD) of Zn^{2+}

The 10 µL of **AQPro** stock solution (1 mM) was diluted with 980 µL of THF in quartz cuvette. The volumes at 1-10 µL of $Zn(NO_3)_2$ stock solutions (100 µM) was added into **AQPro** solution. The final volume of the mixture was adjusted to 1 mL with THF. The fluorophore solution mixed with THF without the metal ion was used as the blank solution. The fluorescence spectra of the blank solution and the mixtures were acquired using an excitation wavelength of 370 nm. The ratio between the fluorescence intensity of the mixture and blank solution (I/I_0) of each metal ion was

plotted against molar concentration of Zn^{2+} as shown in Figure 2.2. The limit of detection (LOD) was calculated according to the following equation:

$$LOD = 3SD/Slope$$

where SD is the standard deviation of blank solution and Slope is calculated from the calibration curve of the plot.
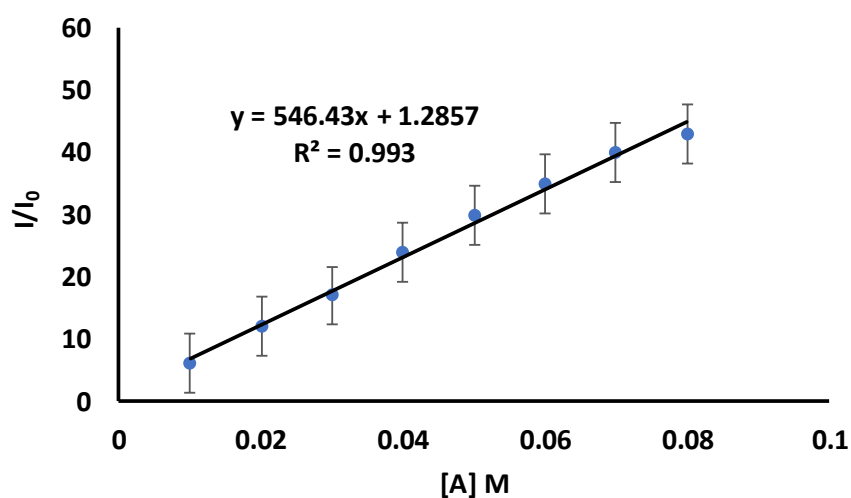
Figure 2.2 the calibration curve for turn-on sensing.

Interference test by competitive binding experiment

The 10 μL of **AQPro** stock solution (1 mM) was diluted with 970 μL of THF in quartz cuvette. The volumes at 10 μL of $Zn(NO_3)_2$ and other metal ions stock solutions (10 mM) was added into **AQPro** solution. The final volume of the mixture was adjusted to 1 mL with THF. The fluorophore solution mixed with THF without the metal ion was used as the blank solution. The fluorescence spectra of the blank solution and the mixtures were acquired using an excitation wavelength of 370 nm. The ratio between the fluorescence intensity of the mixture and blank solution (I/I_0) of each metal ion was used for interference comparison.

2.5   NMR spectroscopy

NMR titration

The 6 mg of **AQPro** was dissolved in 500 μL of THF-d_8. The volume at 2.5-200 μL of ZnCl$_2$ stock solution in THF-d_8 was added into **AQPro** solution. The fluorophore solution without the metal ion was used as the blank solution. The ^{1}H NMR spectra of the blank solution and the mixtures were acquired on a Varian Mercury NMR spectrometer at 400 MHz.

2.6   Fluorescence images for screening study

The fluorophore solution (10 mM, 15 μL) in solvent such as methanol, ethanol, iso-propanol, dimethysulfoxide, acetronitrile and tetrahydrofuran was mixed with each metal ion stock solution (100 mM, 15 μL) in vial. The volume of each mixture was adjusted by solvent to 1.5 mL to afford the final concentration of 1 mM metal ion and 100 μM fluorophore. The fluorophore solution mixed with solvent without the metal ion was used as the blank solution. The fluorescence images of blank solution and mixtures solution were taken with Panasonic Lumix-GF8 digital camera under normal room light or in a dark box equipped with a black light lamp (354 nm, 8 W).

CHAPTER III

RESULTS AND DISCUSSION

3.1   Synthesis and characterization of ligands

The synthesis of amide derivatives of 8-aminoquinoline was achieved in satisfactory to excellent yield by either *N*-acylation with acid chloride for **AQF, AQT** and **AQP** or coupling reaction with carboxylic acid for **AQTHF, AQTHT,** and AQPro. For **AQP**, the pyrrole-2-carbonyl chloride substrate was generated from the reaction of pyrrole-2-carboxylic acid with oxalyl chloride and catalytic amount of DMF. The low yeid of **AQP** was probably due to the poor formation of acid chloride generated prior to the addition of 8-aminoquinoline. Similarly, the synthesis of **HQF** and **HQT**, ester derivatives of 8-hydroxyquinoline, was achieved in moderate yeids by *O*-acylation with acid chloride (Figure 3.1). The **AQF, AQT, AQP, HQF** and **HQT** were purified by recrystallization in EtOAc/hexane 1:4 while the **AQPro, AQTHF** and **AQTHT** were purified by silica gel column chromatography. All purified compounds gave clean ^{1}H NMR and ^{13}C NMR spectra indicating their high purities.

For **HQP** and 8-hydroxyquinoline containing aliphatic rings, the purification by recrytallization was not successful and the attempt to use silica gel column chromatrography for the purification resulted in the decomposition of the ester back to 8-hydroxyquinoline that only small amout of pure **HQP** was recovered just enough for ^{1}H NMR characterization.
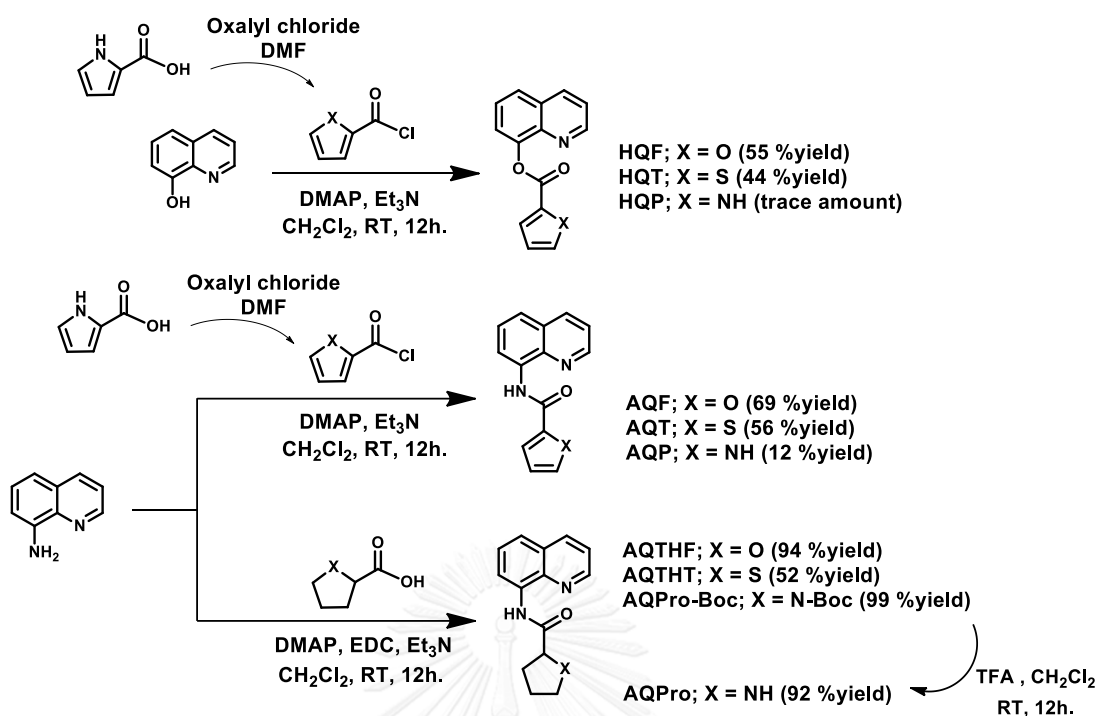
Figure 3.1 Synthetic scheme of 8-aminoquinoline and 8-hydroxyquinoline derivatives.

The ^{1}H NMR spectra of all target compounds are shown in Figure 3.2. The spectra of 8-aminoquinoline derivatives show the amide proton signal (H_g) around 10.8-10.3 ppm which is absent in the spectra of 8-hydroxyquinoline derivatives. The protons of the quinoline ring (H_a-H_f) give the signals around 8.9-7.5 ppm. The protons of heterocyclic aromatic ring in **AQF**, **AQT**, **AQP**, **HQF** and **HQT** show the signals around 8.1-6.3 ppm. For the compounds containing heterocycic aliphatic ring (**AQTHF**, **AQTHT** and **AQPro**), the aliphatic proton signals appear around 4.8-1.9 ppm. **AQP** and **AQPro** also give the N-H signals of pyrrole and proline rings around 11.9 and 3.4 (overlapping with water proton peak in DMSO-d_6) ppm.
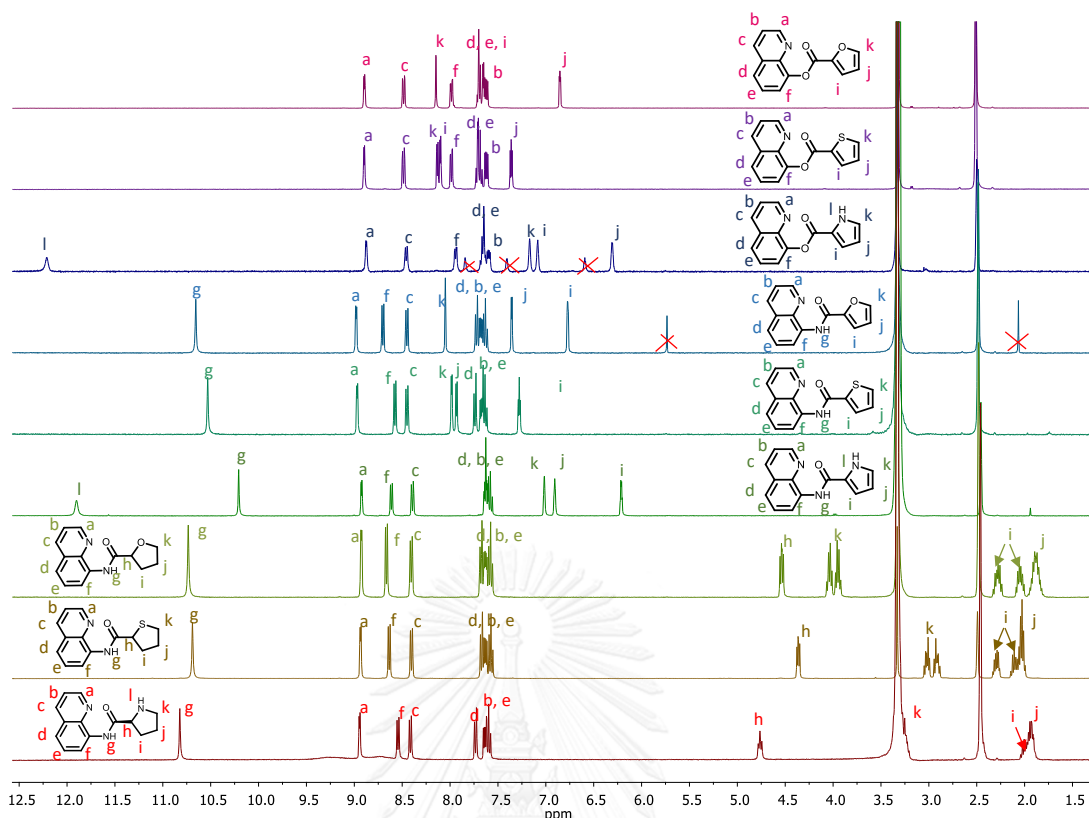
Figure 3.2 ^{1}H NMR spectra of 8-aminoquinoline and 8-hydroxyquinoline derivatives.

3.2 Metal ion sensing

The metal ion sensing properties of all 8 compounds synthesized were screened in comparision with 8-aminoquinoline and 8-hydroxquinoline at 100 μM in ethanol by visual obsevation under black light ($\lambda_{max} \sim$ 354 nm) illumination. Upon the addition of metal salts (1 mM), the 8-hydroxyquinoline (**8HQ**) and its derivatives (**HQF** and **HQT**) gave strong fluorescence with Mg^{2+} and Al^{3+}, the 8-aminoquinoline (**8AQ**) and its derivatives containing heterocyclic aromatic ring (**AQF**, **AQT** and **AQP**) showed no significant fluorescence change while the derivatives containing heterocyclic aliphatic ring (**AQTHF**, **AQTHT** and **AQPro**) showed strong fluorescence with Zn^{2+} and Cd^{2+} (Figure 3.3). From these results, the 8-aminoquinoline derivatives are interesting for further investigation because the derivatives containing aromatic and aliphatic rings showed different fluorescence responses.
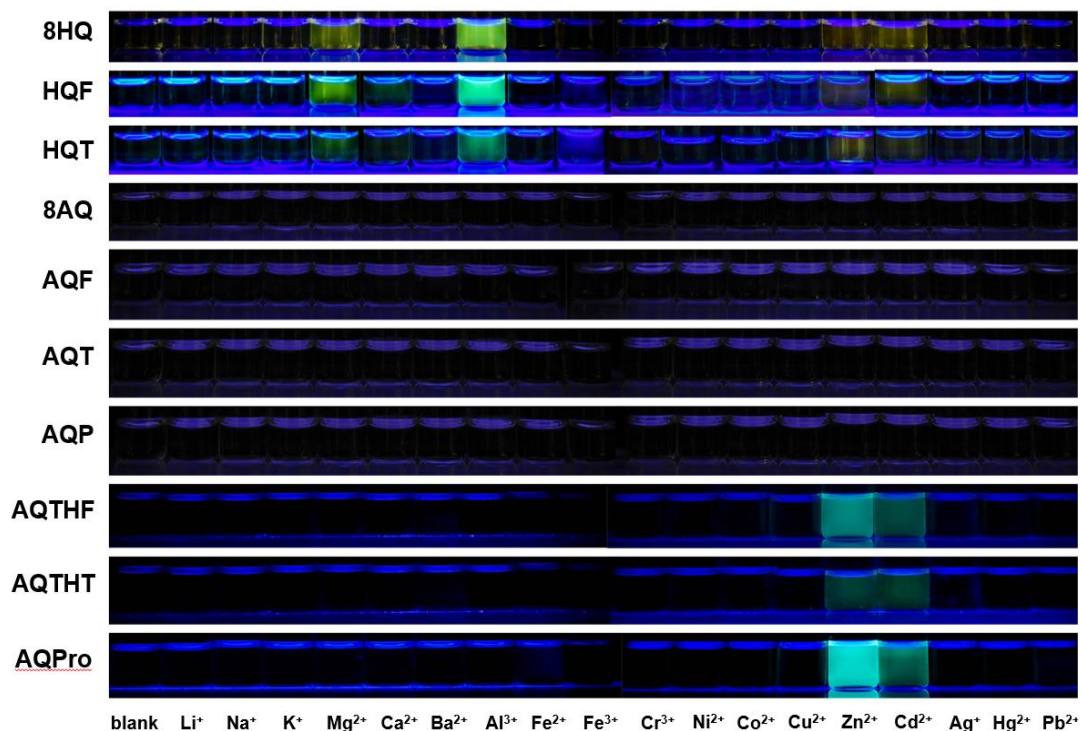
Figure 3.3 All fluorophores (100 µM) upon addition of various metal ions (1 mM) in 99% ethanol aqueous solution under black light.

3.3 Photophysical properties

The absorption and emission of all 8-aminoquinoline derivatives were studied in THF solution (Table 3.1, Figure A31). The absorption stpectra of each fluorophore exhibited the absorption band with the λ_{max} around 320-330 nm and molar absorptivity around 3.7-9.5 x 10^3 M^{-1} cm^{1-} associated with the π-π^* electronic transition of the quinoline chromophore. The derivatives containing aromatic rings i.e. **AQF**, **AQT** and **AQP** possess significantly longer λ_{max} and higher molar absorptivity than the derivatives containing aliphatic rings i.e. **AQTHF**, **AQTHT** and **AQPro** indicating contribution of the additional π-conjugated system to the λ_{max} and molar absorptivity. All of 8-aminoquinoline derivatives synthesized exhibited the maximum emission wavelenght (λ_{em}) around 380-405 nm with fluorescemce quantum yield of 0.09-1.04% and weak observable green fluorescence under blacklight illumination. The low fluorescence is proprably due to the non-radiative PET process between the lone pair

electron of the amide group to the electron poor quinoline ring and the ESIPT process between the amide proton and the electron lone pair of the N in quinoline ring.

Table 3.1 Photophysical data of ligands in THF solution

| Fluorophore	λ_{max}(nm)	ε (M^{-1} cm^{1-})	λ_{em}(nm)	Φ (%)
AQF	329	8027	401	0.214
AQT	329	9412	405	0.068
AQP	332	9557	403	0.112
AQTHF	321	7100	390	1.048
AQTHT	320	4648	380	0.181
AQPro	321	3745	395	0.092

3.4   Fluorescence studies for 8-aminoquinoline derivatives

3.4.1   Selectivity and sensitivity study

The fluorescence enhancement ratios (I/I_0) of all 8-aminoquinoline derivatives obtained from the emission intensity at 498 nm in the presence (I) and absence (I_0) of metal ions in THF solution. The fluorescence of **AQF, AQT, AQP** and **AQTHT** showed insignificant responses to other metal ions tested in THF whereas those of **AQPro** and **AQTHF** exhibited very high fluorescence enhancement to Zn^{2+} and slight enhancement to Cd^{2+} (Figure 3.4) for the corresponding spectra). The results indicate

that the lone pair electrons of hetero atoms in 5-membered nonaromatic ring played important role in binding Zn^{2+} and Cd^{2+} while those of hetero atoms in 5-membered aromatic rings was unable to bind with the metal ions. For the ligand **AQTHT**, the soft lewis base S atom was not suitable for binding with Zn^{2+}.

The chelation enhanced fluorescence (CHEF) of **AQPro** and **AQTHF** was associated with the formation of the complex formation with Zn^{2+} that suppressed the PET and increased rigidity of the ligand [48]. Among six ligands, **AQPro** gave the highest selectivity and sensitivity with Zn^{2+}. Furthermore, the fluorescence quantum efficiency enhancement of **AQPro** by Zn^{2+} in THF solution was found to be as high as 18-Fold (= 0.0168/0.0009). **AQPro** was further investigated in more details for fluorescence sensing properties i.e. solvent effect, pH effect, interference, limit of detection and association constant (K_a) of the ligand-metal complexation.
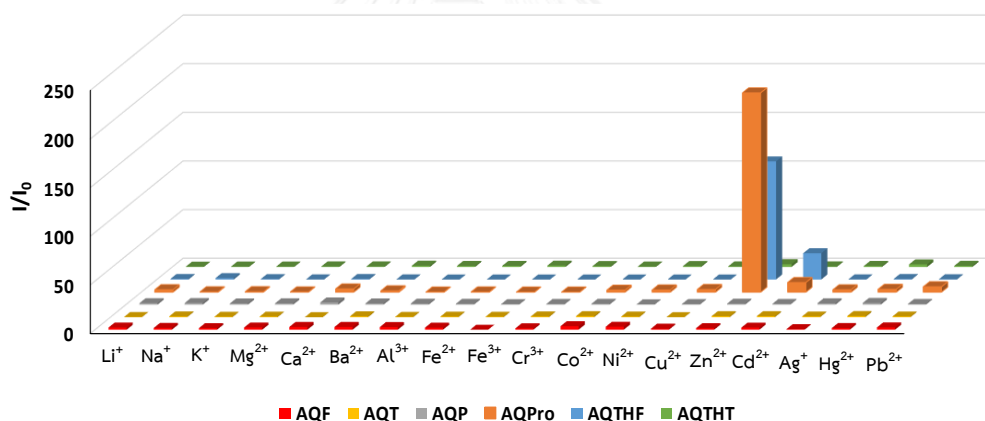

Figure 3.4 Fluorescence enhancement ratios at 498 nm of sensing compounds (10 μM) upon addition of various metal ions (100 μM) in THF solution; λ_{ex} = 370 nm.

3.4.2   Solvent effect

The fluorescence responses of **AQPro** at 498 nm, using λ_{ex} = 370 nm, upon the addition of Zn^{2+} and Cd^{2+} were studied in protic and aprotic solvents i.e. water, methanol, ethanol, 2-propanol, acetonitrile and tetrahydrofuran (THF). The results indicate that THF is the best solvent in terms of both sensitivity and selectivity for Zn^{2+} detection. The fluorescence response is lowest in CH_3CN. It is thus likely that the

presence of a basic O atom in the solvent can promote the binding of the ligand to the metal ions (Figure 3.5). As Cd^{2+} is a softer Lewis acid comparing to Zn^{2+}, the Zn^{2+}/Cd^{2+} selectivity increases with the basicity softness of the solvent which can solvate better with the softer acid. The solvation to Zn^{2+} reduces with the increase of basicity softness of the solvent and thus the ligand binding increases while the solvation to Cd^{2+} and its effect on the ligand binding approximately goes in the opposite direction.
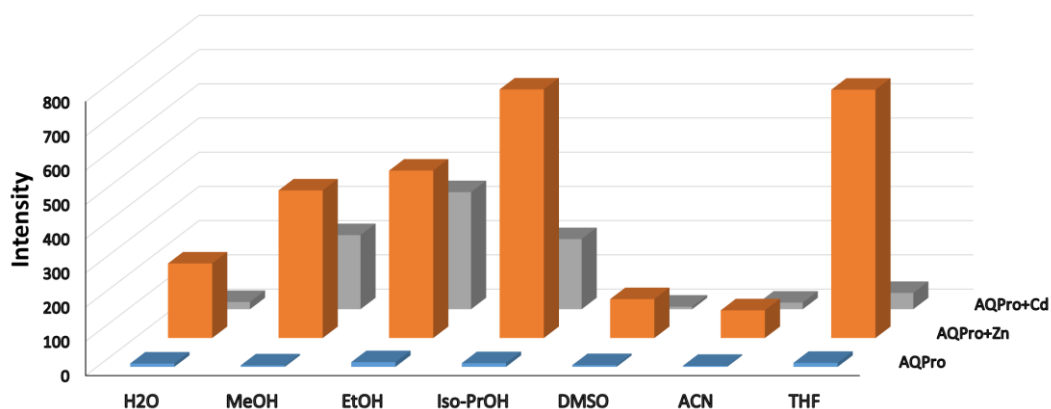
Figure 3.5 Fluorescence signal at 498 nm of **AQPro** (10 µM) in various solvents upon addition of Zn^{2+} and Cd^{2+} ions; λ_{ex} = 370 nm.

3.4.3 pH effects

The pH effects on the fluorescence signal of **AQPro** in the absence and presence of Zn^{2+} were investigated. The fluorescence of **AQPro** itself was not pH sensitive. In contrast, the fluorescence intensity of **AQPro** in the presence of Zn^{2+} considerably increased with the pH and became saturated around pH 9 (Figure 3.6). The results supported that the complexation of **AQpro** to Zn^{2+} involved the deprotonation of the amide proton.
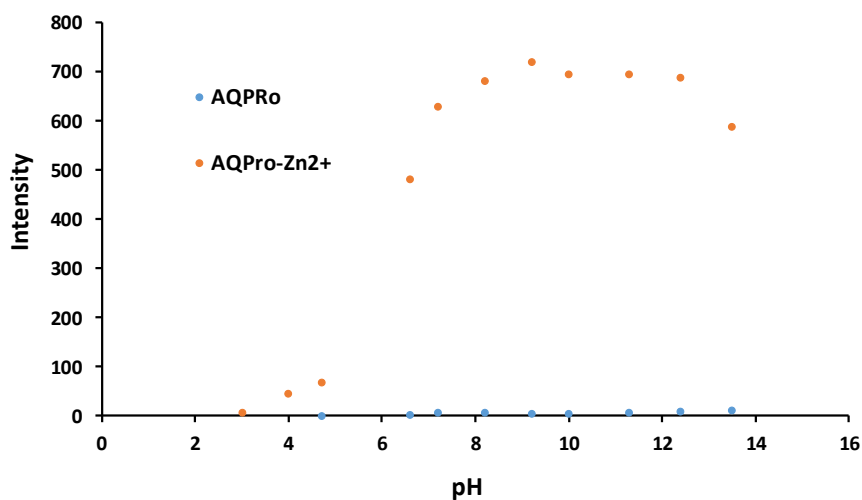
Figure 3.6 Fluorescence intensity (λ_{em} = 493 nm; λ_{ex} = 350 nm) of AQPro (10 μM) in the absence and presence of Zn^{2+} (100 μM) at various pH of Tris-HCl aqueous buffer (10 μM) /EtOH (20:80 v/v).

3.5 Complexation of AQPro and Zn^{2+}

3.5.1 UV-vis absorption

The binding between **AQPro** and Zn^{2+} was investigated by UV-VIS absorption in THF solution at room temperature (25 ^oC). The absorption peak of **AQPro** at 320 nm gradually decreased while a new peak at 370 nm gradually increased upon the addition of Zn^{2+} (Figure 3.7). The large bathochromic shift of the absorption band upon the addition of Zn^{2+} indicated greater electron delocalization in accordance to the deprotonation of the amide proton **AQPro** upon binding with Zn^{2+}.
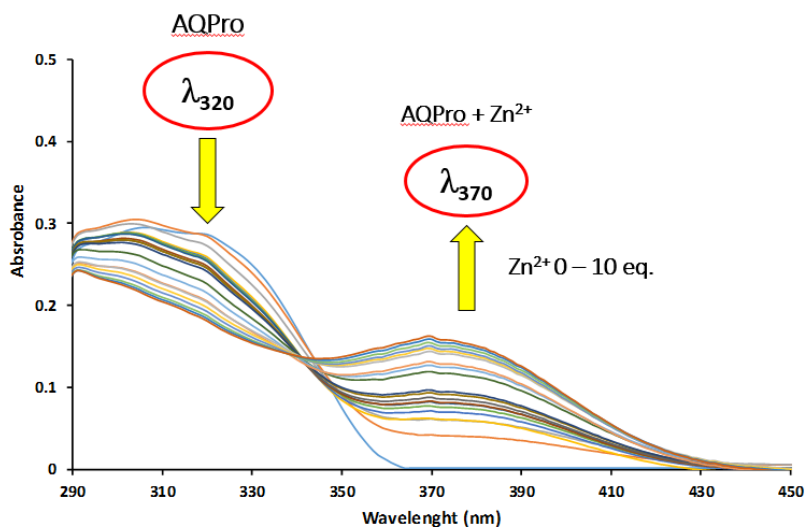
Figure 3.7 UV-VIS absorption spectra of AQPro (100 μM) upon the addition of varied concentrations of Zn^{2+}.

3.5.2 Job's plot

To further determine the stoichiometry of the complexation between **AQPro** and Zn^{2+}, the Job's plot of fluorescence intensity as a function of Zn^{2+} mole fraction. The plot displayed a maximum at the Zn^{2+} mole fraction of 0.33 and 0.50, which suggested either a 2:1 or 1:1 stoichiometric ratios were possible (Figure 3.8).
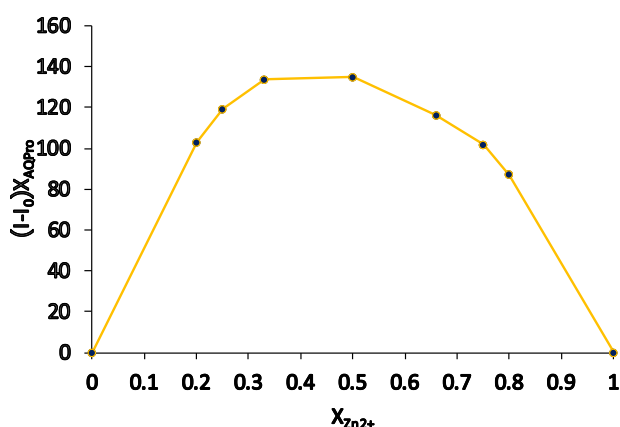
Figure 3.8 Job's plot of fluorescence intensity (at 320 nm) between **AQPro** and Zn^{2+} in THF solution.

3.5.3 Mass spectroscopy

Mass spectrum of **AQPro** with 1 equivalent of Zn^{2+} displayed significant peaks at m/z = 340.02 and 545.16 corresponding to $[Zn \cdot \textbf{AQPro} \cdot Cl]^{+}$ and $[Zn \cdot (\textbf{2AQPro}\text{-H})]^{+}$, respectively (Figure 3.9). The results reveal that the binding raito between Zn^{2+} and **AQPro** can be either 1:1 or 1:2. However, the Job's plot from UV-vis spectroscopy results gave 1:1 binding ratio. Therefore, the 1:2 complex may be a less stable complex which is formed in the mass spectroscopy condition.
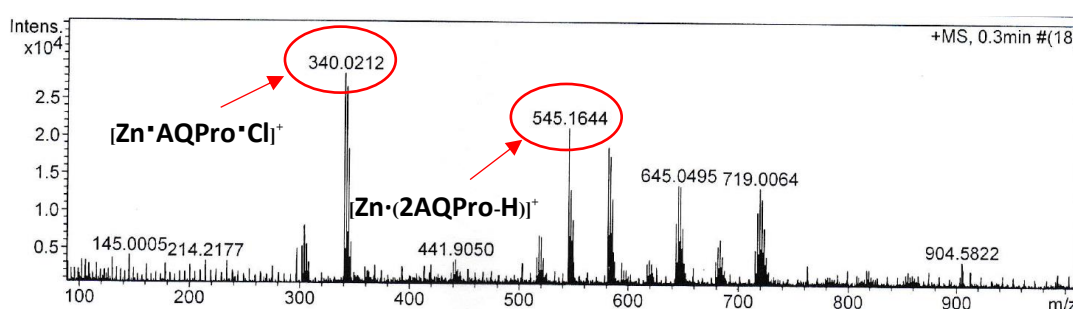
Figure 3.9 Highmass spectrum of **AQPro** (10μM) upon addition of 2 equivalent of Zn^{2+} in methanol.

3.5.4 ^{1}H NMR study

The complexation of **AQPro** with Zn^{2+} was studied by ^{1}H NMR spectroscopy in THF-d_8. The proton chemical shifts of **AQPro** and its complexes were assigned based on J coupling constants in ^{1}H NMR spectrum. The ^{1}H NMR spectrum of **AQpro** showed the amide peak at 10.5 ppm. The proton signals of the quinoline ring (H_a-H_f) were located around 8.8-7.5 ppm and the aliphatic proton signals appeared around 4.9-2.0 ppm. The proline N-H signal appeared at 3.6 (overlapping with solvent residul peak in THF-d_8) ppm (Figure 3.10). The proton signals of **AQPro** did not significantly change upon the addition of Zn^{2+} up to 2 equivalents. The results suggested a relatively low association constant between Zn^{2+} and **AQPro** in THF solution. Upon the addition of 10 equivalent of Zn^{2+}, a new broad peak appeared around 9.2 ppm. This new proton signal may correspond to the quinoline proton in the Zn^{2+}-**AQPro** complexes.
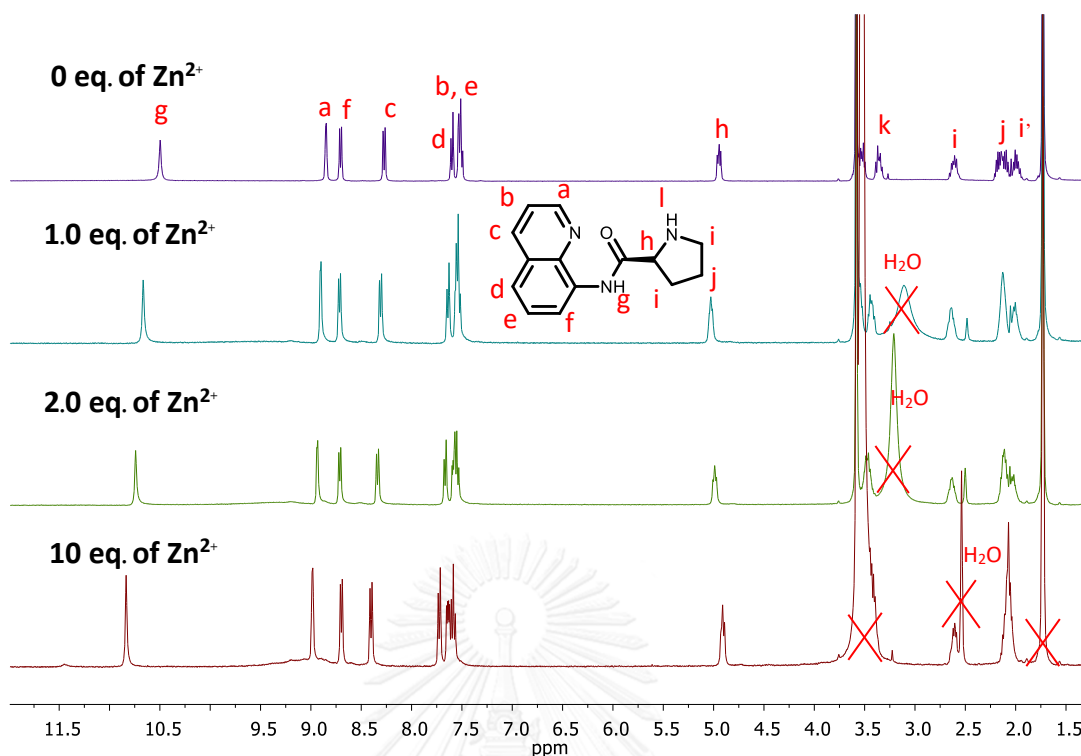
Figure 3.10 ^{1}H NMR spectra of **AQPro** (0.05 M) in THF-d_8 in the presence of various equivalents of Zn^{2+}.

From the pH effects in section 3.4.3, Zn^{2+} induced stronger fluorescence enhancement of **AQPro** under basic condition, it was thus interesting to observe the complexation between **AQPro** and Zn^{2+} by ^{1}H NMR in basic solution. In the presence of 1.0 equivalent CH_3NH_2, the ^{1}H NMR of **AQpro** showed the amide N-H signal at 11.5 ppm in DMSO-d_6. The addition of Zn^{2+} up to 1 equivalent resulted in the disappearance of the amide N-H peak supporting the deprotonation of the amide proton (Figure 3.11b). At 0.5 equivalent of Zn^{2+}, the number of proton signals corresponging to the quinoline protons (H_a-H_f) around 8.8-7.3 ppm increased of which signals at 9.2, 8.1 and 7.9 ppm were assigned to $H_{f'}$, $H_{c'}$ and $H_{a'}$ of the 2:1 complex along with the signals of free ligand and probably the 1:1 complex (For COSEY spectra used in the signal assignment see Figure A32-A37). The proton signals of both free ligand and 2:1 complex totally disappeared when at least 1.0 equivalent of Zn^{2+} was added. At high equivalent of Zn^{2+}, only the 1:1 complex was observed with the quinoline proton signals at 9.0, 8.7 and 8.5 ppm corresponding to $H_{f''}$, $H_{a''}$ and $H_{c''}$, respectively. The other aromatic

signals (H_b, H_d and H_e) in the rage of 7.7-7.2 ppm and aliphatic signals (H_h-H_l) in the range of 4.3-1.3 ppm were also significantly shifted upon the complexation. The spectra of **AQPro** with the addition of Zn^{2+} lower than 0.5 equivalent suggested the conditions where all three species i.e. free ligand, 2:1 complex and 1:1 complex were in equilibrium. These complexes may also be formed under neutral condition but at much lower concentration, due to the low association constant, that cannot be observed in ^1H NMR described in the previous paragraph.
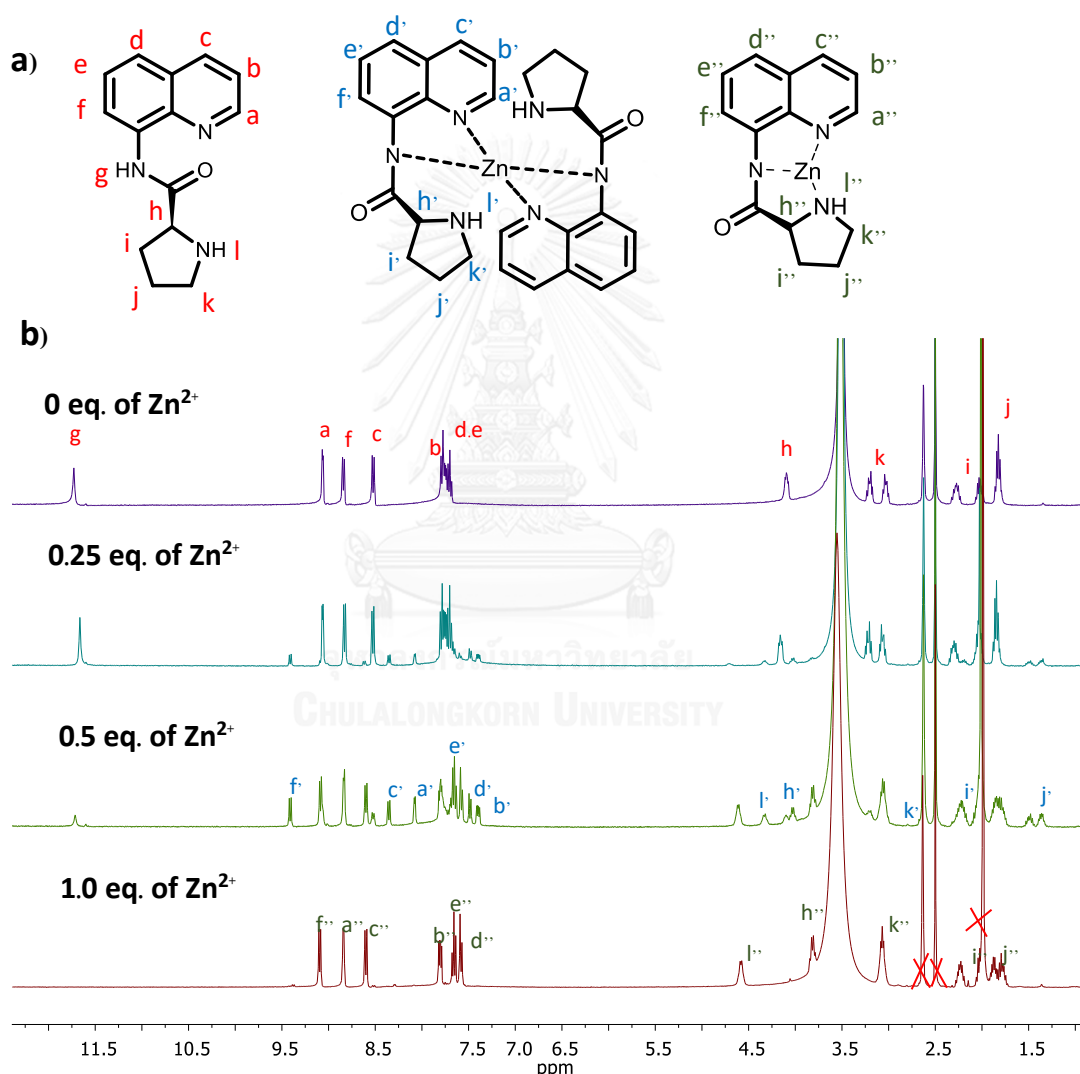
Figure 3.11 a) proposed stucetures of complexes between **AQPro** and Zn^{2+} b) ^1H NMR spectra of **AQPro** (0.05 M) and various equivalents of Zn^{2+} in DMSO-d_6 in the presence of CH_3NH_2 (0.05 M).

3.5.5 The association constant

The association constant (K_a) of the complex formation between **AQPro** and Zn^{2+} was determined by UV-vis titration in nuetral THF solution. The absorbance data at 370 nm of the mixture of **AQPro** (1×10^{-4} M) and Zn^{2+} (1×10^{-5} – 2×10^{-2} M) were used for the curve fitting by Bindfit v0. 5 program available from http://app.supramolecular.org/bindfit/ [49] (Figure 3.12). The fitting was performed for the 2:1 stoichiometric ratio which gave the K_a values of 5.0×10^2 M^{-1} and 1.5×10^4 M^{-2} for the 1:1 and 2:1 complexation, respectively, which represented the stepwise association constants (K_1 and K_2) of 5.0×10^2 and 30 M^{-1}.

Complexation	2:1 ratio	
	K_a	error (%)
AQPro-Zn^{2+}	504.6	3.36
2AQPro-Zn^{2+}	14570.6	13.07
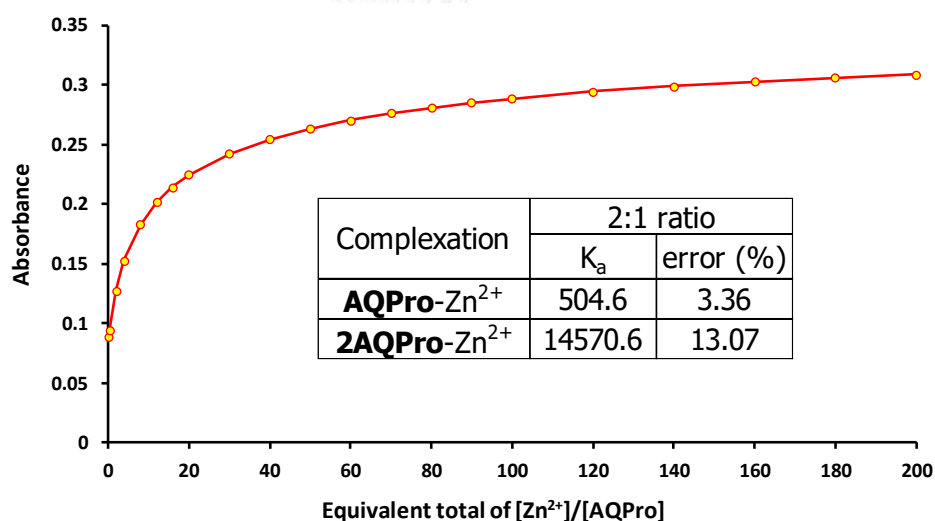
Figure 3.12 Fitting curve and corresponding K_a values assuming 2:1 complexation between **AQPro** and Zn^{2+}.

The plot of mole fractions of all species i.e. **AQPro**, 1:1 and 2:1 complexes in nuetral THF solution could be simulated from the K_a values. At 2 equivalents of Zn^{2+}, the mole fractions of the free ligand, 1:1 and 2:1 complexes shown in the plot were 0.77, 0.07 and 0.16, respectively (Figure 3.13). These calculated mole fraction values agree well with the ^{1}H NMR spectrum obtained from the complexation study in THF-d_8 shown in section 3.5.4.
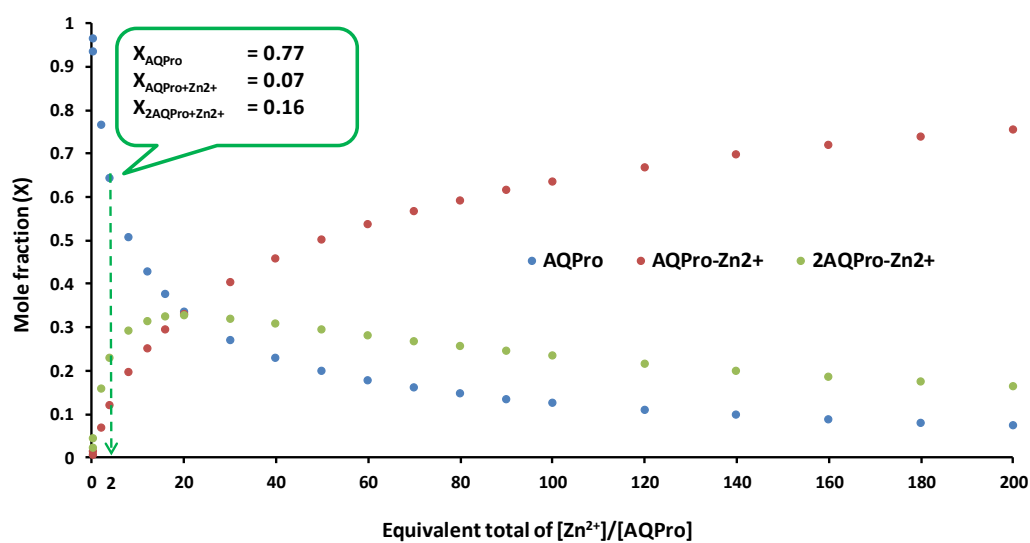

Figure 3.13 Mole fractions of **AQPro**, 1:1 complex and 2:1 complexes simulated by Bindfit v5.0 program using the K_a of 504.6 (1:1) and 14570.6 (2:1) in the 2:1 complexation assumption.

3.5.6 Interferences

Competitive binding of various metal ion versus Zn^{2+} to **AQPro** was evaluated to determine possible interferences. The fluorescence enhancement ratio (I/I_0) of **AQPro** by Zn^{2+} is significantly reduced in the presence of certain metal ions i.e. Al^{3+}, Fe^{3+}, Cr^{3+}, Ni^{2+} and Cu^{2+} (Figure 3.14). The results suggested that **AQPro** could also bind with those metal ions but the binding either led to quenching or indifferent fluorescence responses. The fluorescence enhancement of **AQPro** may thus be used as a positive evidence for the presence of Zn^{2+} but the lack of enhancement should not be taken as a negative proof for the presence of Zn^{2+}.
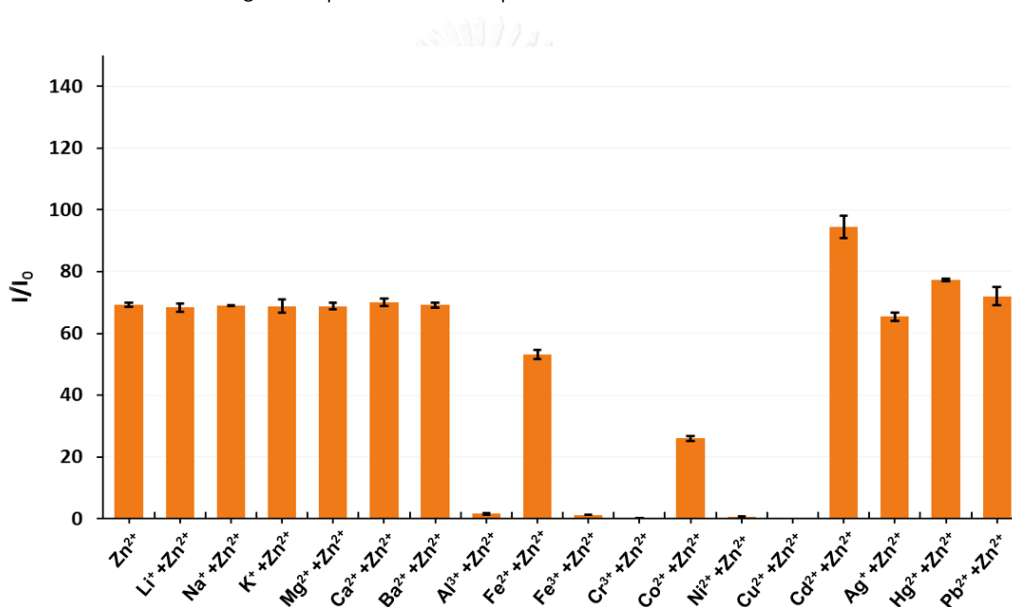
Figure 3.14 Fluorescence responses of AQPro (10 µM) to Zn^{2+} (100 µM) in the presence of each metal ion (100 µM) tested for potential interference in THF solution; (λ_{em} = 498 nm; λ_{ex} = 370 nm).

2.5.6 Fluorescence titration

For quantitative determination of Zn^{2+} concentration, the fluorescence titration of **AQPro** (10 µM in THF solution) with $Zn(NO_3)_2$ (1.0 mM aqueous solution) displayed the maximum emission at 498 nm of which intensity increased with the amount of Zn^{2+} added and reached a saturation around 10 equivalents of Zn^{2+} (Figure 3.15).
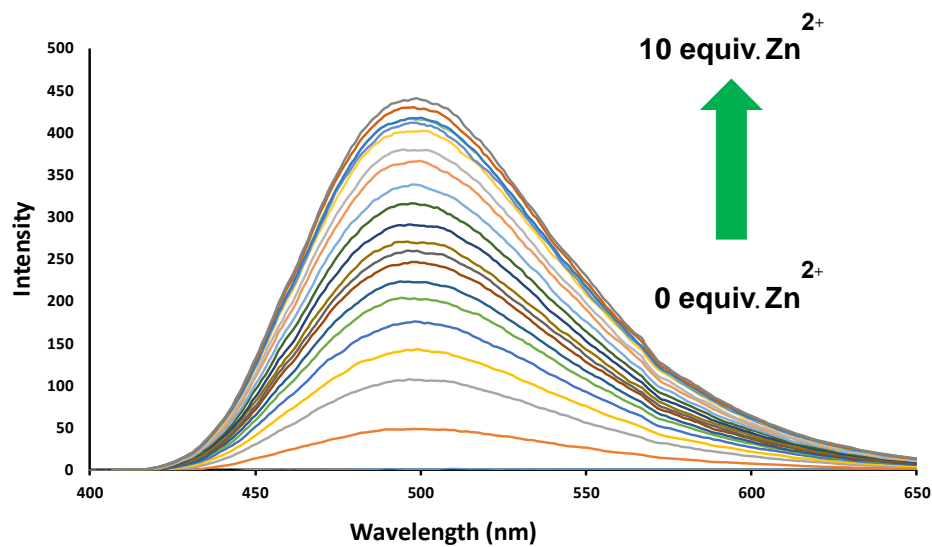
Figure 3.15 Fluorescence spectra (λ_{ex} = 370 nm) of AQPro (10 µM) in THF solution upon addition of Zn^{2+} at various concentration.

The fluorescence intensity ratio (I/I_0) increased almost linearly in the low concentration range of 0.1-1 µM of Zn^{2+} (Figure 3.16 inset). A plot of (I/I_0) at the low concentration range gave a linear calibration line (R^2 = 0.9972) for quantitative determination of Zn^{2+} with the detection limit of 25.7 nM (LOD = 3SD/Slope). This is one of the lowest value for all of the Zn^{2+} sensors based on 8-aminoquinoline derivatives reported to date (TableA1).
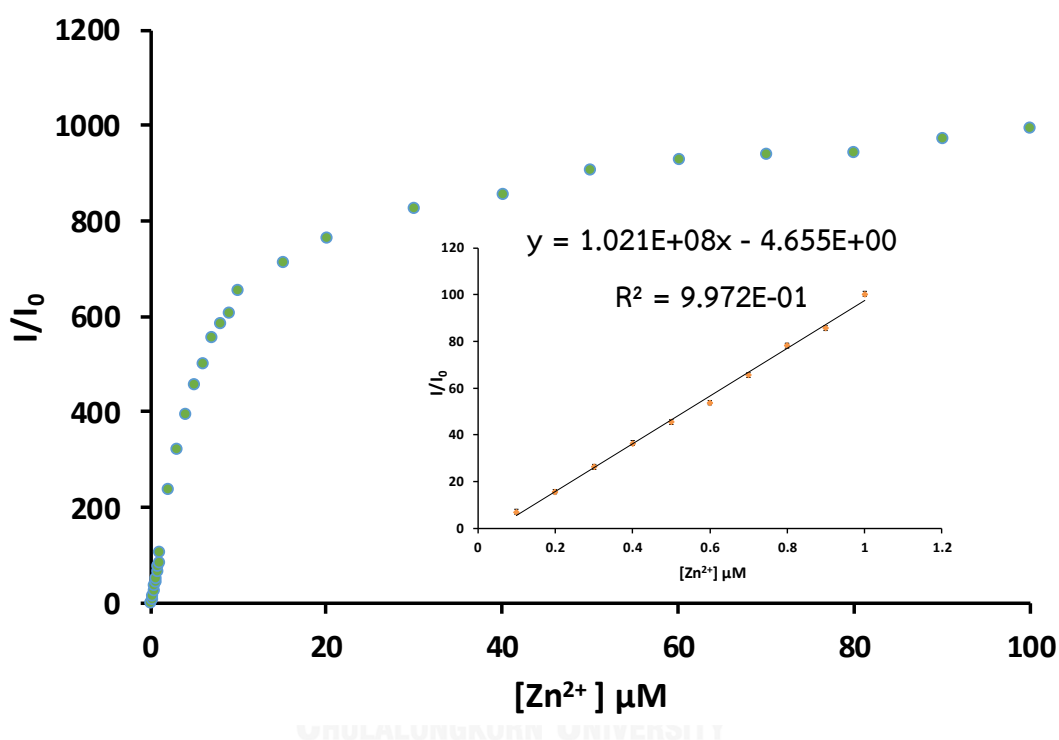
Figure 3.16 Fluorescence intensity ratio as a function of Zn^{2+} concentration; inset: linear calibration line for quantitative determination of Zn^{2+} concentration.

CHAPTER IV

CONCLUSION

Eight quinoline derivatives evaluated as fluorescence sensors for metal ions. In ethanol solution, the amide derivatives containing aliphatic rings (**AQTHF**, **AQTHT** and **AQPro**) gave selective turn-on fluorescence responses to Zn^{2+} and Cd^{2+}. In THF solution, **AQPro** however gave the highest fluorescence enhancement to only Zn^{2+}. The fluorescence enhancement associates with the complexation between **AQPro** and Zn^{2+} that involves the deprotonation of the amide group as confirmed by ^{1}H NMR spectroscopy. Upon the complexation, several non-radiative decay pathways such as PET, ESIPT and geometrical relaxation are probably suppressed. The Job's plot of fluorescence intensity and ^{1}H NMR spectroscopy showed that both 1:1 and 2:1 stoichiometric binding ratio between **AQPro** and Zn^{2+} are possible. The association constant calculated with Bindfit v5.0 program was 5.0×10^{2} M^{-1} and 1.4×10^{4} M^{-2} for 1:1 and 2:1 complexation, respectively. The limit of fluorescence detection of Zn^{2+} with **AQPro** in THF solution was as low as 25.7 nM.

REFERENCES

[1]   Introduction to Fluorescence. in Lakowicz, J.R. (ed.) Principles of Fluorescence Spectroscopy, pp. 1-26. Boston, MA: Springer US, 2006.

[2]   Gunnlaugsson, T., et al. Fluorescent Photoinduced Electron Transfer (PET) Sensors for Anions; From Design to Potential Application. Journal of Fluorescence 15 (3) (2005): 287-299.

[3]   Callan, J.F., de Silva, A.P., and Magri, D.C. Luminescent sensors and switches in the early 21st century. Tetrahedron 61 (36) (2005): 8551-8588.

[4]   Martínez-Máñez, R. and Sancenón, F. Fluorogenic and Chromogenic Chemosensors and Reagents for Anions. Chemical Reviews 103 (11) (2003): 4419-4476.

[5]   de Silva, A.P., et al. Signaling recognition events with fluorescent sensors and switches. Chemical Reviews 97 (5) (1997): 1515-1566.

[6]   Fan, L.-J. and Jones, W.E. Studies of Photoinduced electron transfer (PET) and energy migration in a conjugated polymer system for fluorescence "Turn-on" chemosensor applications. The journal of physical chemistry. B 110 (15) (2006): 7777-7782.

[7]   Valeur, B. and Leray, I. Design principles of fluorescent molecular sensors for cation recognition. Coordination Chemistry Reviews 205 (1) (2000): 3-40.

[8]   Xu, Z., Yoon, J., and Spring, D.R. Fluorescent chemosensors for Zn^{2+}. Chemical Society Reviews 39 (6) (2010): 1996-2006.

[9]   Kim, J.S. and Quang, D.T. Calixarene-Derived Fluorescent Probes. Chemical Reviews 107 (9) (2007): 3780-3799.

[10]   Zhao, J., Ji, S., Chen, Y., Guo, H., and Yang, P. Excited state intramolecular proton transfer (ESIPT): from principal photophysics to the development of new chromophores and applications in fluorescent molecular probes and luminescent materials. Physical Chemistry Chemical Physics 14 (25) (2012): 8803-8817.

[11]   Nishina, N., Mutai, T., and Aihara, J.-i. Excited-state intramolecular proton transfer and global aromaticity. Journal of Physical Chemistry A 121 (1) (2017): 151-161.

[12]   Mutai, T., Sawatani, H., Shida, T., Shono, H., and Araki, K. Tuning of Excited-state intramolecular proton transfer (ESIPT) Fluorescence of imidazo[1,2-a]pyridine in rigid matrices by substitution effect. Journal of Organic Chemistry 78 (6) (2013): 2482-2489.

[13]   Wu, J., Liu, W., Ge, J., Zhang, H., and Wang, P. New sensing mechanisms for design of fluorescent chemosensors emerging in recent years. Chemical Society Reviews 40 (7) (2011): 3483-3495.

[14]   Peng, X., Wu, Y., Fan, J., Tian, M., and Han, K. Colorimetric and ratiometric fluorescence sensing of fluoride: Tuning selectivity in proton transfer. Journal of Organic Chemistry 70 (25) (2005): 10524-10531.

[15]   Carlson, H.J. and Campbell, R.E. Genetically encoded FRET-based biosensors for multiparameter fluorescence imaging. Current Opinion in Biotechnology 20 (1) (2009): 19-27.

[16]   Sapsford, K.E., Berti, L., and Medintz, I.L. Materials for fluorescence resonance energy transfer analysis: Beyond traditional donor–acceptor combinations. Angewandte Chemie International Edition 45 (28) (2006): 4562-4589.

[17]   Wu, J.-S., et al. Fluorescence Turn on of coumarin derivatives by metal cations: A new signaling mechanism based on C=N isomerization. Organic Letters 9 (1) (2007): 33-36.

[18]   Hong, Y., Lam, J.W.Y., and Tang, B.Z. Aggregation-induced emission: phenomenon, mechanism and applications. Chemical Communications (29) (2009): 4332-4353.

[19]   Wang, M., Zhang, G., Zhang, D., Zhu, D., and Tang, B.Z. Fluorescent bio/chemosensors based on silole and tetraphenylethene luminogens with aggregation-induced emission feature. Journal of Materials Chemistry 20 (10) (2010): 1858-1867.

[20]   Thomas, S.W., Joly, G.D., and Swager, T.M. Chemical sensors based on amplifying fluorescent conjugated polymers. Chemical Reviews 107 (4) (2007): 1339-1386.

[21]   Lodeiro, C. and Pina, F. Luminescent and chromogenic molecular probes based on polyamines and related compounds. Coordination Chemistry Reviews 253 (9–10) (2009): 1353-1383.

[22]   de Silva, A.P., Moody, T.S., and Wright, G.D. Fluorescent PET (Photoinduced Electron Transfer) sensors as potent analytical tools. Analyst 134 (12) (2009): 2385-2393.

[23]   Druzhinin, S.I., Mayer, P., Stalke, D., von Bülow, R., Noltemeyer, M., and Zachariasse, K.A. Intramolecular charge transfer with 1-tert-Butyl-6-cyano-1,2,3,4-tetrahydroquinoline (NTC6) and other Aminobenzonitriles. A Comparison of Experimental Vapor Phase Spectra and Crystal Structures with Calculations. Journal of the American Chemical Society 132 (22) (2010): 7730-7744.

[24]   Galievsky, V.A., et al. Ultrafast intramolecular charge transfer with N-(4-Cyanophenyl)carbazole. Evidence for a LE precursor and dual LE + ICT fluorescence. The Journal of Physical Chemistry A 114 (48) (2010): 12622-12638.

[25]   Henary, M.M. and Fahrni, C.J. Excited state intramolecular proton transfer and metal ion complexation of 2-(2'-Hydroxyphenyl)benzazoles in aqueous solution. The Journal of Physical Chemistry A 106 (21) (2002): 5210-5220.

[26]   Zheng, J. Spectroscopy-based quantitative fluorescence resonance energy transfer analysis. in Stockand, J.D. and Shapiro, M.S. (eds.), Ion Channels: Methods and Protocols, pp. 65-77. Totowa, NJ: Humana Press, 2006.

[27]   Higginson, K.A., Zhang, X.-M., and Papadimitrakopoulos, F. Thermal and morphological effects on the hydrolytic stability of aluminum tris(8-hydroxyquinoline) (Alq3). Chemistry of Materials 10 (4) (1998): 1017-1020.

[28]   Pohl, R. and Anzenbacher, P. Emission color tuning in AlQ_3 complexes with extended conjugated chromophores. Organic Letters 5 (16) (2003): 2769-2772.

[29]   Pohl, R., Montes, V.A., Shinar, J., and Anzenbacher, P. Red–green–blue emission from tris(5-aryl-8-quinolinolate)Al(III) complexes. The Journal of Organic Chemistry 69 (5) (2004): 1723-1725.

[30]   Lee, C.B., Uddin, A., Hu, X., and Andersson, T.G. Study of Alq3 thermal evaporation rate effects on the OLED. Materials Science and Engineering: B 112 (1) (2004): 14-18.

[31]   Bhagat, S.A., Borghate, S.V., Kalyani, N.T., and Dhoble, S.J. Novel Na^+ doped Alq3 hybrid materials for organic light-emitting diode (OLED) devices and flat panel displays. Luminescence 30 (3) (2015): 251-256.

[32]   Choong, V.-E., Park, Y., Gao, Y., Mason, M.G., and Tang, C.W. Photoluminescence quenching of Alq3 by metal deposition: A surface analytical investigation. Journal of Vacuum Science & Technology A: Vacuum, Surfaces, and Films 16 (3) (1998): 1838-1841.

[33]   Pathak, R.K., Dessingou, J., Hinge, V.K., Thawari, A.G., Basu, S.K., and Rao, C.P. Quinoline driven fluorescence turn on 1,3-Bis-calix[4]arene conjugate-based receptor to discriminate Fe^{3+} from Fe^{2+}. Analytical Chemistry 85 (7) (2013): 3707-3714.

[34]   Rastogi, S.K., Pal, P., Aston, D.E., Bitterwolf, T.E., and Branen, A.L. 8-Aminoquinoline functionalized silica nanoparticles: A fluorescent nanosensor for detection of divalent zinc in aqueous and in yeast cell suspension. ACS Applied Materials & Interfaces 3 (5) (2011): 1731-1739.

[35]   Meng, X.-m., Wang, S.-X., and Zhu, M.-Z. Quinoline-based fluorescence. various aspects. InTech, 2012.

[36]   Fahrni, C.J. and O'Halloran, T.V. Aqueous coordination chemistry of quinoline-based fluorescence probes for the biological chemistry of zinc. Journal of the American Chemical Society 121 (49) (1999): 11448-11458.

[37]   Zalewski, P.D., et al. Flux of intracellular labile zinc during apoptosis (gene-directed cell death) revealed by a specific chemical probe, Zinquin. Chemistry & Biology 1 (3) (1994): 153-161.

[38]   Zhang, Y., Guo, X., Si, W., Jia, L., and Qian, X. Ratiometric and water-soluble
        fluorescent zinc sensor of carboxamidoquinoline with an alkoxyethylamino
        chain as receptor. Organic Letters 10 (3) (2008): 473-476.

[39]   Zhou, X., et al. Ratiometric fluorescent Zn^{2+} chemosensor constructed by
        appending a pair of carboxamidoquinoline on 1,2-diaminocyclohexane
        scaffold. Tetrahedron 67 (19) (2011): 3412-3419.

[40]   Pal, P., Rastogi, S.K., Gibson, C.M., Aston, D.E., Branen, A.L., and Bitterwolf, T.E.
        Fluorescence sensing of zinc(II) using ordered mesoporous silica material
        (MCM-41) functionalized with N-(Quinolin-8-yl)-2-[3-
        (triethoxysilyl)propylamino]acetamide. ACS Applied Materials & Interfaces 3 (2)
        (2011): 279-286.

[41]   Zhang, Y., et al. Substituent-dependent fluorescent sensors for zinc ions
        based on carboxamidoquinoline. Dalton Transactions 41 (38) (2012): 11776-
        11782.

[42]   Dong, Z., Guo, Y., Tian, X., and Ma, J. Quinoline group based fluorescent
        sensor for detecting zinc ions in aqueous media and its logic gate behaviour.
        Journal of Luminescence 134 (2013): 635-639.

[43]   Ma, Y., Wang, F., Kambam, S., and Chen, X. A quinoline-based fluorescent
        chemosensor for distinguishing cadmium from zinc ions using cysteine as an
        auxiliary reagent. Sensors and Actuators B: Chemical 188 (2013): 1116-1122.

[44]   Goswami, S., et al. Ratiometric and absolute water-soluble fluorescent
        tripodal zinc sensor and its application in killing human lung cancer cells.
        Analyst 138 (16) (2013): 4593-4598.

[45]   Yue, Y., Dong, Q., Zhang, Y., Sun, Y., and Gong, Y. A highly selective "turn-on"
        fluorescent chemosensor based on 8-aminoquinoline for detection of Zn^{2+}.
        Analytical Methods 7 (13) (2015): 5661-5666.

[46]   Choi, Y.W., Lee, J.J., and Kim, C. A highly selective fluorescent chemosensor
        based on a quinoline derivative for zinc ions in pure water. RSC Advances 5
        (75) (2015): 60796-60803.

[47]   Brouwer Albert, M. Standards for photoluminescence quantum yield
         measurements in solution (IUPAC Technical Report). in Pure and Applied
         Chemistry. 2011. 2213.

[48]   Nugent, J.W., Lee, H., Lee, H.-S., Reibenspies, J.H., and Hancock, R.D.
         Mechanism of chelation enhanced fluorescence in complexes of cadmium(ii),
         and a possible new type of anion sensor. Chemical Communications 49 (84)
         (2013): 9749-9751.

[49]   Thordarson, P. Determining association constants from titration experiments in
         supramolecular chemistry. Chemical Society Reviews 40 (3) (2011): 1305-1323.
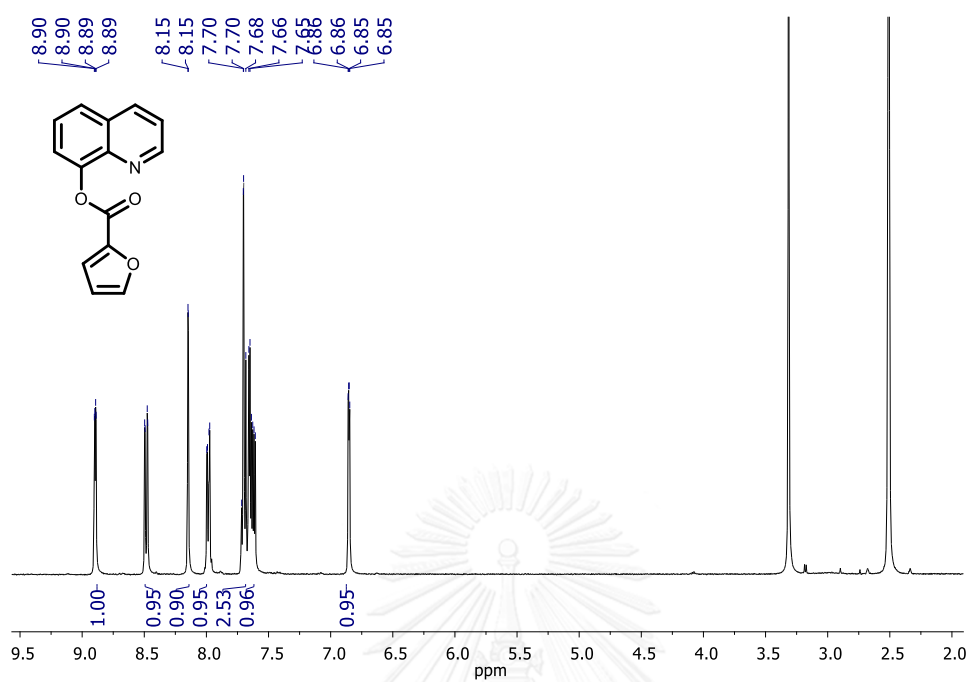
Figure A1 ^{1}H NMR spectrum compound **HQF** in DMSO-d$_6$.
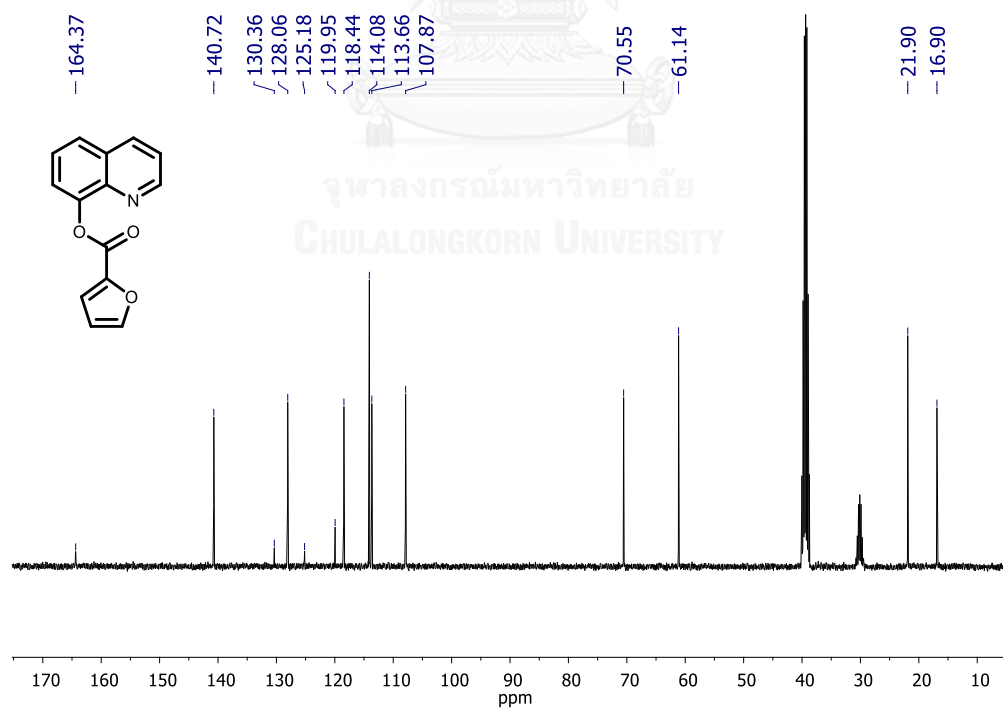
Figure A2 ^{13}C NMR spectrum compound **HQF** in DMSO-d$_6$.

8.90
8.90
8.89
8.89
8.50
8.50
8.48
8.47
8.14
8.14
8.13
8.13
8.11
8.10
8.00
7.99
7.98
7.97
7.73
7.73
7.71
7.71
7.70
7.68
7.67
7.64
7.63
7.62
7.61
7.37
7.36
7.36
7.35

1.00
1.01
0.80
0.90
0.98
1.81
0.99
0.98
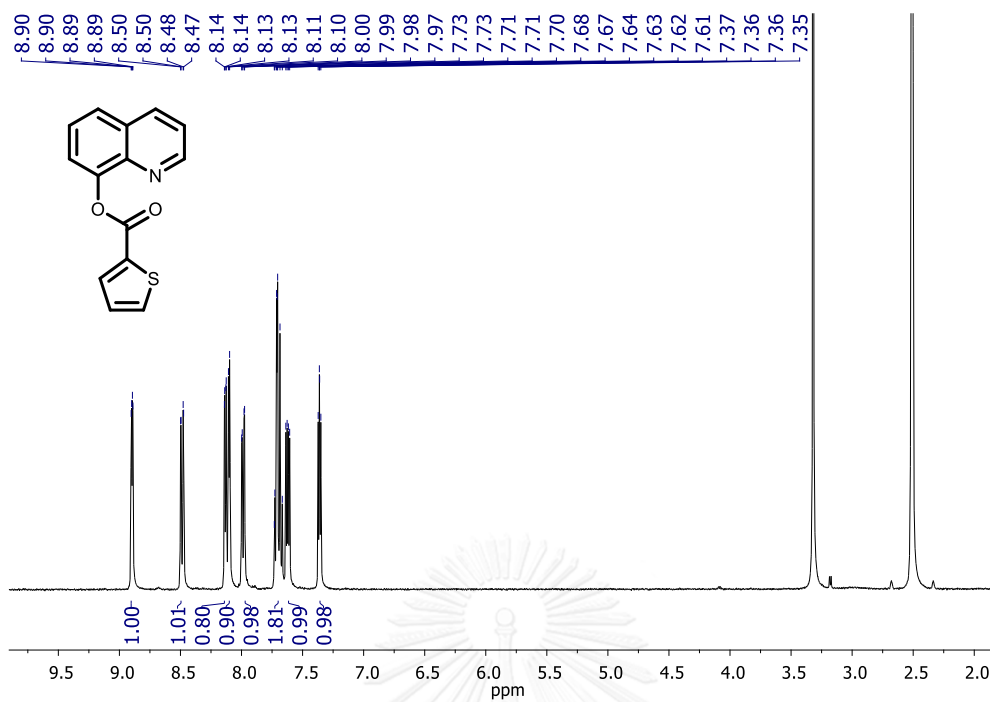
Figure A3 ^{1}H NMR spectrum compound **HQT** in DMSO-d_6.

160.08
150.75
146.59
140.47
136.25
135.21
135.11
131.85
129.12
128.71
126.46
126.41
122.19
121.78
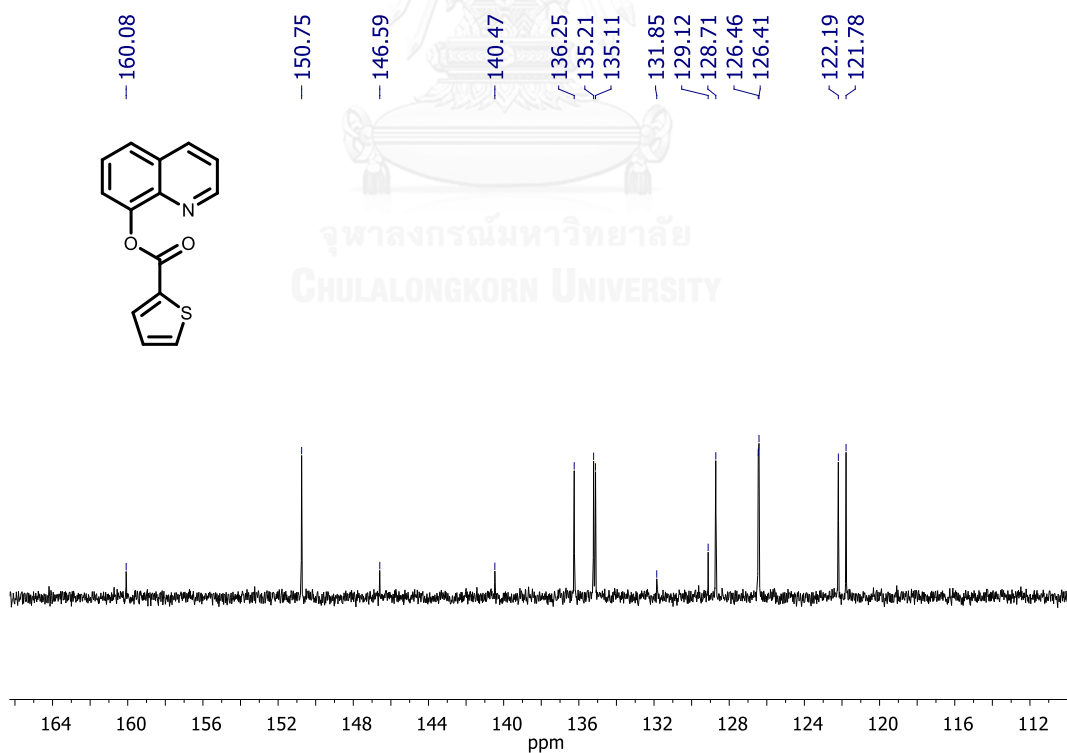
Figure A4 ^{13}C NMR spectrum compound **HQT** in DMSO-d_6.
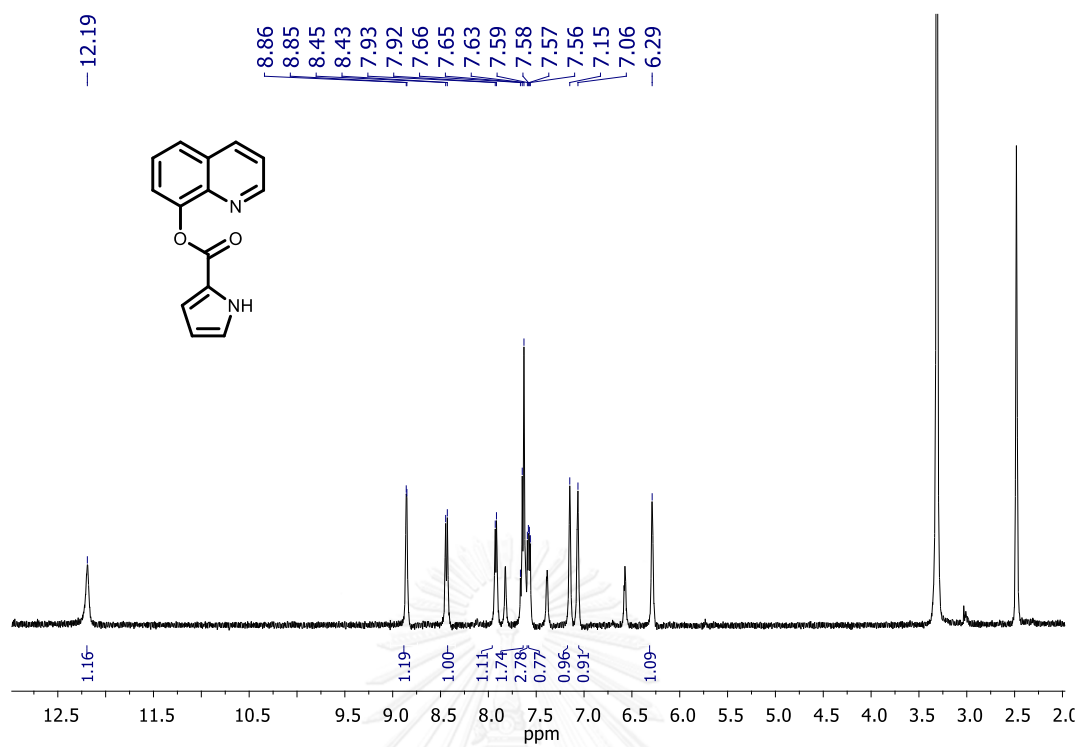
Figure A5 ^{1}H NMR spectrum compound **HQP** in DMSO-d_6.
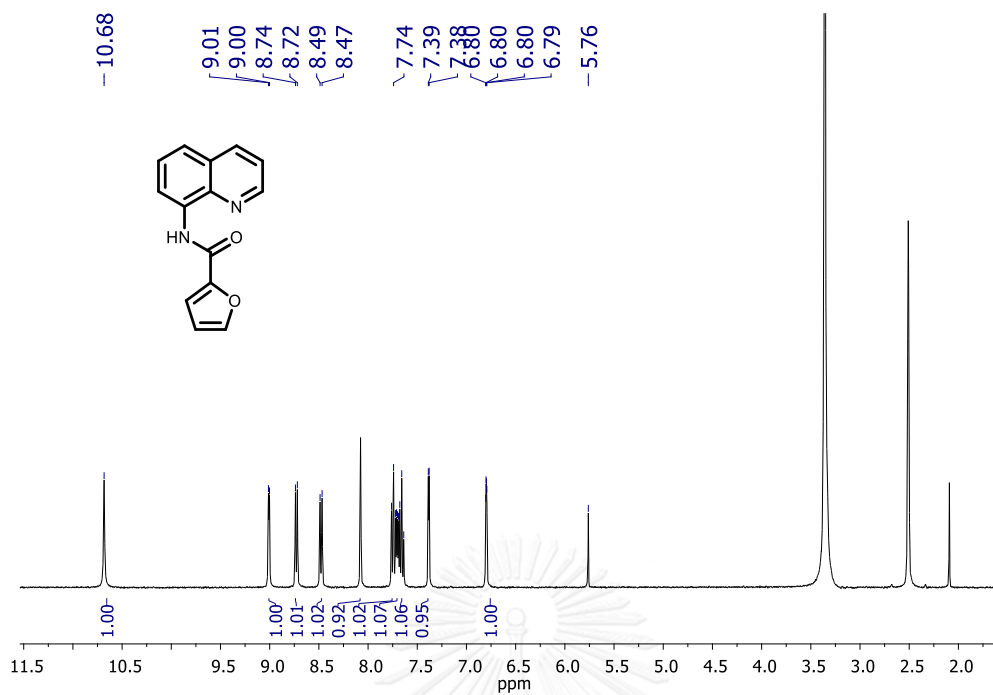
Figure A6 ^{1}H NMR spectrum compound **AQF** in DMSO-d_6.
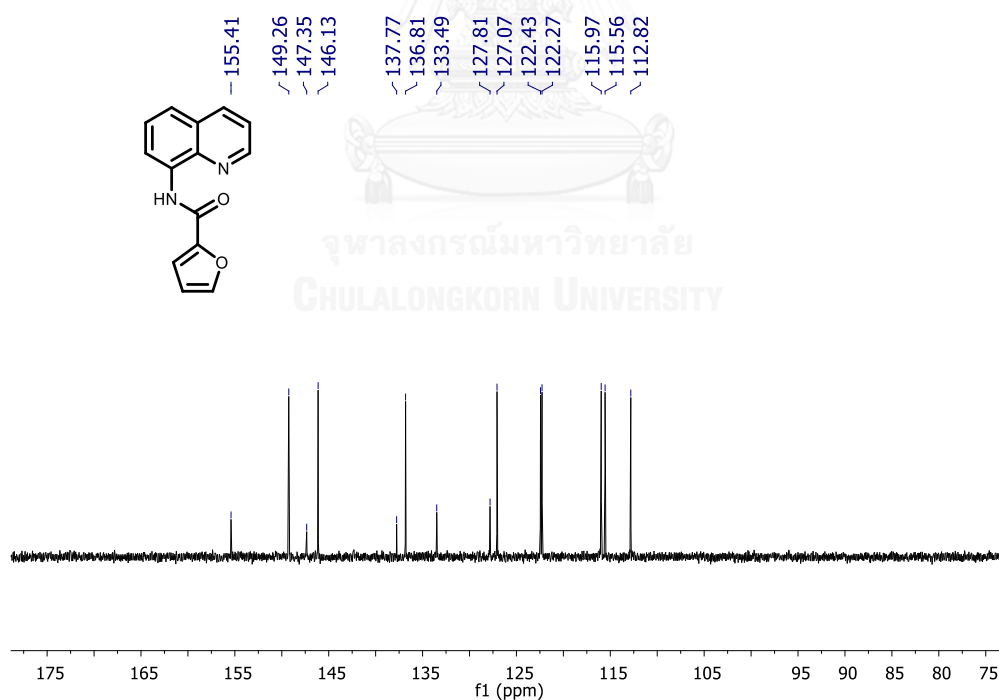
Figure A7 ^{13}C NMR spectrum compound **AQF** in DMSO-d_6.
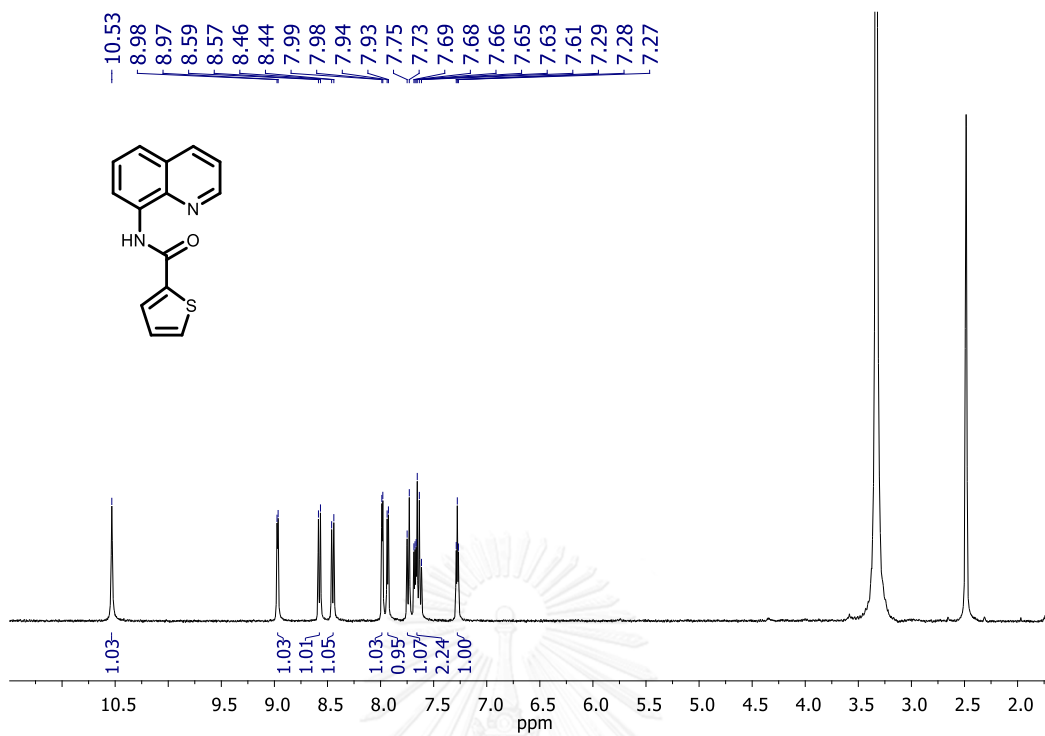
Figure A8 ^{1}H NMR spectrum compound **AQT** in DMSO-d_6.
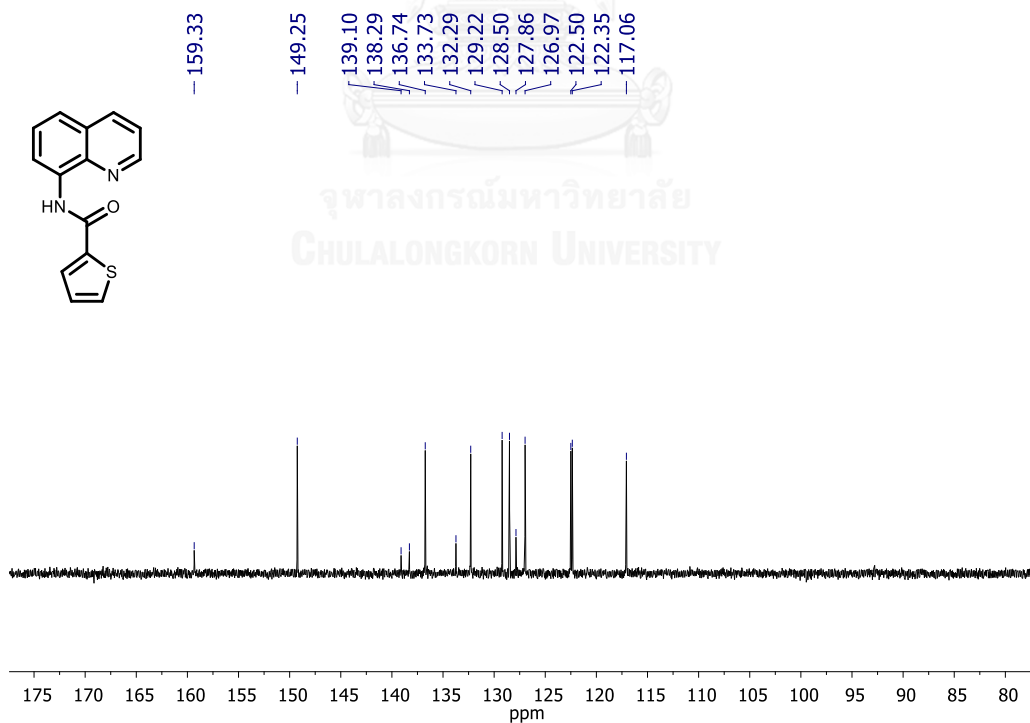
Figure A9 ^{13}C NMR spectrum compound **AQT** in DMSO-d_6.
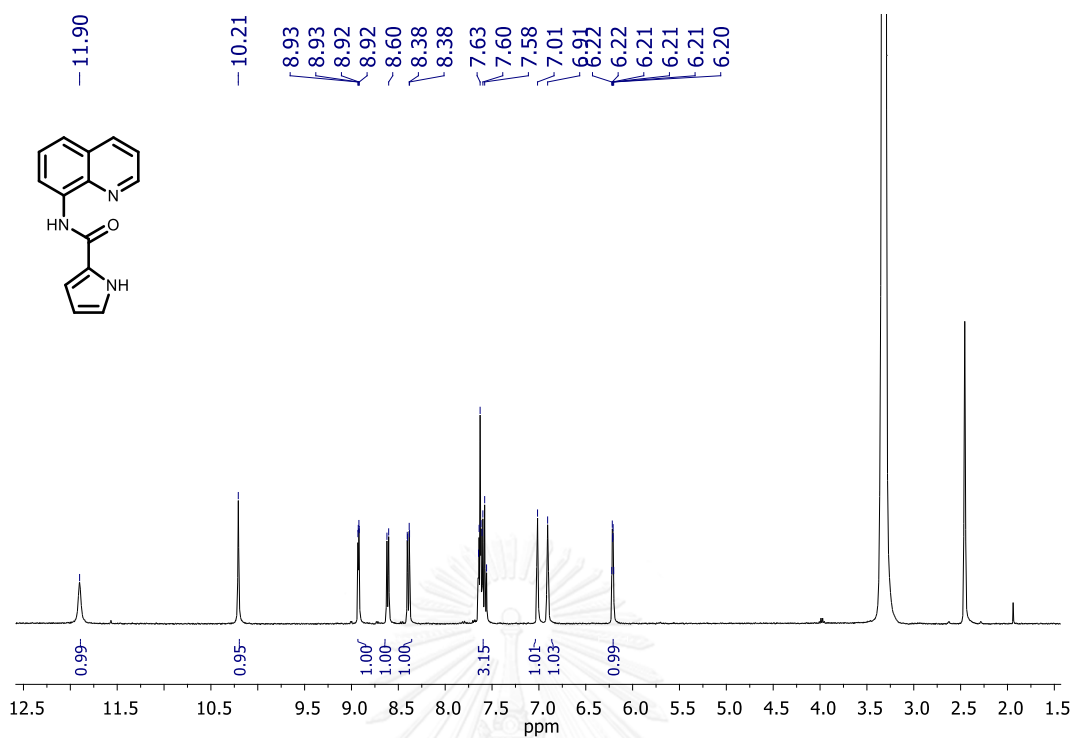
Figure A10 ^{1}H NMR spectrum compound **AQP** in DMSO-d_6.
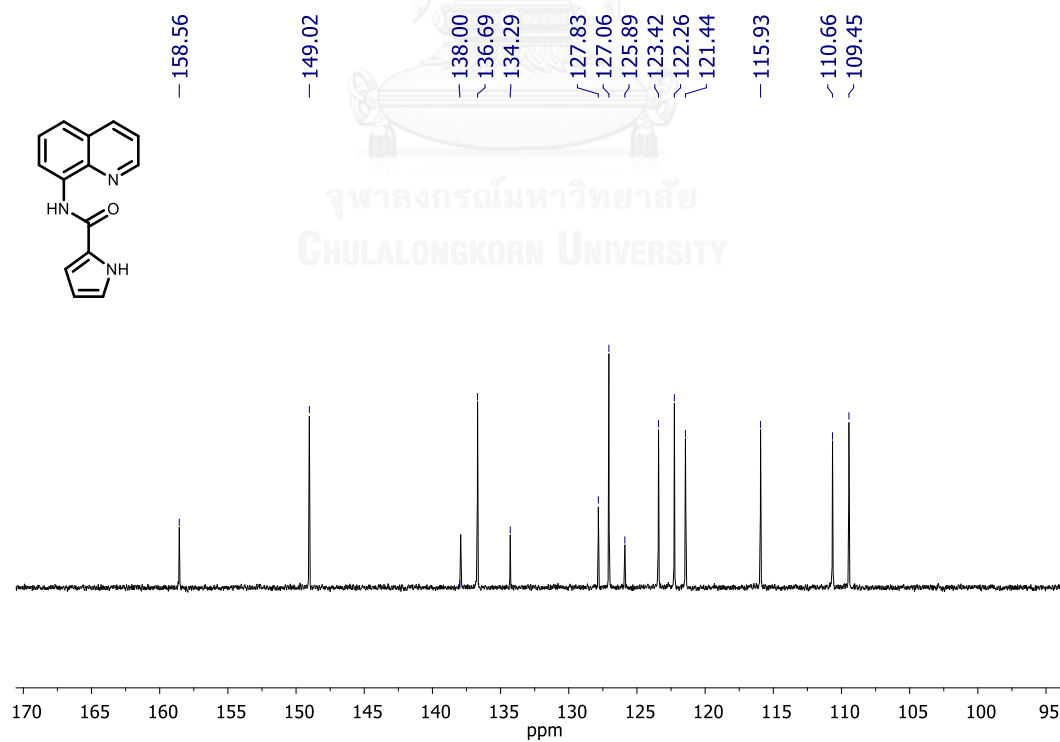
Figure A11 ^{13}C NMR spectrum compound **AQP** in DMSO-d_6.
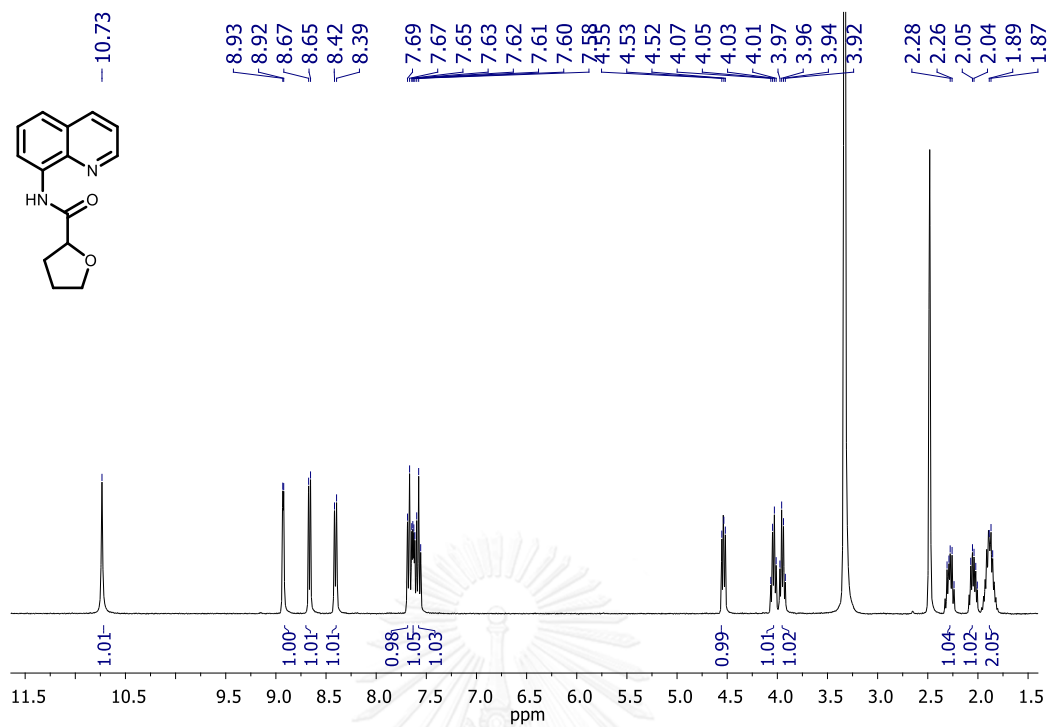
Figure A12 ^{1}H NMR spectrum compound **AQTHF** in DMSO-d_6.
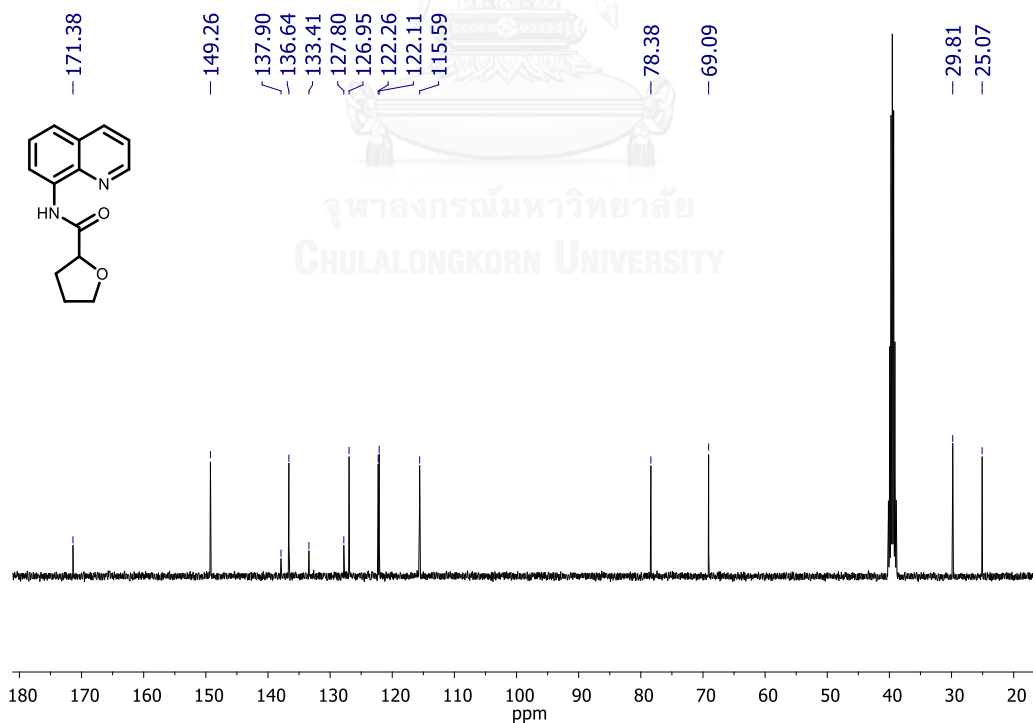
Figure A13 ^{13}C NMR spectrum compound **AQTHF** in DMSO-d_6.
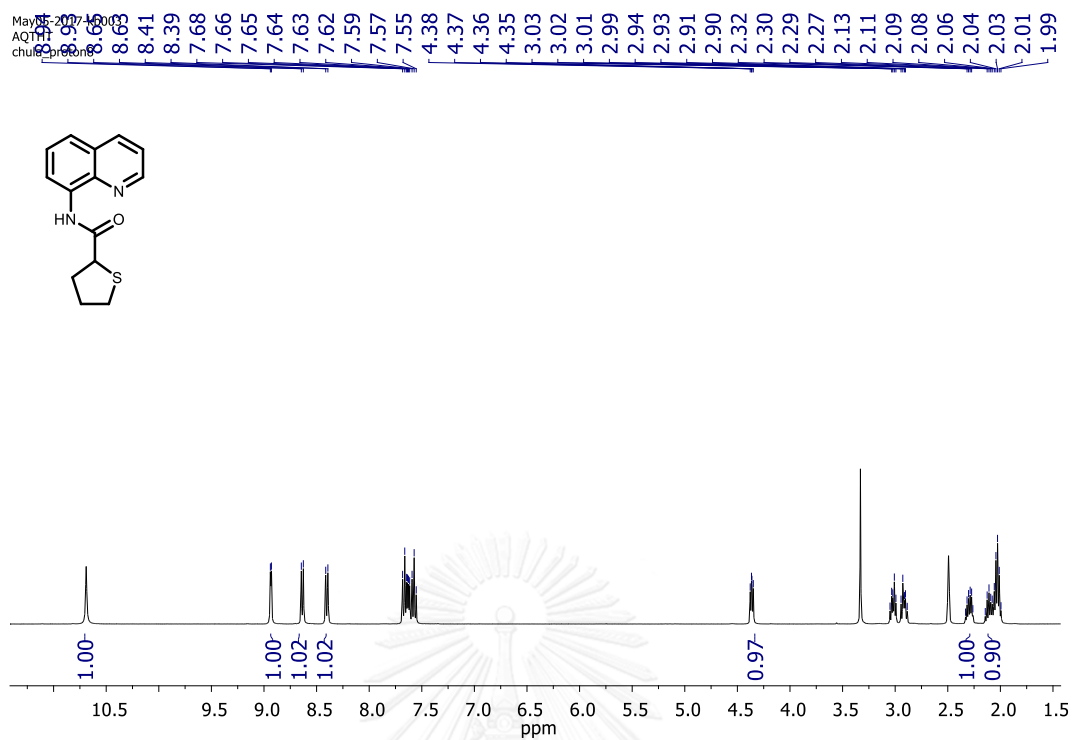
Figure A14 ^{1}H NMR spectrum compound **AQTHT** in DMSO-d_6.
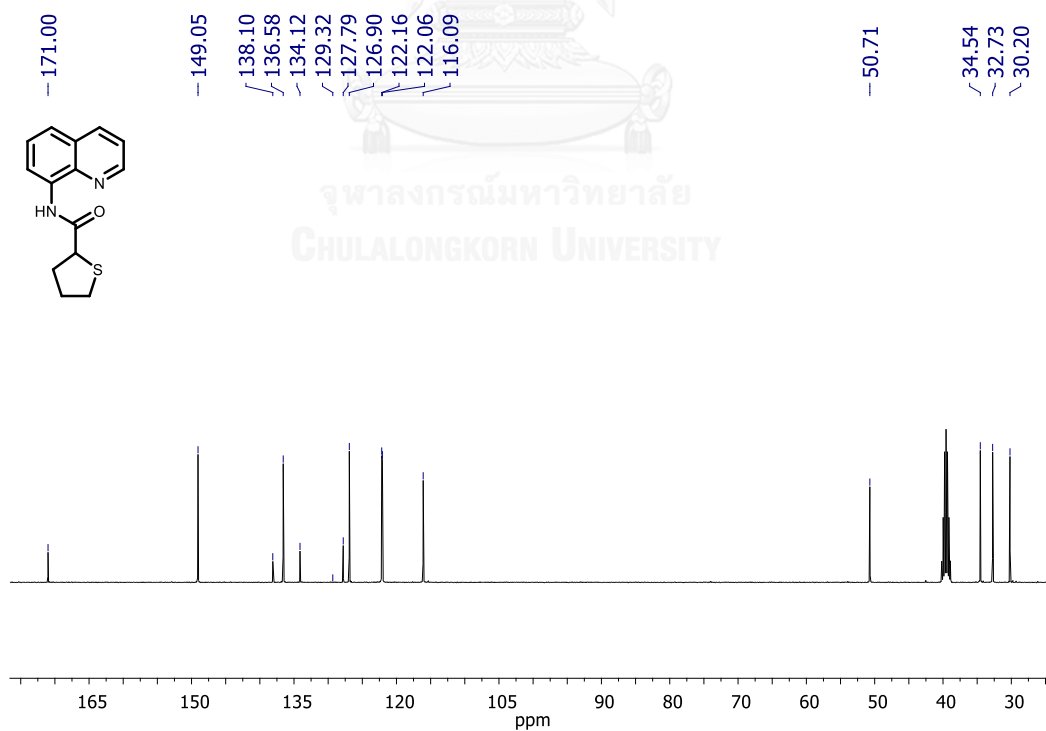
Figure A15 ^{13}C NMR spectrum compound **AQTHT** in DMSO-d_6.
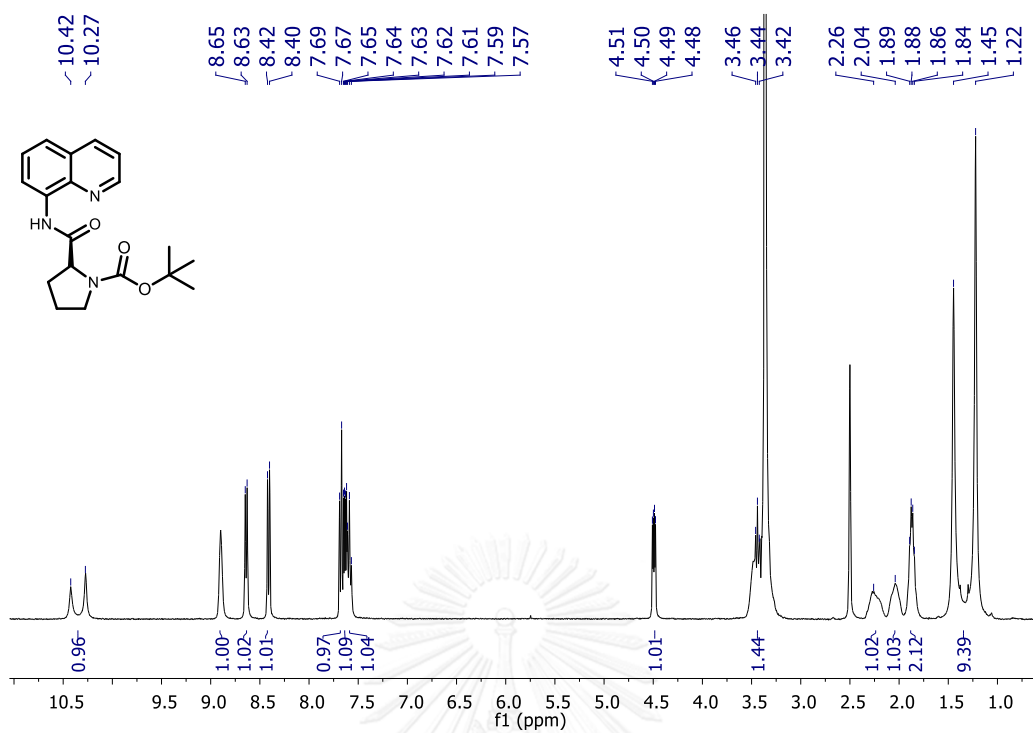
Figure A16 ^{1}H NMR spectrum compound **AQPro-Boc** in DMSO-d_6.
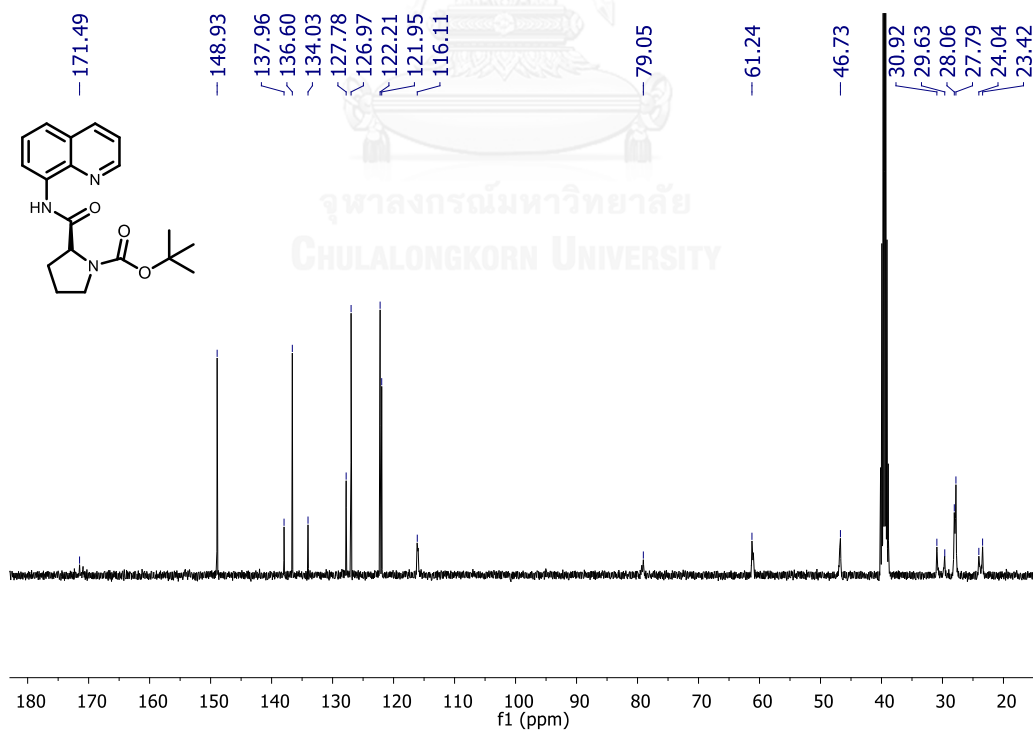
Figure A17 ^{13}C NMR spectrum compound **AQPro-Boc** in DMSO-d_6.
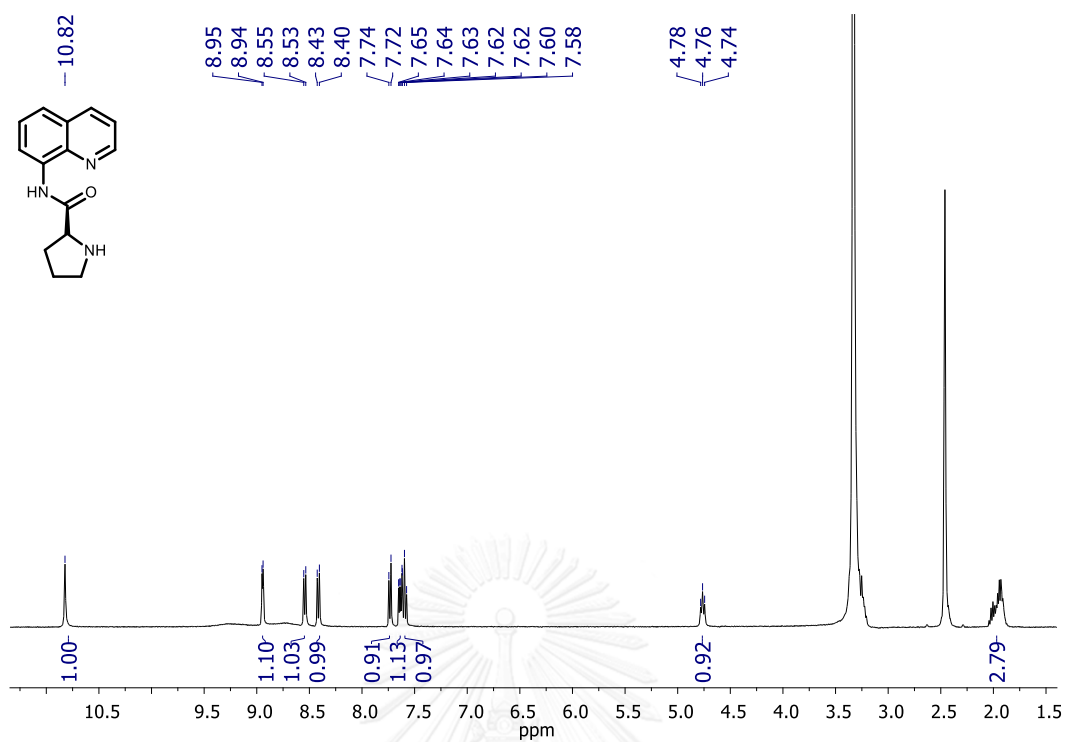
Figure A18 ^{1}H NMR spectrum compound **AQPro** in DMSO-d_6.
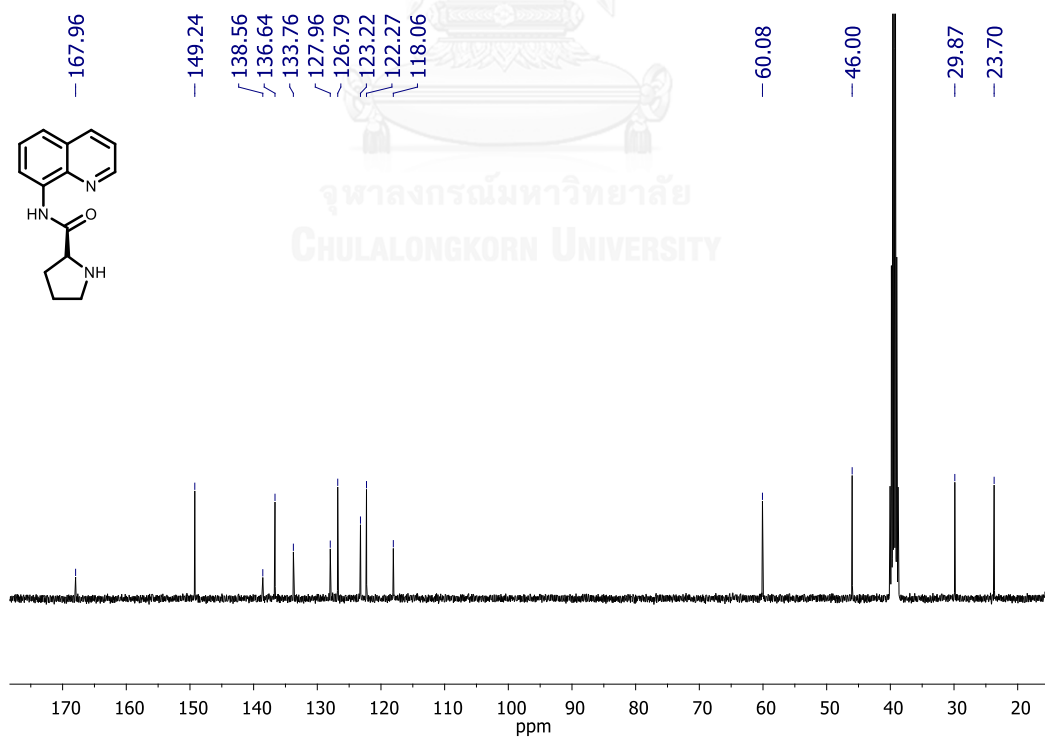
Figure A19 ^{13}C NMR spectrum compound **AQPro** in DMSO-d_6.
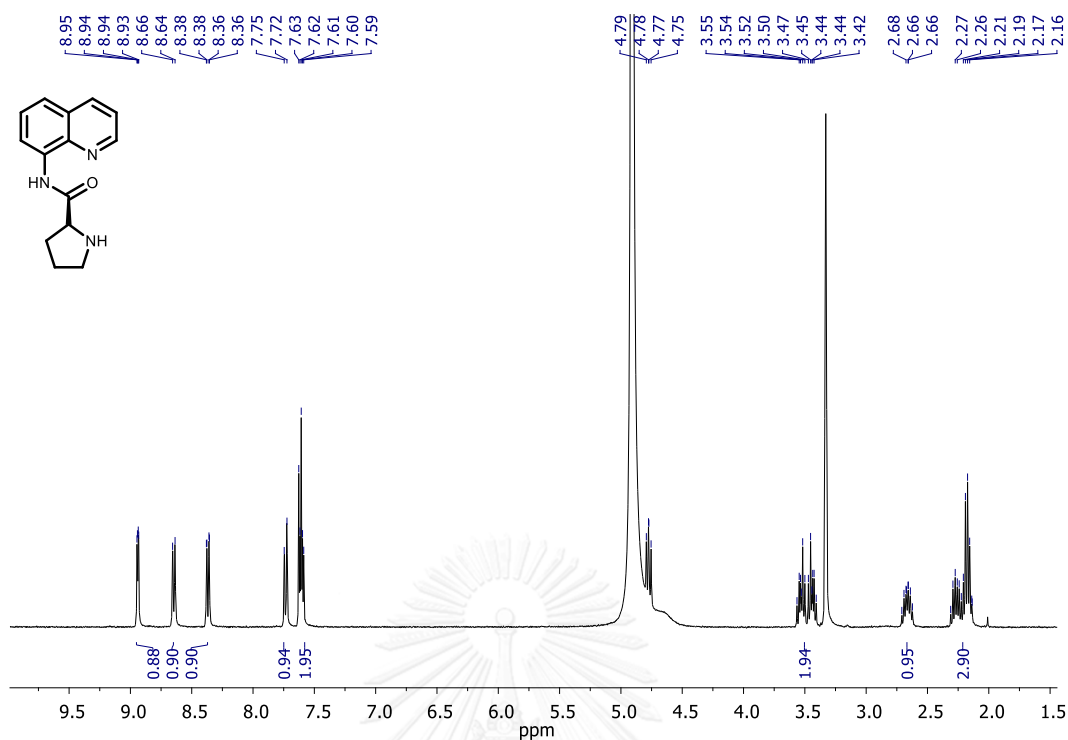
Figure A20 ¹H NMR spectrum compound **AQPro** in Methanol-*d₄*.
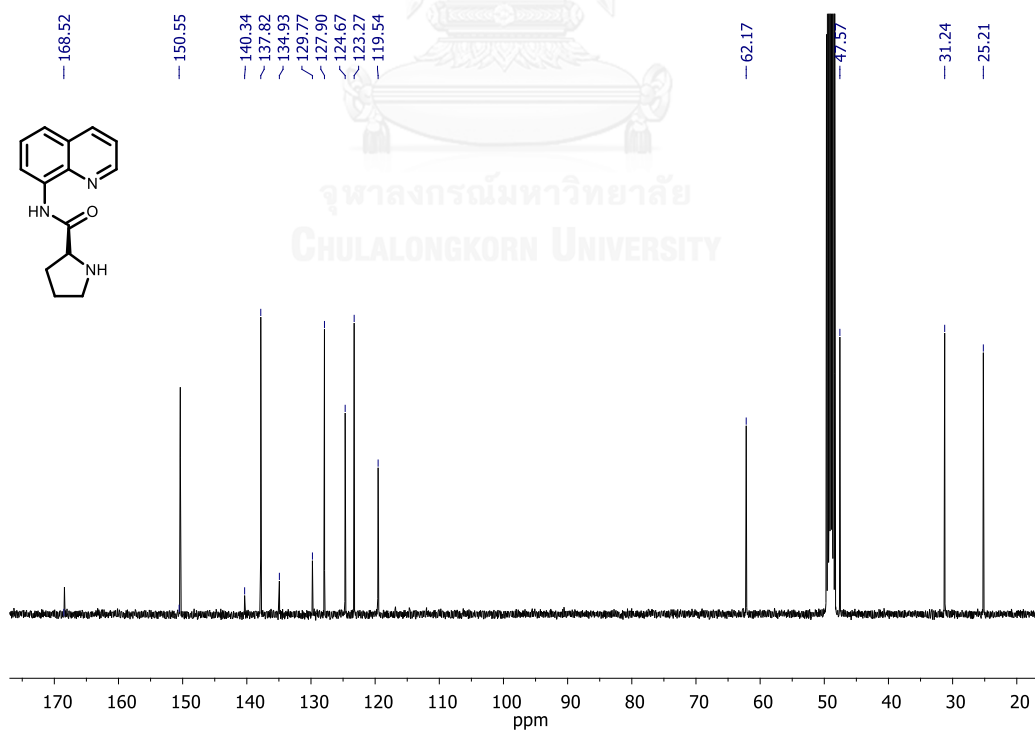
Figure A21 ¹³C NMR spectrum compound **AQPro** in Methanol-*d₄*.
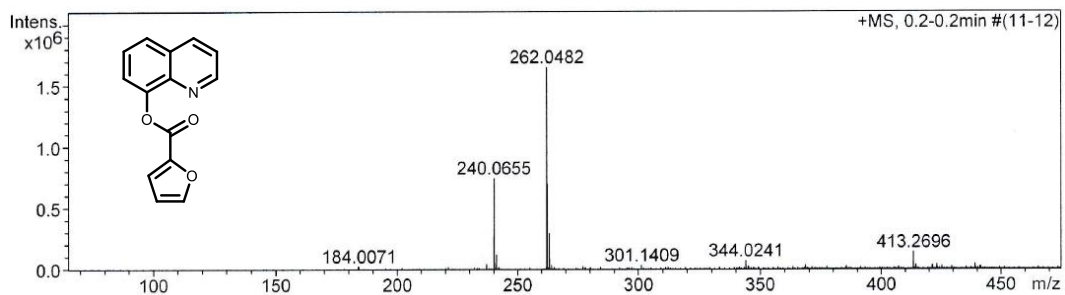
Figure A22 HRMS of **HQF** in methanol.
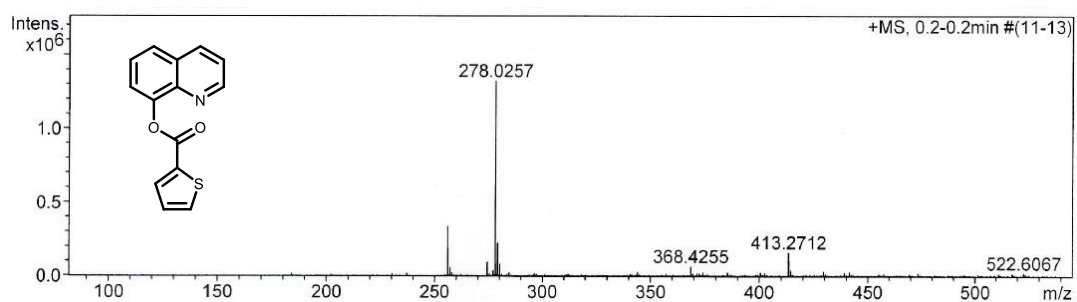
Figure A23 HRMS of **HQT** in methanol.
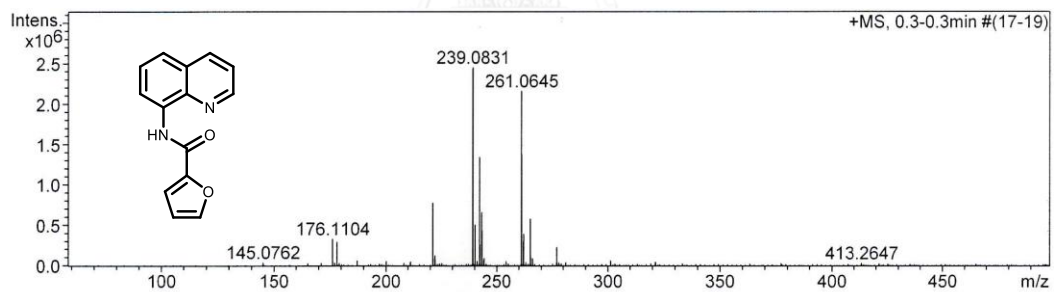
Figure A24 HRMS of **AQF** in methanol.
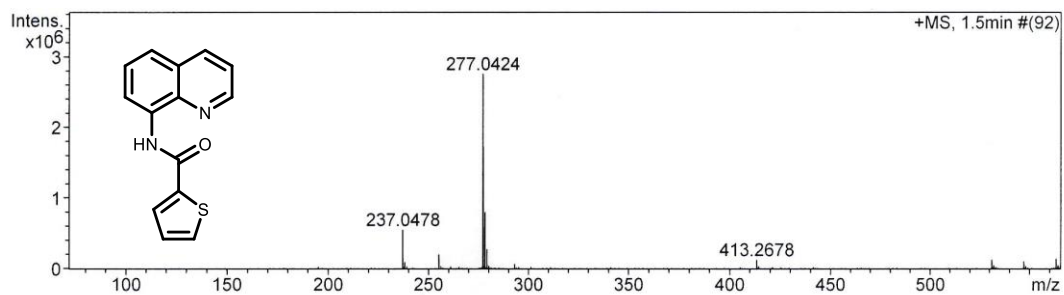
Figure A25 HRMS of **AQT** in methanol.
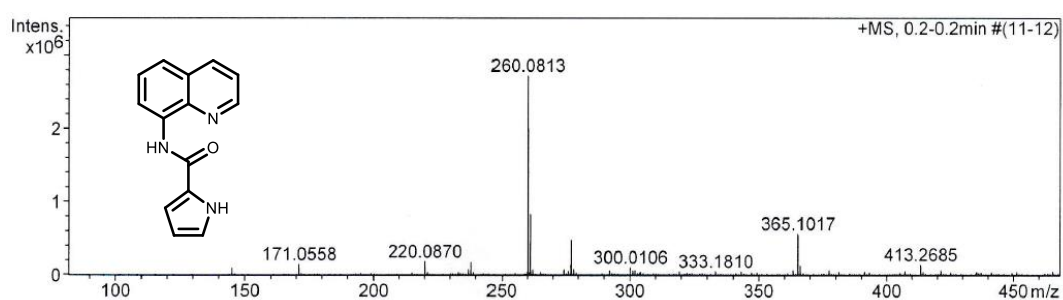
Figure A26 HRMS of **AQP** in methanol.
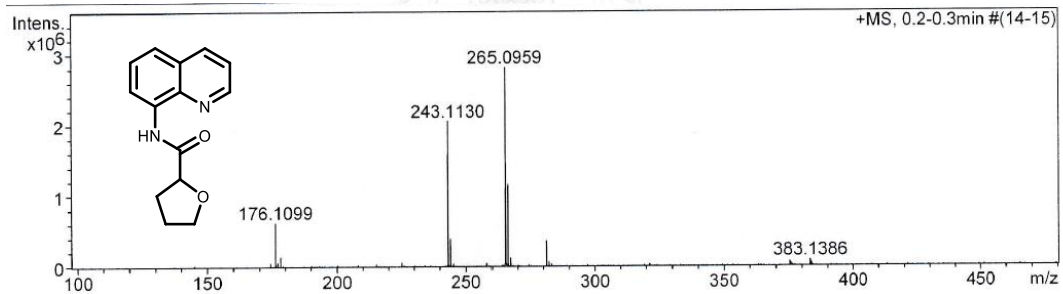
Figure A27 HRMS of **AQTHF** in methanol.
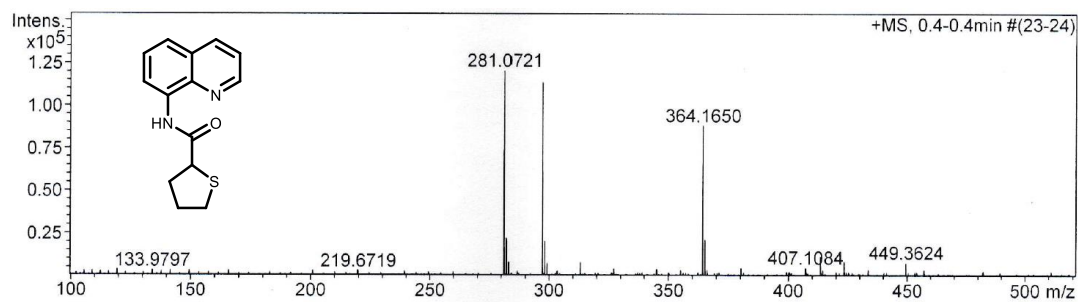
Figure A28 HRMS of **AQTHT** in methanol.
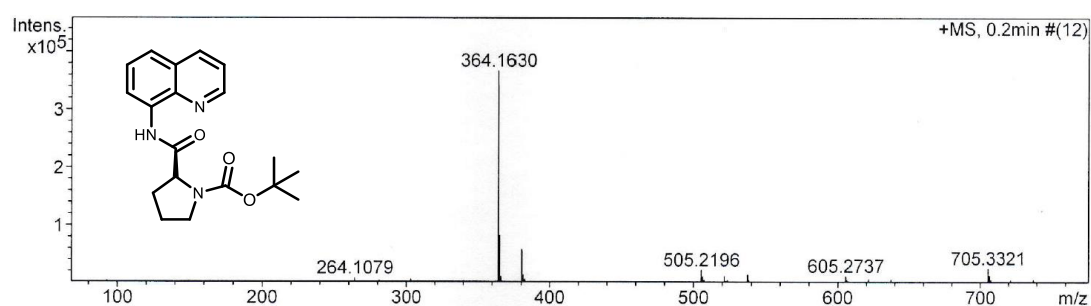
Figure A29 HRMS of **AQPro-Boc** in methanol.
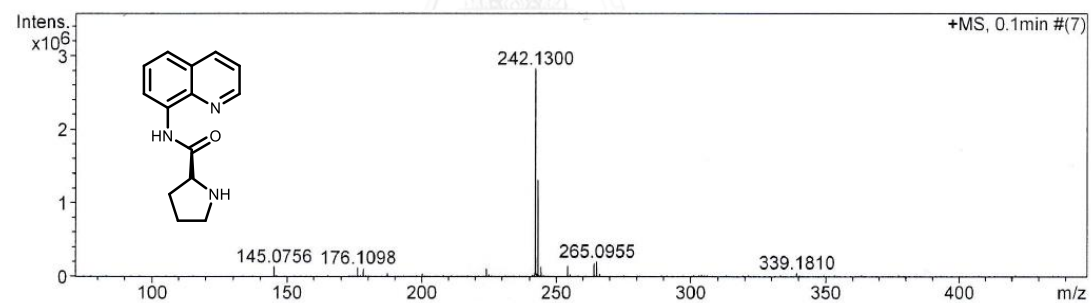
Figure A30 HRMS of **AQPro** in methanol.
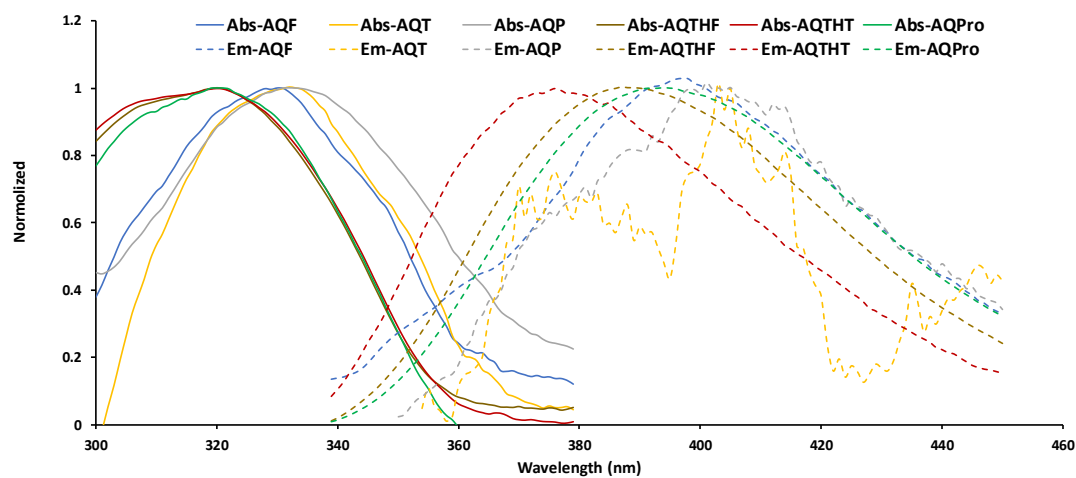
Figure A31 Normalized absorption (solid line) and emission (dash line) spectra of the amide derivatives in THF solution. The λ_{max} of each fluorophore was used as the excitation wavelength in the corresponding emission spectrum.
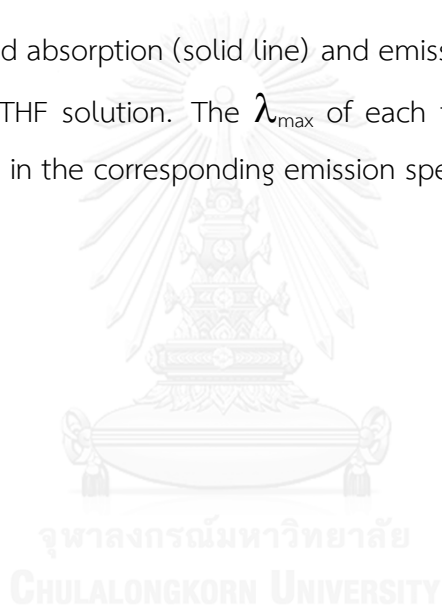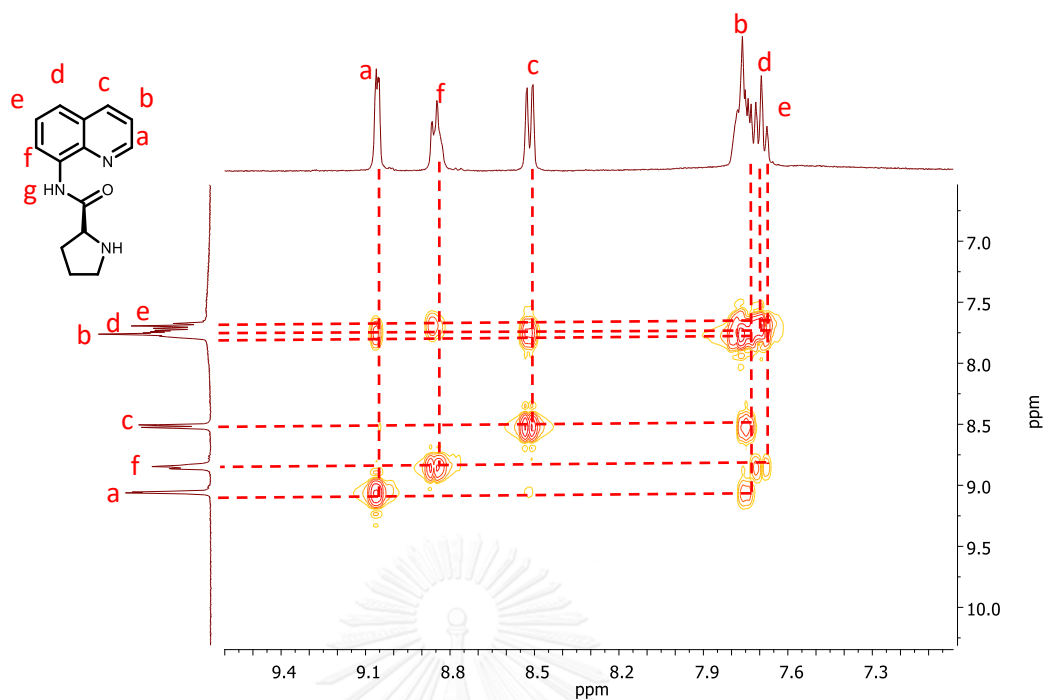
Figure A32 COSY correlation spectra of **AQPro** upon the addition of 1 equivalent of CH$_3$NH$_2$ in DMSO-d_6.
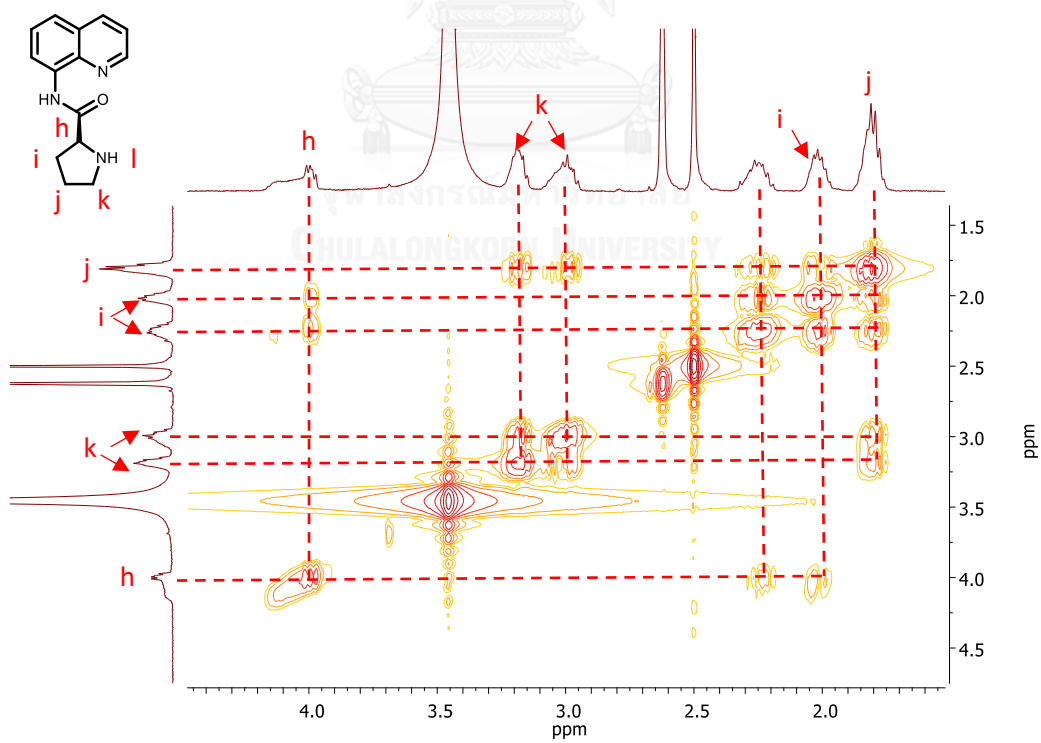
Figure A33 COSY correlation spectra of **AQPro** under basic condition in DMSO-d_6.
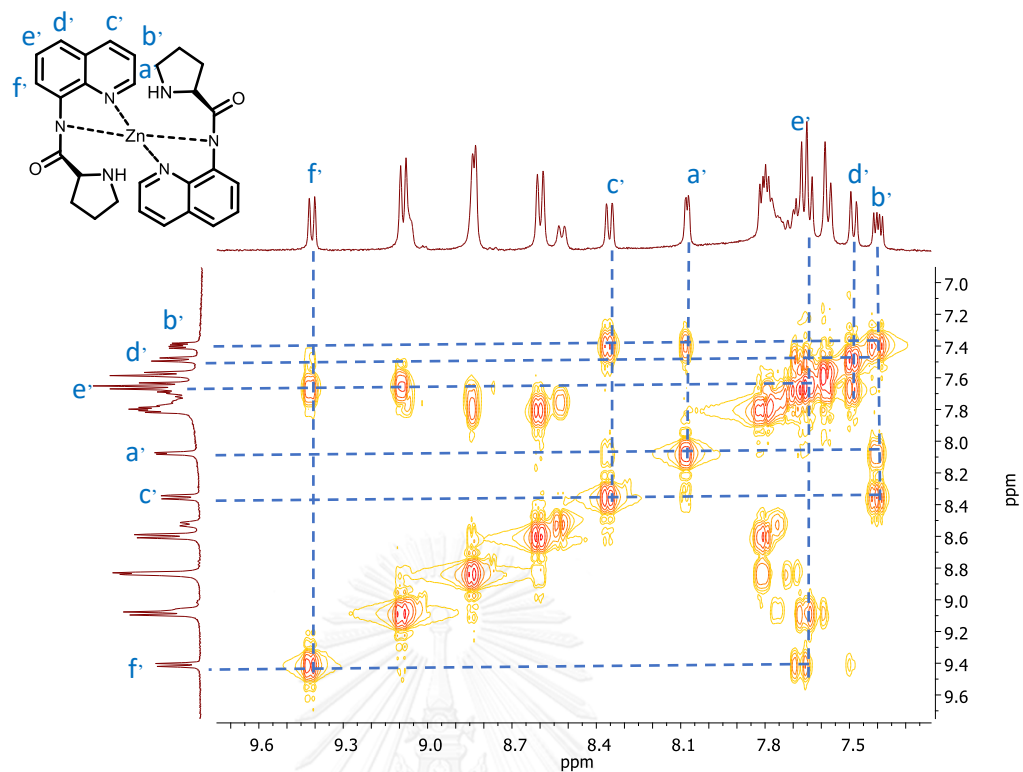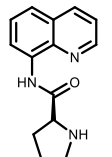
Figure A34 COSY correlation spectra of **AQPro** upon the addition of 0.5 equivalent of Zn^{2+} under basic condition in DMSO-d_6.
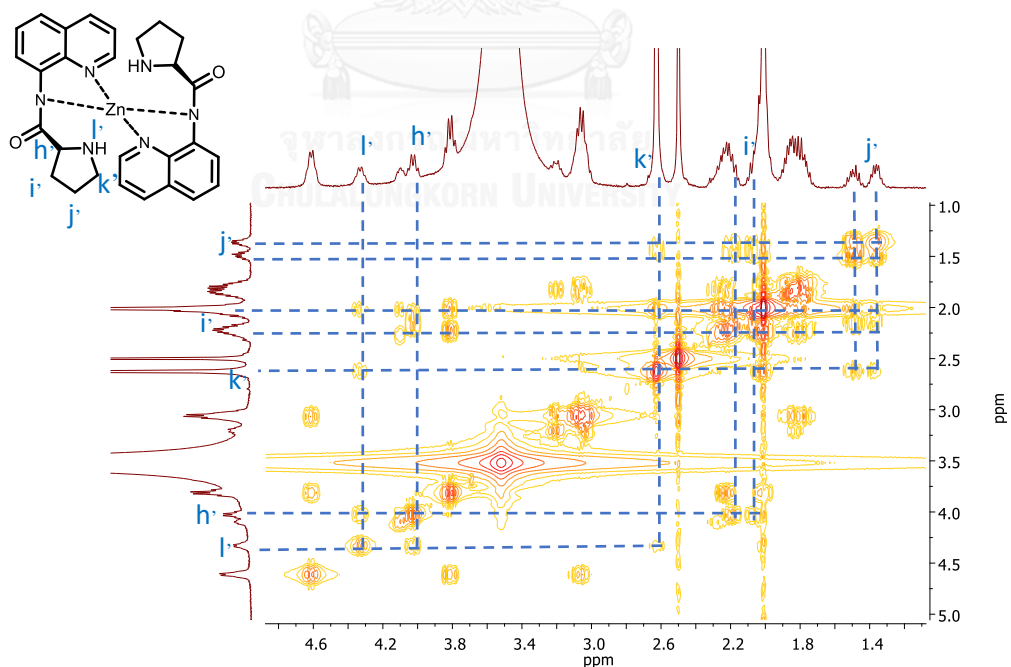
Figure A35 COSY correlation spectra of **AQPro** upon the addition of 0.5 equivalent of Zn^{2+} under basic condition in DMSO-d_6.
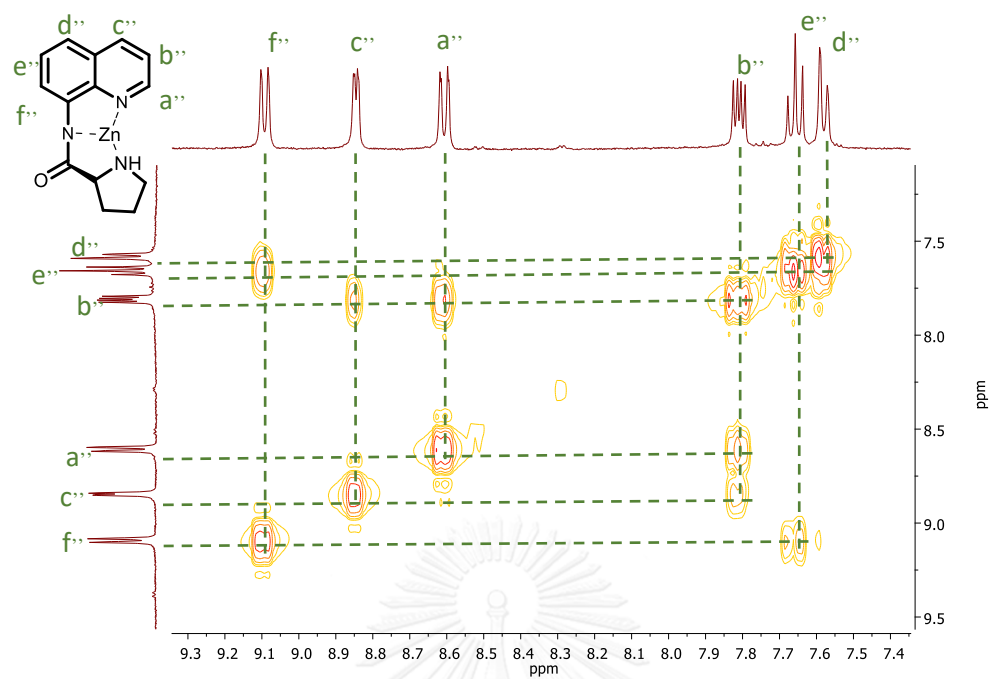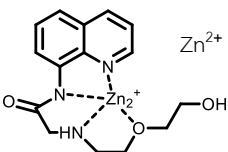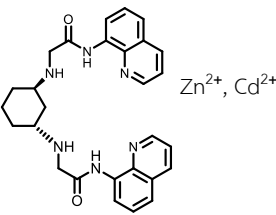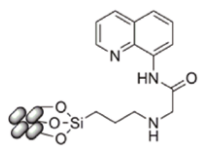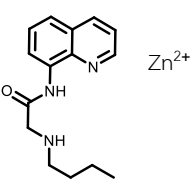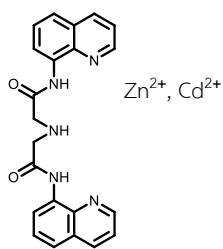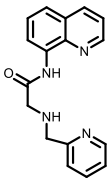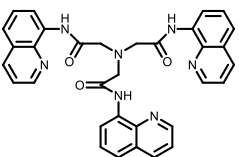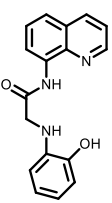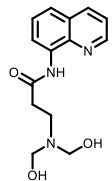
Figure A36 COSY correlation spectra of **AQPro** upon the addition of 1.0 equivalent of Zn²⁺ under basic condition in DMSO-*d₆*.
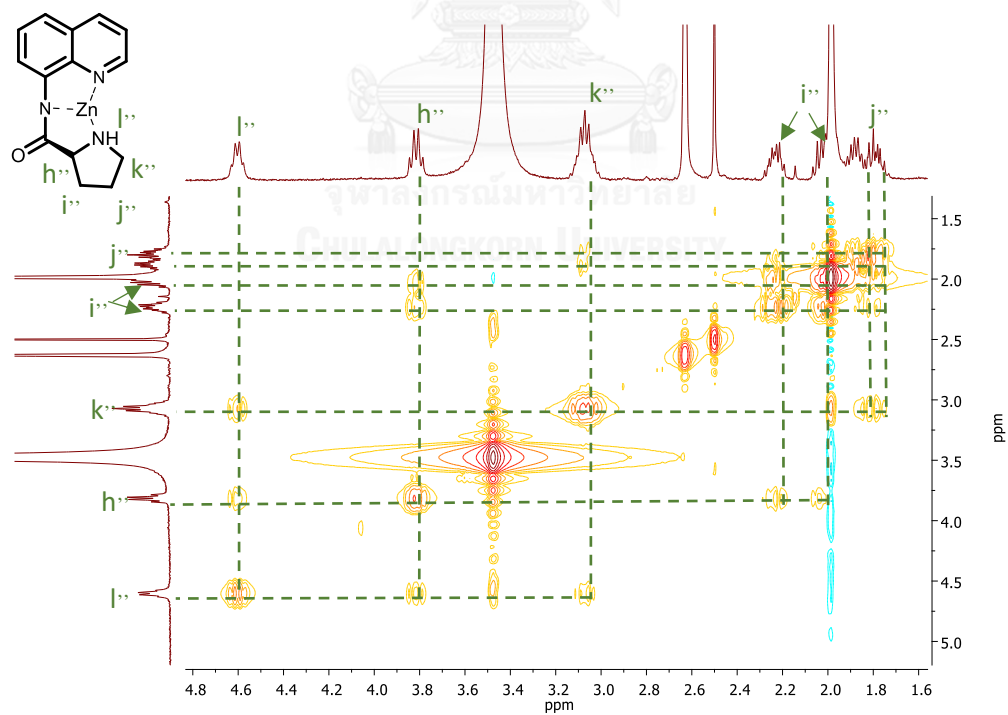
Figure A37 COSY correlation spectra of **AQPro** upon the addition of 1.0 equivalent of Zn²⁺ under basic condition in DMSO-*d₆*.

Table A1 The Zn^{2+} sensor based on 8-aminoquinoline derivatives reported to date

Reference	Selectivity	Media	$K_a(M^{-1})$	LOD (µM)	Φ/Φ_0	interferences	Cell study
[38]	Zn^{2+}	Tris-HCl pH = 7.22, MeOH/H_2O = 1:9 (v/v)	6.7×10^6	-	7.9	Co^{2+}, Cu^{2+}	Yeast cells
[39]	Zn^{2+}, Cd^{2+}	HEPES pH = 7.4, MeOH/H_2O = 5:5 (v/v)	1.8×10^6	0.028	12	Ni^{2+}, Li^+, Na^+, Mg^{2+}, Ca^{2+}	HK-1 cell
[40]	Zn^{2+}	Tris-HCl pH = 7.22	5.7×10^3	0.1	3.31	Fe^{2+}, Co^{2+}, Ni^{2+}, Cu^{2+}	-
[41]	Zn^{2+}	Tris-HCl pH = 7.22, MeOH/H_2O = 1:9 (v/v)	-	1-10	16.3	Co^{2+}, Cu^{2+}	Yeast cells
[42]	Zn^{2+}, Cd^{2+}	Tris-HCl pH = 7.22	8.7×10^6	0.02	-	Co^{2+}, Cu^{2+}	-

Reference	Selectivity	Media	$K_a (M^{-1})$	LOD (μM)	Φ/Φ_0	interferences	Cell study
[43]	Zn^{2+}, Cd^{2+}	HEPES pH = 7.4	1.6×10^6	1-10	8.8	Fe^{2+}, Fe^{3+}, Co^{2+}, Ni^{2+}, Cu^{2+}	-
[44]	Zn^{2+}	Tris-HCl pH = 7.22	5.7×10^3	3.2	15	Fe^{2+}	A549 cells
[45]	Zn^{2+}	Tris buffer pH =7.4 CH_3OH/H_2O = 4:1 (v/v).	5.2×10^5	25.6	-	Ni^{2+}, Cu^{2+}	-
[46]	Zn^{2+}	Bis-tris pH = 7.0	1.4×10^4	4.48	-	Al^{3+}, Fe^{2+}, Fe^{3+}, Co^{2+}, Cr^{3+}, Cu^{2+}	-
This work	Zn^{2+}	THF Solution	5.0×10^2	0.029	18	Al^{3+}, Fe^{2+}, Fe^{3+}, Co^{2+}, Ni^{2+}, Cr^{3+}, Cu^{2+}	-

VITA

Mr. Pasakorn Hansetagan was born on October 4th, 1990 in Bangkok, Thailand. He was graduated with Bachelor Degree of Science, majoring in Chemistry from Srinakharinwirot University in 2012. He has been a graduate student in organic chemistry and become a member of Organic Synthesis Research Unit under supervision of Assist. Prof. Dr. Anawat Ajavakom and Co-advisor Prof. Dr. Mongkol Sukwattanasinitt. He graduated with a Master's degree in Chemistry in academic year 2015. His parent address is 1/146, Ngam Wong Wan Road, Thung Song Hong, Lak Si, Bangkok, Thailand 10210.